Schottky barrier diode fabrication on n-GaN for ultraviolet detection

by

Mmantsae Moche Diale

Submitted in partial fulfillment of the requirements for the degree

PHILOSOPHIAE DOCTOR

In the Faculty of Natural & Agricultural Sciences

Department of Physics

University of Pretoria

PRETORIA

September 2009

Supervisor: Prof. F. D. Auret

© University of Pretoria

TO MY SON

LEBOGANG ONKGOPOTSE

DIALE

UNIVERSITEIT VAN PRETORIA
UNIVERSITY OF PRETORIA
YUNIBESITHI YA PRETORIA

Brain Child

UNIVERSITEIT VAN PRETORIA
UNIVERSITY OF PRETORIA
YUNIBESITHI YA PRETORIA

ACKNOWLEDGMENTS

The opportunity to be at one of the foremost research universities in the world and pioneer GaN research in South Africa is one I will always be grateful for, and there are many people who have inspired, guided and assisted me. I want to thank my supervisor, Professor F. Danie Auret, for accepting me as his student. Thank you for all your support and guidance during my time at the University of Pretoria. It has been both an educational and an emotional experience to work with the Thin Films and Electronic Materials group. The atmosphere was not always enjoyable, but the willingness to learn and apply emotional intelligence has helped me to pull through. I thank Andre Botha and all the members of the microscopy unit for their helpful discussions that led to my first presentation at an international conference as regards this thesis. I wish to express special thanks to Professor Johan Brink for helpful discussions and advice in the experiments that involved the use of optical equipment. I wish to thank Professor Johan Malherbe, the head of the Department of Physics, for his encouragement and interventions during difficult times. I am so glad to have shared this experience with my fellow students in this Department. Gunther Kassier was the first student who worked very closely with me in the endeavour to set-up the optoelectronic station, which was finalized by Louwrens van Schalkwyk. Special thanks to my fellow students and colleagues for answering important questions of the moment: Hannes de Meyer, Machesa Legodi, Claudia Zander, Johan Janse van Rensburg, Sergio Coelho, Cloud Nyamhere, Wilbert Matangi, Albert Chawanda, Rik van Laarhoven, Quinton Odendaal, Walter Meyer, and Augusto Machatine.

Finally I thank my husband Dr OPPP Diale for financial and emotional support.

The financial support of the project stemmed from the National Research Foundation and the University of Pretoria.

UNIVERSITEIT VAN PRETORIA
UNIVERSITY OF PRETORIA
YUNIBESITHI YA PRETORIA

Schottky barrier diode fabrication on n-GaN for ultraviolet detection

by

Mmantsae Moche Diale

Submitted in partial fulfillment for the degree PhD (Physics) in the Faculty of Natural and Agricultural Science, University of Pretoria

Supervisor: Prof. F. D. Auret

There are many potential areas for the utilization of GaN-based nitride materials, including ultraviolet photodetectors. Ultraviolet photodetectors are used in the military for missile plume detection and space communications. Medically, ultraviolet photodiodes are used in monitoring skin cancer. Schottky barrier metal-semiconductor contacts are choice devices for the manufacture of ultraviolet photodiodes due to higher short wavelength sensitivity and fast response. They also require simple fabrication technology; suffer lower breakdown voltages, and record larger leakage currents at lower voltages as compared to p-n structures of the same semiconductor material. Thus the formation of a Schottky contact with high barrier height, low leakage current, and good thermal stability in order to withstand high temperature processing and operation are some of the most important factors in improving the performance of Schottky barrier photodiodes to be used for ultraviolet detection. The first stage of this study was to establish a chemical cleaning and etching technique. It was found that KOH was suitable in reducing C from the surface and that $(NH_4)_2S$ further reduced the surface oxides. The next phase of the work was to select a metal that will allow UV light to pass through at a high transmission percentage: a combination of annealed Ni/Au was found to be ideal. The transmission percentage of this alloy was found to be above 80%. The next phase was the fabrication of Ni/Au Schottky barrier diodes on GaN to study the electrical characteristics of the diodes. Electrical

characterization of the diodes showed that the dominant current transport mechanism was thermionic emission, masked by the effects of series resistance, which resulted from the condition of the GaN surface. Finally, we fabricated GaN UV photodiodes and characterized them in the optoelectronic station designed and produced during this research. Device responsivity as high as 31.8 mA/W for GaN and 3.8 mA/W for AlGaN were recorded. The calculated quantum efficiencies of the photodiodes were 11 % for GaN and 1.7 % for AlGaN respectively

Keywords: Al(GaN), Schottky, photodiodes, Ultraviolet, responsivity, quantum efficiency.

UNIVERSITEIT VAN PRETORIA
UNIVERSITY OF PRETORIA
YUNIBESITHI YA PRETORIA

TABLE OF CONTENTS

ACKNOWLEDGEMENTS iv

ABSTRACT v

1 Introduction **1**
1.1 Introduction 1
1.2 Aims of the study . 6
1.3 Synopsis of thesis 6
References 7

2 GaN-based materials for Ultraviolet detectors **8**
2.1 Introduction 8
2.2 Progressive development of GaN 8
2.2.1 Growth Methods 9
2.2.2 Substrates to GaN 12
2.2.3 High n-type conductivity 13
2.2.4 Doping of GaN 14
2.2.5 Effects of defects on GaN devices 15
2.3 Properties of GaN-based materials 16
2.4 Applications of GaN 19
2.5 AlGaN photodetectors 21
2.6 Ohmic contacts to AlGaN 22
References 24

3. Schottky Barrier Ultraviolet Photodetectors **31**
3.1 Introduction 31
3.2 Ultraviolet photodetectors 31
3.2.1 Active area of semiconductor diode 33
3.2.2 Responsivity 33
3.2.3 Operation Voltage 35
3.2.4 Dark current-voltage characteristics 35
3.2.5 Response speed 36
3.2.6 Capacitance 37
3.2.7 Series resistance 37
3.3 Schottky-Mott theory and its modifications 38
3.4 Current transport mechanisms 41
3.5 Theory of ultraviolet photodetectors 43
References 45

4 Experimental Techniques **47**
4.1 Introduction 47
4.2 Sample preparation 47
4.3 Surface characterization 48
4.3.1 Auger Electron Spectroscopy 48
4.3.2 Scanning Electron Microscopy 49
4.3.3 Atomic Force Microscopy 50
4.4 Electrical and Optical Characterization 51
References 55

EXPERIMENTAL RESULTS **56**

5 Analysis of GaN Cleaning procedures **57**
5.1 Introduction 57
5.2 Experimental 60
5.3 Results and Discussion 63
5.3.1 Atomic Force Microscopy 63
5.3.2 Auger Electron Spectroscopy 75
5.4 Conclusions 78
References 80

6 Study of metal contacts on GaN for transmission of UV light **81**
6.1 Introduction 81
6.2 Choice of metal for transparent contacts 82
6.3 Experimental 83
6.4 Results and Discussion 83
6.5 Conclusions 90
References 91

7 Chemical treatment effect on Au/GaN diodes **92**
7.1 Introduction 92
7.2 Experimental 94
7.3 Results and Discussion 94
7.3.1 Capacitance-Voltage 94
7.3.2 Current-Voltage 96
7.4 Conclusions 99
References 100

8 Fabrication of GaN/AlGaN Schottky barrier photodiodes	**101**
8.1 Introduction	102
8.2 Experimental	103
8.3 Results and Discussion	104
8.4 Conclusions	111
References	112
9 Conclusions	**113**
List of Publications	**116**

CHAPTER 1

1.1 Introduction

The ultraviolet (UV) region of electromagnetic radiation occupies a section of wavelengths ranging from 400 to 10 nm [1]. It is highly ionizing and activates many chemical processes on different types of materials and living beings. It is divided into four categories: near UV with wavelength range 400 to 300 nm, middle UV from 300 to 200 nm, far or vacuum UV from 200 to 100 nm and extreme UV from 100 to 10 nm. The lower wavelength radiation that generally reaches the earth's surface is the first mentioned. Middle UV radiation is absorbed by the ozone layer while far UV radiation is absorbed by molecular oxygen. Extreme UV radiation is absorbed by all types of atomic and molecular gases and is not supposed to reach the earth's surface at all. As a function of its effects on the biosphere, the UV regions are arbitrarily called: UVA from 400–320 nm, UVB from 320-280 nm and UVC from 280-180 nm [2]. The different regions for the UV section of the electromagnetic spectrum are shown in Table 1.1 below.

Table 1.1: UV radiation wavelength range and corresponding names [2].

Category	Wavelength (nm)
UV - A	400 – 320/315
UV - B	315/320 – 280
UV - C	280 – 180
Vacuum UV	200 – 10

Category	Wavelength (nm)
Near UV	400 – 300
Middle UV	300 – 200
Far UV	200 – 122/100
Extreme UV	121/100 – 10

Further classification of the radiation wavelength is termed the solar-blind and visible blind regions. Some UV radiation from the sun is absorbed by the ozone in a certain range of wavelengths, thus not reaching the earth's atmosphere. Figure 1.1 indicates this condition with a comparison between the regions above and below the atmosphere. Some detectors require that the UV signal be detected in the background of the sun. It is evident from the figure that the amount of solar radiation reaching the earth's surface drops greatly around 300 nm (4.1 eV). Thus a solar blind detector detects UV radiation below 300 nm. The wavelength range of AlGaN makes it possible to have both visible-blind and solar blind UV detectors, depending on the energy of the radiation to be detected.

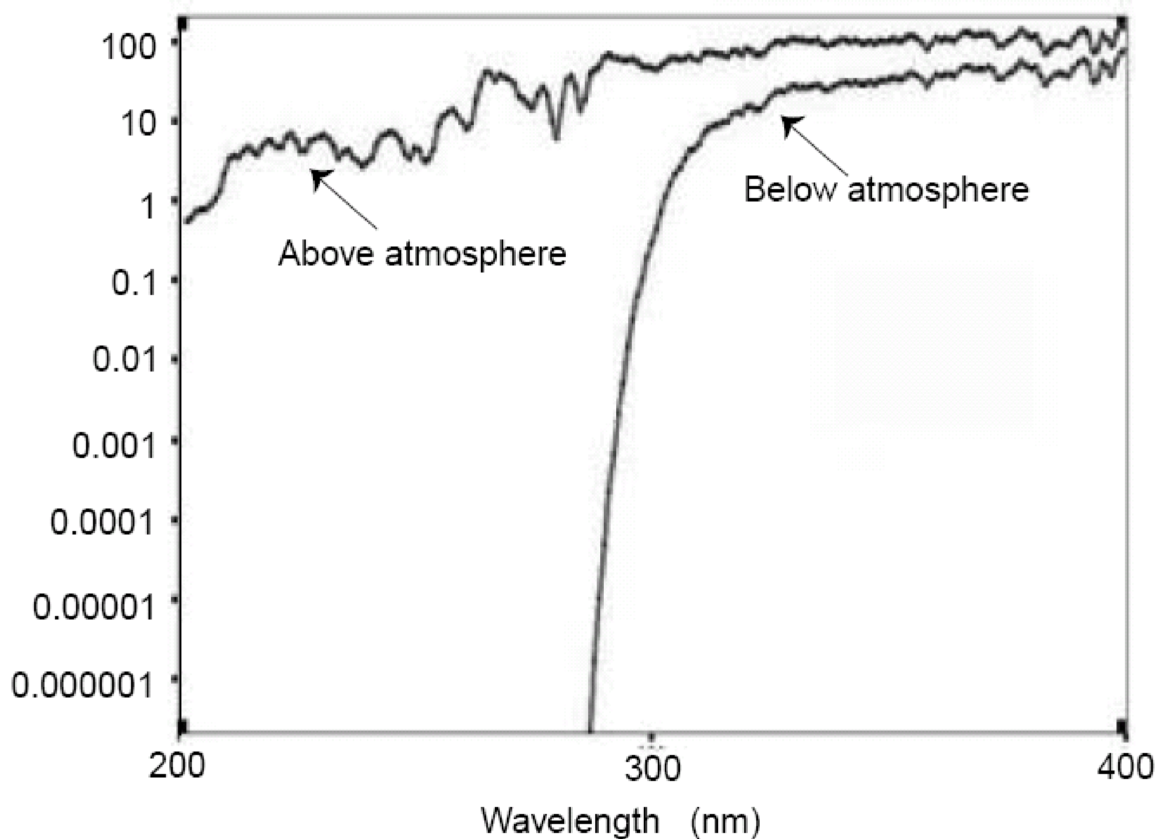

Figure 1.1: Solar UV above and below the atmosphere of the earth, from 1976 US standard atmosphere [3].

In addition, figure 1.2 clearly depicts the solar blind and visible blind regions. Visible blind indicates those regions where UVB radiation is active while solar blind refers to the regions where UVC is dominant. UVB never reach the earth surface in general, but due to ozone layer depletion, there may be some effects of on the biosphere.

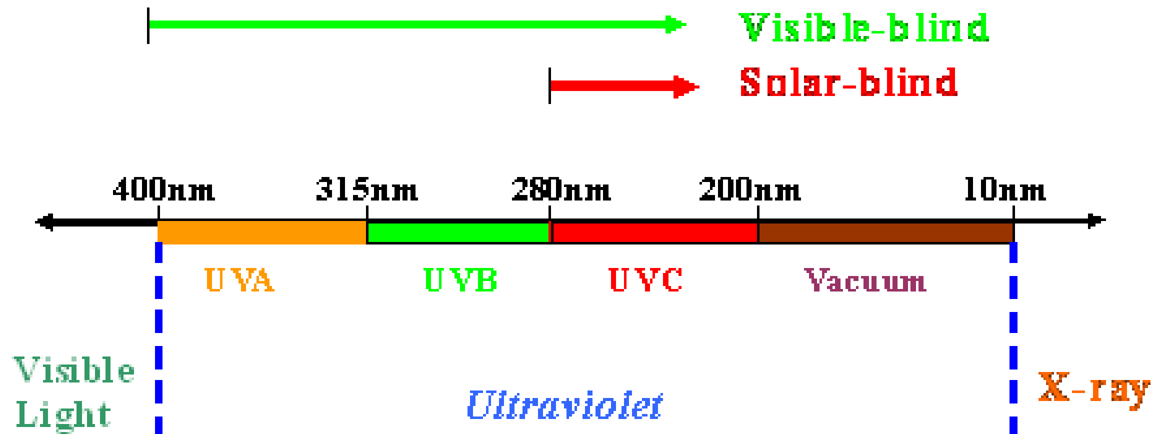

Figure 1.2: Regions of electromagnetic radiation, showing the different ultraviolet sections and their borders [4].

The main source of UV radiation is the sun. The energy per unit of time reaching the earth at right angles to the light rays that are observed outside the earth's atmosphere is 1353 W/m^2, of which only 121.8 W/m^2 (9%) constitute the total UV radiation [4]. The UV radiation on earth and its effects depend on the solar altitude angle lying between any line directed to the sun and the projection on the horizontal plane. Thus the amount of UV radiation at different places on the earth depends on the position of the sun during the day and the season of year. Research in Germany has shown that a decline in the amount of ozone has been observed to be high in spring, indicating an increase in UV radiation at that time of the year [5]. UV radiation is also produced artificially from electroluminiscence of certain types of matter, when ions, atoms and molecules are accelerated at high voltages.

A global scale called Solar Ultra Violet Index (UVI) is used to describe the level of UV radiation on the biosphere; it is usually seen on TV during the weather forecast. The UVI is a form of

warning to mankind to protect oneself against such a radiation effect. The values range from zero to ten and above, indicating the strength of UV radiation. These values depend on the geographical region and time of day [6]. In many places, the UVI is very high around midday and it is required that one must be protected from the effects of the sun. When the UVI is less than three, a person may be free from these harmful effects, but anything above this calls for protection.

The effects of UV radiation on the biosphere lead to issues such as sunburn, skin cancer and eye cataracts. Sunscreens, hats and sunglasses are used together for maximum protection from UV radiation. Issues with regards to these protection systems include the correct amount of sunscreen protection, known as the Sun Protection Factor (SPF), in the solutions that are applied. The values differ from skin to skin and from person to person. A common practice amongst some fair skinned people is to expose themselves to UV radiation in order to pigment their skin. Overexposure may lead to erythema and premature aging, which may be followed by skin cancer and eye cataracts [7]. Snow, white sand, water and any similar substances increase one's UV exposure by reflection and this is not good for one's eyes.

However, UV radiation effects are beneficial to humankind well being in terms of the activation of vitamin D, the most important of sun energy and stimulation of photosynthesis [8]. Sterilization of water and the removal of micro-organisms from foods and in the pasteurization process require the use of UV radiation. Such radiation is used in modern refrigeration to keep food and air free of micro-organisms during long storage, giving them longer life. In biotechnology, UV radiation is used in the synthesis of vitamins D_2 and D_3. In addition, UV flytraps are used to control pests, killing them through shock once attracted to the light.

UV detection has been achieved by photomultiplier tubes (PMT), thermal detectors, and charged-coupled devices (CCD). PMT displays high gain and low noise and can reduce the infiltration of low energy photons, but these are large fragile instruments that require much power. Thermal detectors such as pyrometers and bolometers are used in the calibration processes of UV detectors, but are slow and their response is wavelength independent. Semiconductor photodiodes and CCDs are narrow bandgap solid-state devices that require

moderate bias. As solid-state devices, photodetectors are small, lightweight and insensitive to magnetic fields. Their low-cost, good linearity and sensibility, and capability of high-speed operation make them suitable for UV detection. Si, GaAs, and GaP have been used in the fabrication of UV detectors [9]. These materials are suitable for devices operating in the visible and infrared sections of the electromagnetic radiation. UV detectors made from these materials need filters to stop interference of low energy radiation.

The most common semiconductor UV enhanced devices are made of Si, displaying some limitations due to the narrow and indirect bandgap of Si. Si-based UV photodiodes have been made as p-n junction photodiodes and charge inversion photodiodes. In p-n-junction UV photodiodes, the junction is typically situated at a depth of 0.2 μm and the devices are coated with a SiO_2 surface layer, acting as surface passivation and anti-reflection coating [10]. The charge inversion photodiodes are similar to metal-oxide semiconductor structures designed for field effect transistors. Photodetection occurs as a result of the presence of the electric field at the Si/SiO_2 interface. This is the region of high UV radiation absorption and requires control of the surface recombination at the Si/SiO_2 interface, which is very critical for the performance of the device. Si, GaP, CsI and GaAs-based UV detectors suffer radiation aging, as their bandgap is far lower than the UV photon energies.

Diamond, SiC, GaN and ZnO are wide bandgap (WBG) semiconductors suitable for the fabrication of UV detectors [11]. The wide bandgap is itself an important advantage for UV detectors because it enables room-temperature operation and provides important intrinsic visible blindness. Thermal conductivity of the wide bandgap materials is very high compared to that of Si, which renders devices suitable to operate in high temperature and high power environments. Electron velocities of the WBG semiconductors are lower than those of conventional semiconductors, but at high electric fields, these become larger. A further interesting feature of WBG semiconductors for operation in the lower wavelengths of the electromagnetic spectrum is the ability to display negative electron affinity [12], which makes electrons readily available when the semiconductor interacts with appropriate photon energies. In this thesis, GaN-based materials are used in the study of ultraviolet detectors.

1.2 Aims of the study

In this work, the focus falls on the optimization of Schottky diodes suitable for use as UV detectors on GaN-based semiconductors. The performance of metal contacts on semiconductors depends on the quality of the surface prior to metallization, the chemicals used in preparing the surface, the morphology of the surface, the adhesion of the metal to the semiconductor, reproducibility, resistance to radiation damage and thermal stability. The aims of the study were to establish the following:

- Cleaning procedures for GaN for the purpose of metallization.
- GaN for device patterning using wet etch processes.
- Choosing a metal contact with high UV light transmission.
- Fabrication of Schottky barrier UV detectors.
- Setting-up an electro-optical characterization station for the evaluation of the UV detectors.

1.3 Synopsis of the thesis

The focus of this work has been described. This chapter serves as a prelude to the GaN UV detectors and offers the motivation for the study. Chapter 2 consists of the literature review on GaN semiconductors for UV detectors. Chapter 3 presents a theoretical overview of Schottky Barrier diodes, while Chapter 4 contains the experimental details of the research. Chapter 5 furnishes the results of all experiments and Chapter 6 presents the conclusions.

REFERENCES

[1] Razeghi M. and Rogalski A., Journal of Applied Physics **79** (1996) 7433.

[2] Goldberg Y. A., Semiconductor Science and Technology, **14** (1999), R41.

[3] Parish G., PhD Thesis, University of Santa Barbara (2001)

[4] Coulson K. L, Solar and Terrestrial Radiation, Academic Press, New York (1975).

[5] Winkler P. and Trepte S., Gesundhetswesen, Suppl. **66** (2004) S31.

[6] Koepke P., De Backer H., Ericson P., Feister U., Grifoni D., Koskela T., Lehman A., Lityska Z., Oppenrieder A., Staiger H. and Vanicek K., UV Index Photobiology, International Radiation Symposium (2000).

[7] Mackie R. M., Progress in Biophysics and Molecular Biology, **92** (2006) 92.

[8] Schmalwieser A. W. and Schauberger G., ICB2005, Garmisch-Partenkirchen, Germany

[9] Rogalski A., Progress in Quantum Electronics **27** (2003) 59.

[10] Korde R. and Geist J., Applied Optics **26** (1987) 5284.

[11] Monroy E., Omness F. and Calle F., Semiconductor Science and Technology **18** (2003) R33.

[12] Nemanich R. J., English S. L., Hartman J. D., Sowers A. T., Ward B. L., Ade H. and Davies R. F., Applied Surface Science **146** (1999) 287.

CHAPTER 2

GaN-based materials for Ultraviolet Detectors

2.1 Introduction

In this chapter, the basic information about GaN-based materials is presented. The issues that affected the development of GaN are discussed in section 2.2. This is followed by a discussion of the properties and applications of GaN-based materials. Finally, a review of AlGaN photodiodes is done.

2.2 Progressive development of GaN-based materials

GaN is one of the most successful materials used to make optoelectronic devices operating in the blue and ultraviolet region (UV) of the electromagnetic spectrum. Most colours in the visible range have been covered by other semiconductors with Si and GaP containing devices operating in the infrared (IR) region. Since the 1990s, there has been notable growth in the research and development of GaN devices [1]. However, the success of such devices has been limited by material issues such as the presence of high-unintended donor concentrations [2], lack of suitable substrates [3] and growth methods. These issues resulted in dislocation densities as high as 1×10^{10} cm^{-2}, leading to uncontrollable electronic properties in GaN crystals [4,5]. Similarly, AlN and InN suffered in the same manner in their development, and both are useful in bandgap engineering, producing AlGaN and InGaN respectively. In and Al content in GaN can be tailored to select a specific wavelength for device fabrication [6]. InGaN and AlGaN are used to introduce green and UV wavelengths respectively. Figure 2.1 presents a graph of bandgap tuning with Al and In in GaN. SiC, diamond, and ZnO are inserted for comparison.

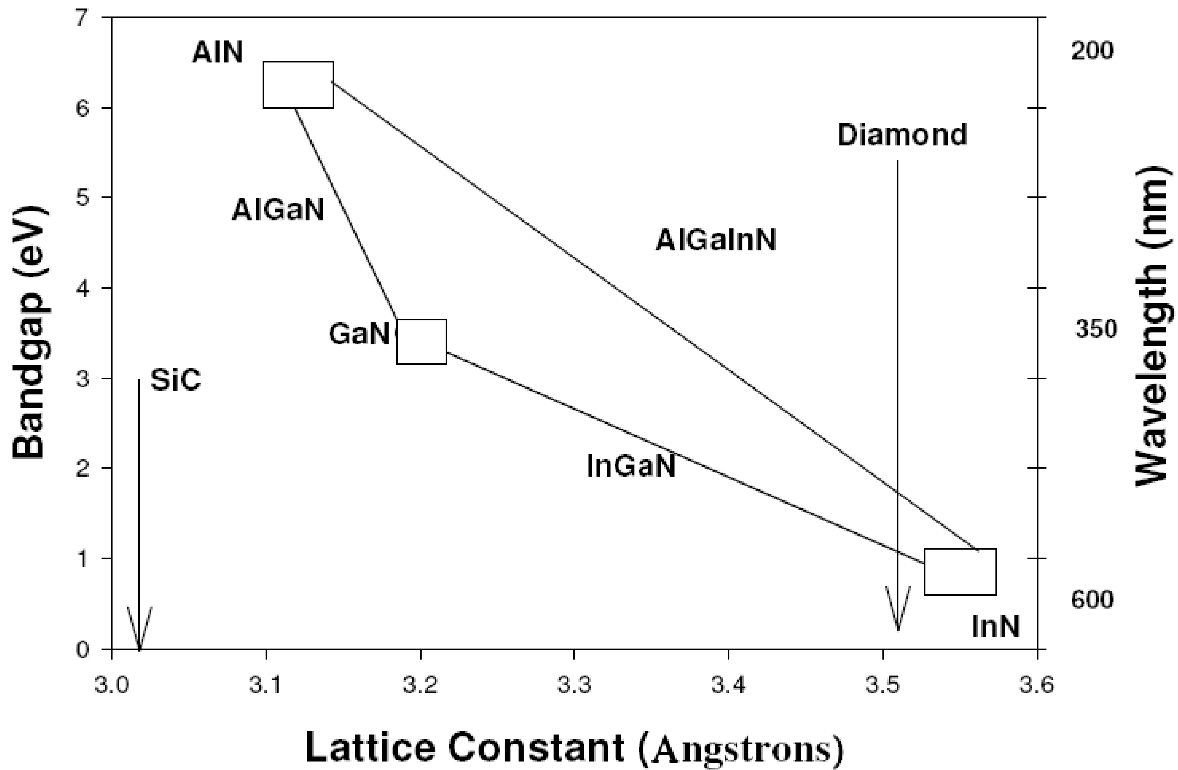

Figure 2.1: Bandgap of GaN-based materials for UV detectors. SiC, ZnO and diamond are inserted for comparison.

2.2.1 Growth methods

In an effort to improve the quality of GaN crystals and reduce dislocation density, several growth methods were used. The growth methods that have been used are vapour phase epitaxy (VPE), which includes both hydride (HVPE) [7] and metal organic vapour phase epitaxy (MOVPE) [8], and molecular beam epitaxy (MBE) [9]. MOVPE is a chemical vapour deposition method, also termed metal organic chemical vapour deposition (MOCVD), organometallic chemical vapour deposition (OMCVD) or organometallic vapour phase epitaxy (OMVPE). This method uses ammonia (NH_3) and trimethyllgallium (TMG) as precursors for nitrogen and gallium, respectively. In the case of other nitrides, trimethyllaluminium (TMAl) and trimethylinduim (TMIn) are used as sources for Al in AlN and In in InN, respectively. The chemical equation for the growth of GaN is given by:

$$Ga(CH_3)_3 + NH_3 \rightarrow GaN + CH_4 \qquad (2.1)$$

The MOCVD method requires a high partial pressure for NH_3 and a high growth temperature, ranging from 1000 to 1100°C. The first step is growing the material at low temperature producing GaN crystallites that covers the substrate. The final film is grown at a higher temperature to control and reduce contamination in the material. GaN is doped with Si or Mg for n-type and p-type doping. In n-type doping, Si is sourced from methyl silane, while in p-type doping Mg is sourced from biscyclopentadithyl. Figure 2.2 shows the growth process of the III-Nitrides. The carrier gas introduces the required element for the growth of GaN and the by products are expelled from the system, with the semiconductor growing onto a substrate.

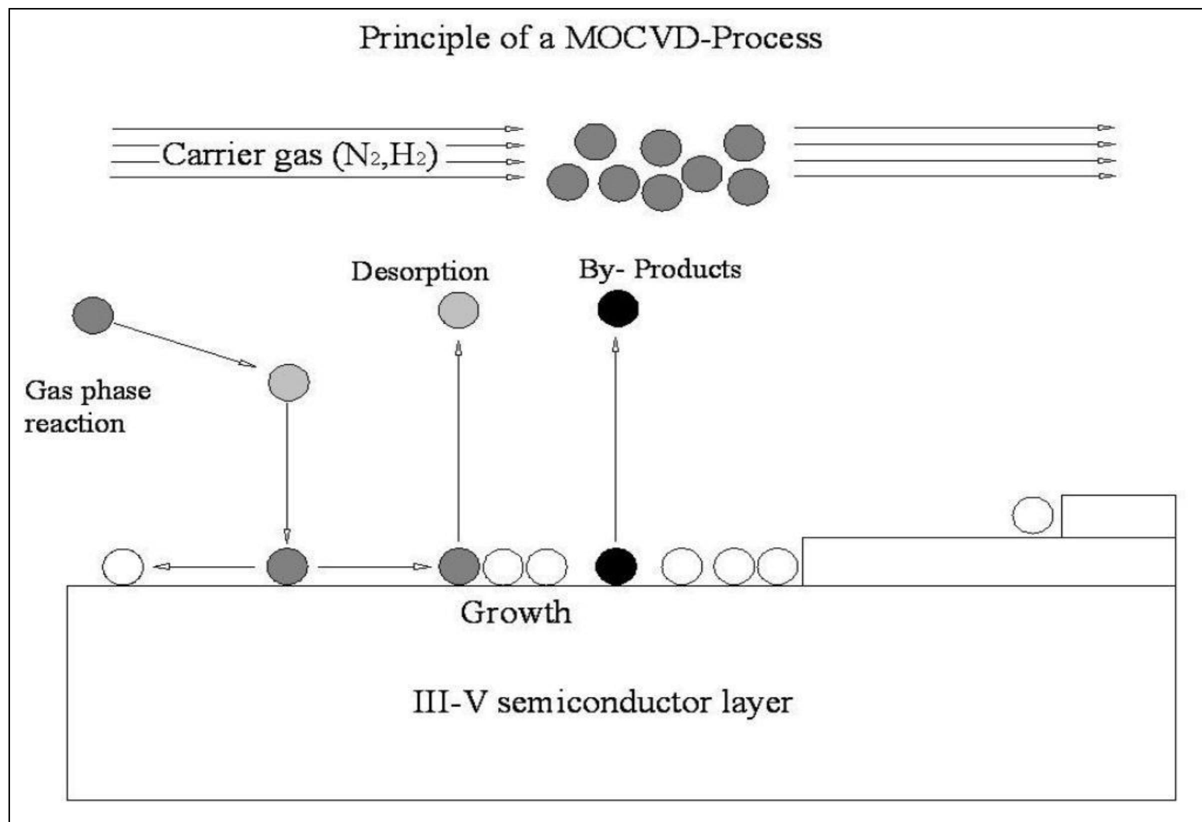

Figure 2.2: MOCVD growth process for III-Nitrides.

MBE is an ultra high vacuum technique for growing semiconductor crystals. High purity Ga is heated in an effusion cell until it evaporates and deposits slowly onto a substrate. Nitrogen atoms are supplied from a plasma source. The growth of GaN is controlled by conditions that allow

atoms of Ga and N to be deposited layer by layer onto a heated substrate. The MBE method operates in an ultra high vacuum chamber to minimize crystal contamination during growth. This method is capable of producing heterostructures with sharp interfaces and of growing zinc-blende structure GaN (normally, GaN is grown in a wurtzite structure). The chamber is also equipped with Si, Mg, In and Al effusion cells for alloying purposes. The disadvantage of the MBE method is the low growth temperature, 700 to 800°C as compared to MOCVD where temperatures are 1000 to 1100°C. GaN is a thermodynamically unstable material in a vacuum and the thin film may decompose into Ga and N in the MBE, when the deposition rate becomes lower than the decomposition rate due to a temperature difference between the chamber and the substrate. The low substrate temperature reduces surface atom mobility, resulting in increased densities of defects [10]. Figure 2.3 shows the schematics of the MBE growth method.

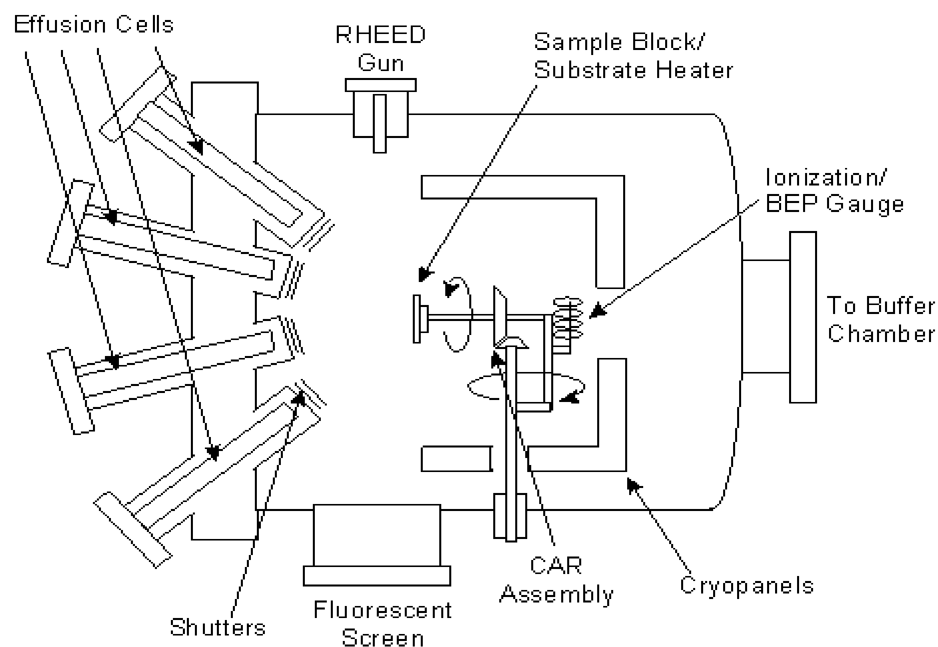

Figure 2.3: MBE growth process for III-Nitrides [11].

2.2.2 Substrates for GaN

In addition to the growth method, the crystal quality of semiconductors depends on the suitability of the substrate. In growing GaN, sapphire (α-Al_2O_3), GaAs, Si, SiC, $LiGaO_2$, $LiAlO_2$ and ZnO have been used as a substrate [3]. The criterion for choosing a suitable substrate is lattices match. In addition, practical properties such as crystal structure, surface finish and composition, chemical, thermal and electrical properties are also considered. Currently, it has become important to study the effects of treatments of a substrate (e.g. heating or chemical processing) prior to the deposition of GaN. For example, it has been shown that wet etching of sapphire prior to the deposition of GaN crystals reduces threading dislocations [12]. α-Al_2O_3 has been extensively used as a substrate for GaN. It has a crystal orientation parallel to GaN c-plane, and the lattice mismatch is about 15 %, leading to a dislocation density of about 10^{10} cm^{-2}. α-Al_2O_3 has a rhombohedral structure and is highly anisotropic. Like GaN, it exhibits extremely high chemical and thermal stability with a melting point of 2040 °C. Its bandgap of 9.1 eV permits excellent optical transmission. Furthermore, the coefficient of the thermal expansion of α-Al_2O_3 is greater than that of GaN, resulting in comprehensive stress in the grown film during cooling. Such stress causes cracks in both GaN and α-Al_2O_3.

A continually improving technique to produce GaN with less threading dislocations is the epitaxial lateral overgrowth (ELOG), considered to be an alternative substrate [13]. Figure 2.4 depicts the schematics of the ELOG substrate. The ELOG technique takes advantage of the large anisotropy of the GaN growth rate in the [0001] direction, controlling dislocations through the patterned substrate such that they do not reach the surface of the final layer as shown in figure 2.4 (D). GaN thin buffer layer is grown on sapphire as a usual practice for GaN growth as shown in figure 2.4 (A). A dielectric material such as SiO_2 or SiN mask is then patterned onto the GaN buffer layer {figure 2.4 (B)}. The thin film is then grown onto the patterned GaN buffer layer {figure 2.4 (C)}. Using MOCVD, ELOG and several of its variations has been shown to significantly reduce the dislocation density of GaN crystals to as low as 10^6 cm^{-3} [14].

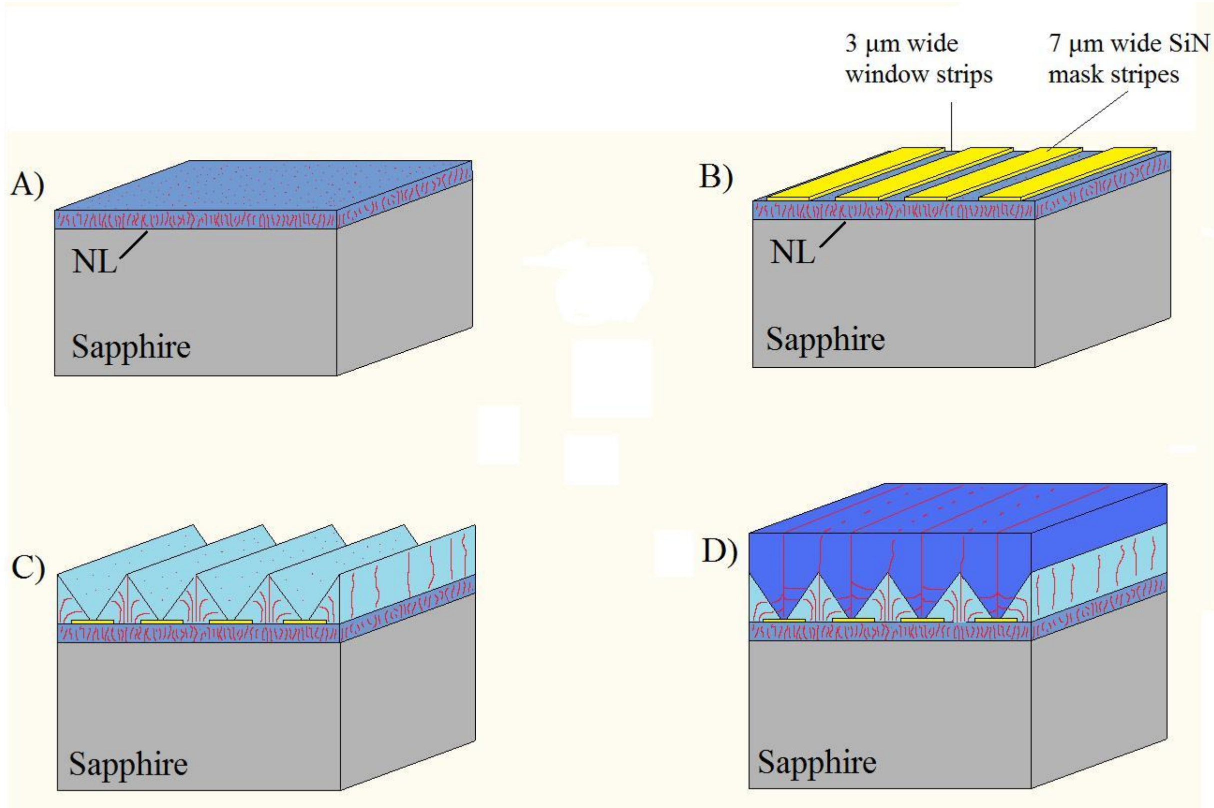

Figure 2.4: Schematic representations of 2 step ELOG for GaN, where NL is the GaN nucleation layer [13].

2.2.3 High n-type Conductivity

The first GaN crystals were observed to possess high n-type conductivity, which was attributed to nitrogen vacancies. This is an unresolved issue in GaN research. Published reports [15,16,17,18] suggest impurities such as Si, C, O, and H as being responsible for n-type conductivity. Park et al. have reported that Si and C are responsible for n-type doping in GaN films [15], where C atoms are acting as compensating acceptors in the crystal, influencing the electron concentration. Van de Walle et al. reported that O, a shallow donor in GaN, is responsible for high background n-type conductivity while Zhang et al. claim that H is responsible for this phenomenon [16,17]. In addition to n-type conductivity, there is a strong presence of parasitic yellow band (YB) luminescence associated with point defects in GaN crystals. Ogino et al. suggested that the YB is a transition that takes place between a shallow donor and a deep accepter level [18]. This suggestion was demonstrated by Saarinen et al. using

positron annihilation spectroscopy, and they concluded that the intensity of YB is directly proportional to the concentration of Ga vacancies [19]. Reynolds et al. have studied the source of yellow luminescence in GaN. They concluded that Ga vacancies, in partnership with the O atom at a nitrogen site, are responsible for point defects producing the YB [20]. More recently, researchers have again suggested that the YB is associated with O impurities in GaN [21]. Related to the impurities discussed above, defects have been studied using Deep Level Transient Spectroscopy (DLTS), which identified vacancies and interstitials in semiconductors. Defects in materials act as electron and hole traps, affecting the current transport in devices. In HVPE grown GaN, three electron traps have been shown by DLTS: E1, E2 and E3 with activation energies 0.264, 0.580 and 0.665 eV [22], with E1 and E2 appearing in concentrations above 2 X 10^{13}cm^{-3} in MOVPE [23]. Auret et. al. have also reported two electron traps, E_c - 0.23 eV and E_c - 0.58 eV, in non-intentionally doped MOVPE GaN with activation energies 0.27 and 0.61 eV [24].

2.2.4 Doping of GaN

Doping of GaN plays a crucial role in the performance of devices as it alters GaN's electrical properties by enhancing its conductivity. Using Si in n-type doping of GaN, a carrier density as high as 2.2 x 10^{19} cm^{-3} and a Hall mobility of 287 cm^2/Vs have been recorded [25]. In addition, Si doping has led to a reduction of threading dislocation density in GaN, through the formation of SiN, which stops the propagation of edge dislocation from reaching the surface of the crystal.]. In the case of p-type doping, group II elements like Mg, Be, Ca, Zn, and a combination of Mg and Be have been used. Mg doping is the most efficient, allowing the production of semi-insulating p-type crystals. The highest carrier density in Mg doped GaN has been recorded as 8 x 10^{18} cm^{-3} with the correspondingly low resistivity of 0.8 Ω cm. For p-GaN growth with Ga-polarity, the incorporation of Mg has a tendency to introduce stacking faults, thus inverting the polarity to N-face, and reducing threading dislocation from reaching the surface [26]. These are also defects introduced into the material which exert adverse effects on the performance of devices.

2.2.5 Effects of defects in GaN devices

GaN, like all semiconductors, contains defects due to growth conditions, method of growth, doping, and the substrate used. Dislocations are observed directly from the substrate where the growth begins from a low temperature nucleation layer. Growth processes with both the continuous nucleation layer and the one formed by isolated islands end with vertical threading dislocations. Dislocations in GaN are identified as edge-type, screw type and mixed character type. All these defects influence device performance, including the different types of photodiodes. GaN photodiodes are characterized by high gain, long response time and a responsivity that is dependent on frequency and optical power. Gain is defined as the ratio of the excess–carrier recombination lifetime and the electron transit time across the diode. Since electrons have very high mobility in GaN, high gain will be affected by a long stay of carriers in traps, reducing the probability of recombination. High gain thus occurs at the expense of the long response time of minority carriers. Published works have attributed the mechanism of the long response times and high gain in n-type GaN photoconductors to acceptor levels trapping the photogenerated holes [27, 28, 29]. Traps in the semiconductor material occur as a result of both point defects and dislocations. Hole traps can be reduced by altering the growth conditions for GaN-based materials, and this has proved to have an effect on the photoresponse [30]. Leakage currents in photodiodes consist of the dark current at the reverse bias and have different sources. Surface leakage currents result from surface states and tunneling induced near the surface, and is reduced by surface chemical treatments including passivation. Passivation is responsible for tying up dangling bonds and thus reduces the density of surface states. Reduced leakage currents have been reported in devices grown on ELOG GaN p-n structures and Schottky photodiodes, which are characterized by reduced threading dislocation densities [31]. Low leakage current improves the response time and sharpness of the cut-off wavelength in ELOG GaN [32].

2.3 Properties of GaN-based materials

GaN, with its famous nitride family, AlN and InN, are wide band gap semiconductors that occur in both zincblende and wurtzite structures. Figure 2.5 shows the schematics of GaN wurtzite structure, showing the Ga-face and the n-face. In wurtzite form, the direct band gap of GaN is recorded at 3.5 eV while that of AlN is 6.23 eV [33]. The bandgap of InN was recorded earlier as 1.9 to 2.05 eV [34] while more recently, a new band gap of 0.7 to 1.0 eV [35] was recorded. In cubic form the bandgaps of GaN and AlN are direct while that of InN is indirect [36]. Alloying GaN with InN and AlN allows for the tuning of band gaps and emission wavelengths. AlGaN is suitable for the fabrication of UV solar-blind detectors. By varying the Al content, the responsivity cut-off wavelength can be varied from 280 nm [37] to as low as 240 nm [38].

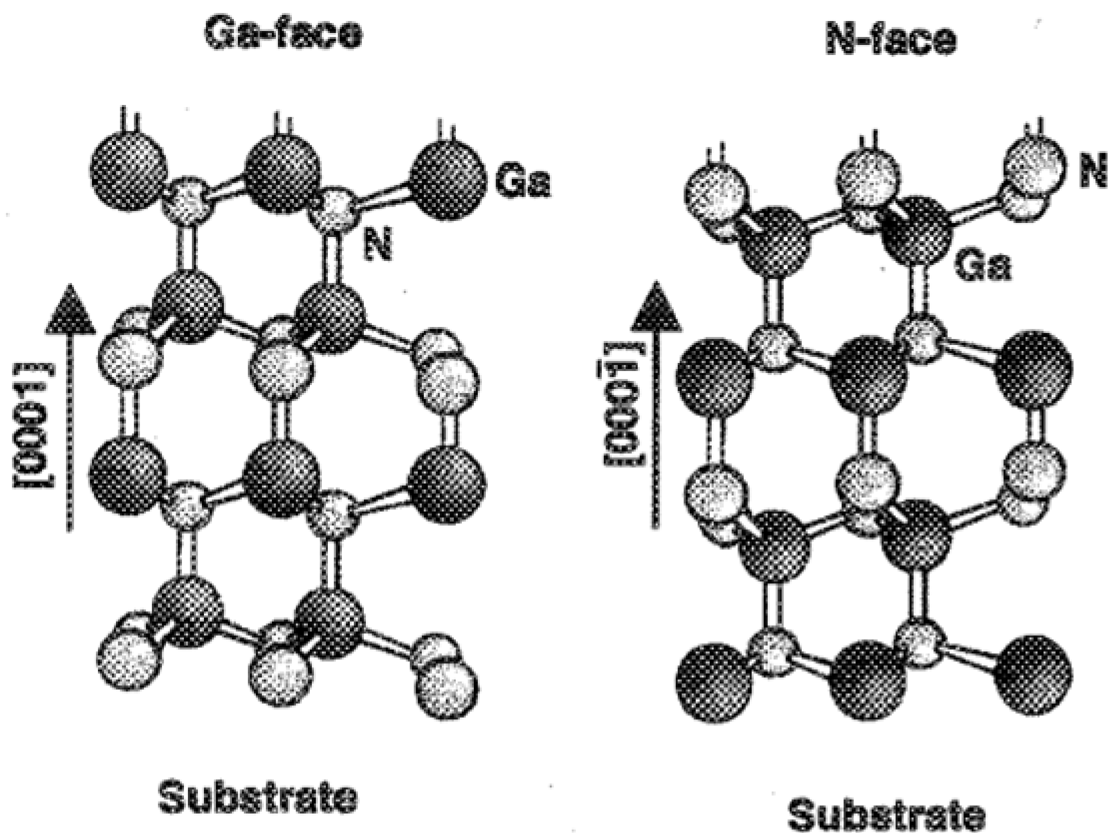

Figure 2.5: Schematic representations of wurtzite GaN, where Ga-face and N-face are indicated by opposite directions [39].

GaN based materials possess excellent transport properties suitable for high power, high temperature and high frequency devices. The electron saturation velocity of GaN is 2.5×10^7 cm.s^{-1} at a field 10^5 Vcm^{-1} [40]. The electron mobility of epitaxial GaN has been recorded at 1000 cm^{2}V^{-1}s^{-1} for epitaxial layers [41,42]. The value of low temperature mobility in doped GaN is recorded above 7000 cm^{2}V^{-1}s^{-1} [43]. GaN based materials have high breakdown fields of up to 5×10^6 V^{-1}cm^{-1} [44]. SiC is one wide bandgap semiconductor that possesses a higher thermal conductivity than GaN, which makes it superior to GaN for high temperature devices. However, GaN, with a thermal conductivity greater than 2.1 Wcm^{-1}°C^{-1}, enjoys the direct bandgap advantage [45].

The wurtzite (hexagonal) structure GaN based materials are grown along the [0001] direction while the zincblende (cubic) crystals are grown along the [1111] direction, as shown in figure 2.5. These are polar axes, which cause GaN-based semiconductors to contain strong lattice polarization effects. Large spontaneous polarization is suitable for applications in high temperature piezoelectronics and in pyroelectronic sensors. Properties such as piezoelectricity and pyroelectricity are important elements in detector technology. Piezoelectric semiconductors are able to generate electric potentials in response to applied mechanical stress, while pyroelectric materials are capable of generating electric charges in response to heat flow. When heat is applied it changes the temperature of the material by means of thermal convection, diffusion or radiation. GaN and AlN are believed to contain some spontaneous polarization, leading to high piezoelectric constants, which furthermore leads to high piezoelectric polarization in strained films [46].

The pyroelectric response in GaN-based materials results from the piezoelectric effects of temperature-induced strain. There exists a primary piezoelectric effect, which is dominant during fast heat transfer such as the immersion of a device in a medium with high flow velocity. In such a medium, a GaN-based sensor generates a response voltage that is proportional to heat flow. For example, there is a difference in the thermal expansion coefficients of the substrate and the pyroelectric material produces strain in response to temperature changes owing to the applied strain (piezoelectric strain), which in turn generates an electric charge [47]. It has been shown that the pyroelectric voltage coefficient in GaN can be as high as 7×10^5 V/m-K [48] and is

higher than that of the best-known high temperature pyroelectric material, $LiTaO_3$, whose pyroelectric voltage is 5 x 10^5 V/m-K [49]. In GaN based materials, strong polarization effects result from piezoelectric polarization, which depends on the lattice strain and spontaneous polarization. Spontaneous polarization exerts a strong influence on the electrical properties of heterostructures such as the electron density. Spontaneous polarization arises as a result of large ionicity associated with covalent metal nitrogen bonds and low symmetry in wurtzite material. It also causes an unstable electric field that may decrease or increase the interfacial carrier concentration. In heterostructures where strain is present, the polarization charge is inextricably connected to the present free carriers in the semiconductor. The magnitude of this charge is measured by converting it to the number of electrons: it can be in the mid 10^{13} cm^{-2} level for AlN/GaN interfaces [46]. This is very high compared to AlAs/GaAs heterostructures, where the number of electrons is less than 10% of that of the AlN/GaN structure. AlGaN/GaN devices, in particular, high-electron-mobility-transistor (HEMT), have an extremely large charge density as a result of the two dimensional electron gas (2DEG) formed at the AlGaN/GaN interface, occurring even without doping in the AlGaN. Figure 2.6 shows the energy band of a basic HEMT, indicating the position of 2DEG. Table 2.1 furnishes a summary of some of the properties of III-nitride semiconductors.

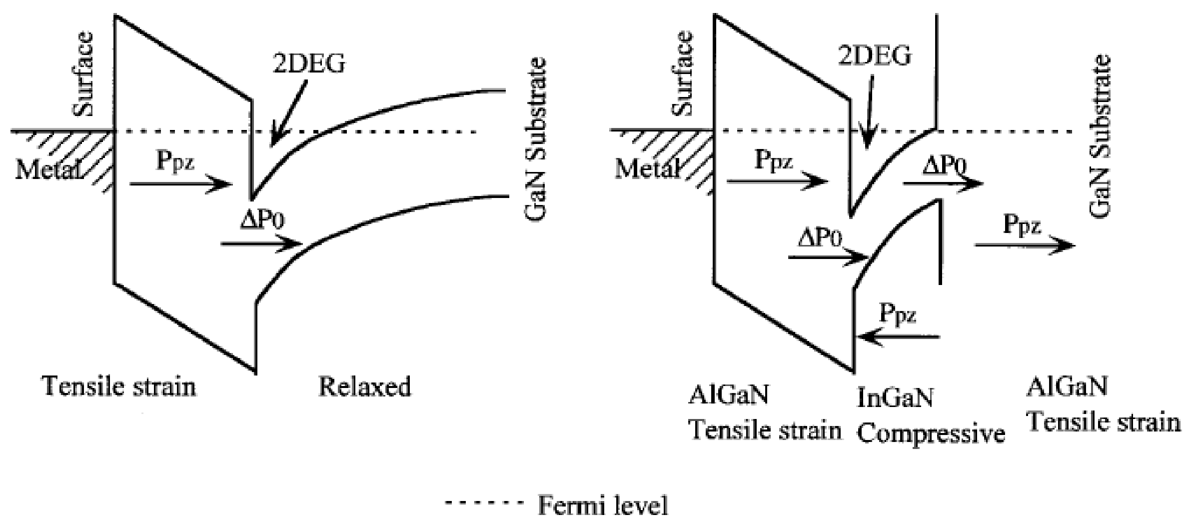

Figure 2.6: AlGaN/GaN structure showing the 2DEG caused by spontaneous and piezoelectric polarization [50].

Table 2.1: Properties of Wurtzite III-Nitrides Semiconductors.

Property	**Units**	**AlN**	**GaN**	**InN**
Crystal Type		Wurtzite	Wurtzite	Wurtzite
Energy Band Gap	eV	6.2	3.39	1.89
Electron Mobility	cm^2/Vs	135	1000 (bulk)	1100
Hole Mobility	cm^2/Vs	15	30	10
Breakdown Fields	V/cm	1.4×10^5	$>5 \times 10^6$	1.4×10^5
Saturation Velocity	cm/s	1.4×10^7	2.5×10^7	2.5×10^5
Thermal Conductivity	W/cmK	2	1.5	6.4×10^{-5}
Lattice Constant, *a*	Å	3.11	3.19	3.54
Lattice Constant, c	Å	4.98	5.18	5.76

2.4 Applications of GaN-based materials.

III-nitrides are suitable semiconductor materials for use in optoelectronic devices, as both emitters and detectors. They can also be used to fabricate high power and high temperature electronic devices [51]. The allowed energy bandgaps of these materials are suitable for band-to-band light generation with colours ranging from potentially red to UV wavelengths, rendering them an advantageous addition to the already existing semiconductor systems for colour displays. It has been demonstrated that nitrides can be used as Bragg reflectors [52], UV detectors [53], UV and visible light emitting diodes (LEDs) for applications in flat panel displays, lighting and indicator lights on devices, advertisements and traffic signals [54]. As coherent sources, lasers are important for high-density optical read-write technologies [55]. The diffraction-limited optical storage density increases approximately quadratically as the probe

laser wavelength is reduced, making the GaN-based materials suitable for coherent sources at lower wavelengths of the electromagnetic radiation. Optical storage enables the storage and retrieval of data in vast quantities. Medical applications of UV LEDs and lasers include surgery [56], phototherapy of neonatal jaundice [57], photodynamic therapy [30], photo-polymerization of dental composites [30], phototherapy of seasonal affective disorder [30], and sterilization [58]. When used in surgery, UV lasers are seen as most suitable due to the fact that UV can sterilize. In photosynthesis, the high brightness LEDs are suitable for the growing of plants and for photo bioreactors [59]. Finally, the LEDs and laser diodes (LDs) are suitable for use in optical measurements such as time domain and frequency domain spectroscopy [60]. Furthermore, exposure to UV-B radiation causes skin cancer to fair skinned people. The use of AlGaN ultraviolet detectors will help prevent such disease, where a handheld device will be able to communicate to user how much ultraviolet radiation was absorbed.

There is great concern all over the world about the contribution of uncontrolled effluents to global warming which is an unexpected change in climate. The effluents stem from aerosols, car fumes, industries and wild fires, and add to the concentration of CO_2 in the atmosphere. When installed in jet engines, cars and furnaces, the UV detectors would monitor and control contaminants for a cleaner environment. In addition, UV detectors operating in the solar-blind region of the electromagnetic spectrum, when made from GaN-based materials, record a high detectivity and are useful in the detection of UV-C (280 nm to 10 nm) and UV-B (320 nm to 280 nm) [61]. UV-C and UV-B are not detectable naturally because the ozone layer is a natural UV filter for all radiation less than 280 nm [35]. It has been observed that power lines emit UV-C radiation as a result of ionization of nitrogen around them.

2.5 Al_xGaN_{1-x} photodetectors

Since the first GaN UV photoconductive photodiode reported by Khan in 1992 [62], all types of photodiode structures have been developed. These are linked directly with the advancement of GaN and AlGaN growth, progress in p-type doping and the improvement of both ohmic and Schottky contact technology. The first developments were focused on the fabrication of visible-blind and solar-blind UV detectors in which the Al mole fraction plays a crucial role in determining the detection band edge [63]. The next stages of development of the photodiodes were focused on the advancement of detector parameters: high responsivity [64], high quantum efficiency [65], high detectivity [66], and UV imaging using focal plane arrays [67]. Photoconductive photodiodes [68], p-n junctions [24], metal-semiconductor-metal (MSM) [69] and Schottky barrier (SB) diodes [55] have already been reported. The success of Schottky barrier photodetectors depends on the structure of both the metallization and the AlGaN used for fabrication. Khan et al. reported the first high quality UV Schottky photodetectors. They used the Cr/Au metal system for the preparation of the ohmic contacts and Ti/Au for Schottky barriers. The spectral responsivity of these detectors reached a maximum value at 365 nm. Miyake et. al. used a Ti/Al structure for the fabrication of ohmic contacts and Ni/Au for Schottky contacts. The transmittance of the Ni/Au electrode in the near UV and VUV region was up to 60 %. The responsivity of the AlGaN detector operating in the UV-VUV wavelength range was found to be 100-265 nm [53].

In recent advances, Tut et. al. demonstrated solar-blind photodetectors with low noise, high detectivity and high quantum efficiency [70]. The AlGaN epitaxial layers were grown on sapphire substrate using MOCVD. A thin nucleation layer of AlN was first deposited on sapphire, to control the cracking of AlGaN. Unintentionally doped GaN mesa isolation with 0.5 µm thickness was grown onto AlN. This was followed by the deposition of a highly doped (2 x $10^{18}cm^{-3}$; 0.6 µm) GaN ohmic contact layer. The diffusion barrier, expected to increase the solar blindness of the photodetector, was deposited as a layer of 0.2 µm n-AlGaN. The growth of the Schottky heterostructure was completed with the deposition of a 0.8 µm undoped AlGaN active layer. Ti/Al (100 Å/ 1000 Å) ohmic contacts were deposited onto the highly doped GaN since it was difficult to produce high quality ohmic contacts onto AlGaN. Au Schottky contacts of 100 Å

were deposited onto the active layer. The photodiodes exhibited a low leakage current: less than 3 fA and 10 fA for reverse bias voltages of 12 V and 17 V respectively. The spectral response of solar blind photodetectors was measured at the 250 - 400 nm spectral range. When the applied voltage increased from 5 V to 20 V, the peak responsivity increased from 61 mA/W at 250 nm to 147 mA/W at 256 nm. The responsivity reached saturation for voltages greater than 20 V, indicating a total depletion of the undoped AlGaN absorption layer. A cut-off wavelength of the diodes was reached at 267 nm, which ensures the true solar blindness operation of the diodes. The zero-bias (photovoltaic) quantum efficiency was very low. A maximum quantum efficiency of 71% was measured at 256 nm under 20 V reverse bias.

2.6 Ohmic contacts on AlGaN/GaN

Early studies of ohmic contacts on GaN used Al and Au metallization, which yielded specific contact resistivities in the range of 10^{-4} and 10^{-3} Ωcm [71]. Addition of Ti/Au to Ti/Al improved the specific contact resistivity to 10^{-6} Ωcm [72]. In taking the Ti/Al metal structure further, Wu et al. confirmed that Ti/Al functions very effectively, except at a high annealing temperature [73]. It was realized that at such temperatures, Al melts and tends to form balls on the surface of GaN, increasing the surface's roughness. Rough surfaces are detrimental to the performance of a device because they cause an increase in contact resistivity. As a follow-up on the Ti/Al structure, Fan et al. designed a multilayer ohmic contact, using Ti/Al/Ni/Au (150 Å/2200 Å /400 Å /500 Å) [74]. The measured ohmic contact resistivities were 1.19×10^{-7} and 8.9×10^{-8} Ωcm, respectively. Ti was introduced due to its capability to form a reactive interface with GaN; annealing the metal enhances the formation of TiN as a result of the reaction with GaN. Lack of N from GaN increases the electron concentration through the formation of the N vacancy. Al passivates the GaN surface, while forming a Ti/Al metal layer. It has also been observed that the ratio of Al to Ti in nitrides has an influence on the specific contact resistance. Ti is capable of forming TiN during annealing, which makes the surface highly reactive. During annealing, metallic Ga from GaN has a tendency to diffuse through the metal contact. Al is then used to prevent out-diffusion of Ga to the surface. Thus the Ti/Al system is enough to produce good ohmic contacts as a result of their capability to form thin AlN, TiN and AlTiN at the interface. In addition, it was found that the Ti/Al structure reduces the

contact resistance by varying conditions such as the annealing and ambient temperature. A Ti/Al/Ni/Au structure has been successfully used in optimizing the specific contact resistance.

Similar metal combinations have been used to make ohmic contacts on AlGaN, with Ti/Al structures being kept as basic [75]. Ti/Al/Ti/Au (200 Å, 1000 Å, 450 Å, 600 Å) combinations were reported, with a Ti layer deposited onto AlGaN, thus enhancing adhesion to the semiconductor. It was also found the reaction of Ti with residual surface oxide to form TiO_2 is beneficial to the device being fabricated. TiO_2 has a bandgap of 3.05 eV, which is smaller than the GaN bandgap (3.5 eV). The TiO_2 bandgap compared to other surface oxides on AlGaN, Ga_2O_3 (bandgap 4.4 eV), and Al_2O_3 (bandgap of 8.8 eV) reduces surface states. Using Ti alone for ohmic contact formation would require annealing temperatures as high as 900°C via TiN formation. The interaction of Al with N in AlGaN occurs at lower temperatures than the TiN formation; hence an ohmic contact is formed by Ti/Al/Ti combinations, when Al diffuses through the surface Ti layer. Au is used to protect oxidation of surface metal, whether it is Ti or diffused Al. Hence, Ti/Al/Ti/Au combinations are used with modifications to the second Ti layer replaced by Mo, Ni, and Pt [76]. All these combinations are regarded as reducing contact resistivity.

REFERENCES

[1] Compound Semiconductor, March 2005, p12.

[2] Maruska H. P. and Tietjen J. J., The preparation and properties of vapor-deposited single-crystalline GaN, Applied Physics Letters **15** (1969) 329.

[3] Liu L. and Edgar J. H., Substrates for gallium nitride epitaxy, Material Science and Engineering **R37** (2002) 61.

[4] Lester S. D.,Ponce F. A., Craford M. M. G., Steigerwald D. A., High dislocation densities in high efficiency GaN-based light-emitting diodes, Applied Physics Letters **66** (1995) 1249.

[5] Ponce F. A., Cherns D., Young W. T.and Steeds J. W., Characterization of dislocations in GaN by transmission electron diffraction and microscopy techniques, Applied Physics Letters **69** (1996) 770.

[6] Mohammad S. N., Salvador A. A. and Morkoc H., Emerging gallium nitride based devices, Proceeding IEEE **83** (1995) 1306.

[7] Morkoc H., Comprehensive characterization of hydride VPE grown GaN layers and templates, Material Science Engineering **R33** (2001) 135.

[8] Uchida K., Watanabe A., Yano F., Kouguchi M., Tanaka T. and Minagawa S., Nitridation of sapphire substrate surface and its effects on the growth of GaN, Applied Physics Letters **79** (1996) 3487.

[9] Waltereit P. and Brandt O., Influence of AlN nucleation layers on growth mode and strain relief of GaN grown on 6H-SiC(0001) Applied Physics Letters **74** (1999) 3660.

[10] Rubin M and Weber E, US Patent # IB 1290

[11] http://projects.ece.utexas.edu/ece/mrc/groups/street_mbe/mbechapter.html

[12] Wang J., Guo L. W., Jia H. Q., Xing Z. G., Wang Y., Chen H. and Zhou J. M., Lateral epitaxial overgrowth of GaN films on patterned sapphire substrates fabricated by wet chemical etching, Thin Solid Films **515** (2006) 1727.

[13] Gibart P., Metal Organic Vapour Phase Epitaxy of GaN and Lateral Overgrowth, Progress Reports Physics **67** (2004) 667.

[14] Lee I-H, Polyakov A. Y, Smirnov N. B., Govorkov A. V, Markov A. V., Pearton S. J., Deep-level studies in GaN layers grown by epitaxial lateral overgrowth, Thin Solid Films **516** (2008) 2035.

[15] Park S-E., Han W. S., Lee H. G. and Byungsung O., Effects of native defects on electrical and optical properties of undoped polycrystalline GaN, Journal of Crystal Growth **253** (2003) 107.

[16] Van de Walle C. G., Stampfl C. and Neugebauer J., Deep level related yellow luminiscence in p-GaN grown by MBE, Journal of Crystal Growth **189/190** (1998) 505.

[17] Zhang J-P., Sun D-Z., Wang X-L., Kong M-Y. Zeng Y-P., Li J-M. and Lin L-Y., Hydrogen contaminants and its correlation with background electrons in GaN, Semiconductor Science Technology **14** (1999) 403.

[18] Ogino T and Aoki M,Mechanisms of yellow luminescence in GaN, Japanese Journal Physics. (Japan), **19** (1980) 2395.

[19] Saarinen K, Observations of native Ga vacancies by positron annihilation, Physical Review Letters **79** (1997) 3030.

[20] Reynolds D. C., Look D. C., Jogai B., Van Nostrand J. E., Jones R. and Jenny J., Sources of yellow luminescence in GaN grown by gas–source molecular beam epitaxy and the green luminescence band in sigle crystals ZnO, Solid State Communication. 1**06** (1998) 701.

[21] Nyk M., Jablonski J. M., Strek W. and Misiewicz J., Yellow emission of GaN nanocrystals embedded in silica xerogel matrix, Optical Material **26** (2004) 133.

[22] Hacke P., Detchprohm T.,Hiramatsu K., Sawaki N., Tadatomo K. and Miyake K., Degradation mechanisms in AlGaN/InGaN/GaN light sources, Applied Physics Letters **76** (1994) 304.

[23] Hacke P., Nakayama H., Detchprohm T.,Hiramatsu K. and Sawaki N. Deep levels in upper band-gap region of lightly Mg-doped GaN, Applied Physics Letters **68** (1996) 1362.

[24] Auret F. D., Goodman S. A., Koschnick F. K., Spaeth J.-M, Beaumont B. and Gibart P, Proton bombardment induced electron traps in epitaxialy grown n-GaN, Applied Physics Letters **74**, (1999) 407

[25] Eiting C. J., Grudowski P. A. and Dupuis R. D.P- and N-type doping of GaN and AlGaN epitaxial layers grown by metalorganic chemical vapour deposition, Journal of Electronic Material. **27** (1998) 206.

[26] Calleja E., **Sanchez**-Garcia M. A., Calle F., Naranjo F. B., Munoz E., Jahn U., Ploog K., Calleja J. M., Sarinen K. and Hautojarvi P., Molecular beam epitaxy growth and doping of III-nitrides on Si(111): layer morphology and doping efficiency, Material Science and Enginering **B82** (2001) 2.

[27] Binet F., Duboz J.Y., Rosencher E., Scholz F., and Hãrle V., Mechanisms of recombinations in GaN photodetectors, Applied Physics Letters **69** (1996) 1202.

[28] Huang Z.C., Mott D.B., Shu P.K., Zhang R., Chen J.C., and Wickenden D.K., Optical quenching of photoconductivity in GaN photoconductors, Applied Physics Letters **82** (1997) 2707.

[29] Monroy E., Garrido J.A, Muñoz E., Izpura I., Sánchez F.J., Sánchez-García M.A., Calleja E., Beaumont B., and Gibart P., High performance GaN p-n junctions photodetectors for solar ultraviolet applications, Semiconductor Science and Technology **13** (1998) 1042.

[30] Huang Z.C., Mott D.B., Shu P.K., Chen J.C., and Wickenden D.K., Improvement of metal-semiconductor-metal GaN photodetectors, Journal of Electronic Material **26** (1997) 330.

[31] Kozodoy P., Ibbetson J.P., Marchand H., Fini P.T., Keller S., Speck J.S., DenBaars S.P, and. Mishra U.K, Electrical characterization of GaN p-n junctions with and without p-n junctions, Applied Physics Letters **73,** (1998) 975.

[32] Parish G., Keller S., Kozodoy P., Ibbetson J. P., Marchand, H., Fini P. T, Fleischer S.B., DenBaars S. P., Mishra U. K. and Tarsa E.J., High performance (Al,Ga)N-based solar-blind ultraviolet p-i-n detectors on laterally overgrown GaN, Applied Physics Letters **75** (1999) 247.

[33] Vurgaftman I., Meyer J. R. and Ram-Mohan L. R. J., Band parameters for III-V semicobnductors and their alloys, Applied Physics Letters **89** (2001) 5815.

[34] Davvydov V. Y., Klochikin A. A., Emstev V. V., Kurdyukov D. A., Ivanov S. V., Vekshin V. A., Bechstedt F., Furthmuller J., Aderhold J., Graul J., Mufrui A. V., Harima H.,

Hashimoto A., Yamomoto A., Haller E. E., Bandgap of hexagonal InN and InGaN alloys, Physica Status Solidi (b) **234** (2002) 787.

[35] Levinshtein M. E., Rumyantsev S. L., and Shur M. S., Editors "Properties of advanced Semiconductor Materials: GaN, AlN, InN, BN, SiC, and SiGe",John Wiley and Sons, New York (2001).

[36] Davvydov V. Y., Klochikin A. A., Seisyan R. P., Emstev V. V., Ivanov S. V., Bechstedt F., Furthmuller J., Harima H., Mudryi A. V., Aderhold J., Semchinova O., and Graul J., Absorption and emission of hexagonal InN: Ebidence of narrow fundamental bandgap, Physica Status Solidi (b) **229** (2002) R1.

[37] Tut T., Butun B., Gokkavas M., Ozbay E, Solar-blind AlxGa1-xN-based avalanche photodiodes, Applied Physics Letters **87** (2005) 223502.

[38] Monroy E., Calle F., Munoz E., Omnes F. Gibart P. and Munoz J. A., Applied Physics Letters **73** (1999) 1171

[39] Ambercher O., Smart J., Shealy J. R., Wemann N. G., Chu K., Murphy M., Schaff W. J., Eastman L. F., Dimitrov R., Wittmer L., Stutzmann M., Rieger W. and Hilsenbeck J., Journal Applied Physics **85** (1999) 3222.

[40] Albrecht J. D., Wang R. P., Ruden P. P., Farahmand M. and Brennan K. F., Electron transport characteristics of GaN for high temperature device modeling, Journal of Applied Physics **83** (1998) 4777.

[41] Heying B., Smorchkova I., Poblenz C., Elsass C., Fini, B. Denbaars S., Mishra U. and Speck J. S., Optimization of surface morphologies and electron mobilities in GaN by plasma-assisted molecular beam epitaxy, Applied Physics Letters **77** (2000) 2885.

[42] Ambacher O., Smart J., Shealy J. R., Wenmann N. G., Chu K., Murphy M., Schaff W. J., Eastman L. F., Dimitrov, R., Wittmer L., Stutzman M., Rieger W. and Hilsenbeck J., Two-dimensional electron gases induced by spontaneous and piezoelectric polarization charges in N- and Ga-phase AlGaN/GaN, Journal of Applied Physics **85** (1999) 3222.

[43] Morkoc H., Cingolani R., Lampbrecht W., Gil B., Jiang H-X, Lin J., Pavlidis D. and Shenai K., Material properties of GaN in the context of electronic devices, MRS Internet Journal Nitride Semiconductors **R 4S1** (1999) G1.2.

[44] Harima H., Properties of GaN and related compounds studied by means of Raman scattering, Journal of Physics: Condense Matter **14** (2002) R967.

[45] Florescu D. I., Asnin V. M. and Pollak F. H., Thermal conductivity measurements of GaN and AlN, Compound Semiconductor **7** (2001) 62.

[46] Bernardini F., Fiorentini V., and Vanderbilt D., Photoluminiscence in n-doped In0.1Ga0.9N/In0.01Ga.099N multiple quantum wells, Physical Review B **56** (1997) R10024.

[47] Shur M. S., Bykhovski A. D. and Gaska R., Pyroelectric and Piezoelectric properties of GaN-based materials, MRS Internet Journal Nitride Semiconductors Res. **4S1** (2000) G1.6.

[48] Shur M. S. and Khan M. A., AlGaN/GaN doped channel heterostructure field effect transistors, Physica Scripta **T69** (1997) 103.

[49] Fraden J., Handbook of Modern Sensors, Springer, New York (1996) 536.

[50] Morkoç H., Cingolani R. and Gil B., " Polarization effects in nitride semiconductor device structures and performance of modulation doped field effect transistors, Solid State Electronic, **43** (1999) 1753

[51] Yoshida S., Ishii H., Li J.., Wang D., and Ichikawa M., A high-power AlGaN/GaN heterojunctions field effect transistor, Solid State Electronics **47** (2003) 589.

[52] Fritz I. J. and Drummond T. J., AlGaN quarter-wave reflector stack grown by gas-source MBE on (100)GaAs, Electronic Letters **31** (1995) 68.

[53] Munoz E., Monroy E., Pau J. L., Calle F., Omnes F. and Gibart P., III-V nitrides and UV detection, Journal of Physics: Condense Matter **13** (2001) 7115.

[54] Tsao J. Y., Solid-State lighting : lamps, chips and materials fo tomorrow, IEEE Circuits & Devices **20** (3) (2004) 28.

[55] Miyajima T., Tojyo T., Takeharu A., Katsunori Y., Kijima S., Hino T., Takeya M., Uchida S., Tomiya S., Funato K., Asatsuma T., Kobayashi T and Ikeda M., GaN blue laser diode, Journal of Physics: Condense Matter **13** (2001) 7099.

[56] Mead R.D.,Miyake C. I. and Lowenthal D. D., US Patent **5**,742, 626 (1998).

[57] Vreman H. J., Wong R. J. and Stevenson D. K., Phototherapy: Current methods and future directions, Seminars in Perinatology, **28** (2004) 326.

[58] Shodeen K., Davenpot S. and Melgaard H. L., Patent 5,446,289, (1995).

[59] Day T. A., Ruhland C. T. and Xiong F. S., Multiple trophic levels in UV-B assessments- completing the ecosystem, Journal of Photochemistry and Photobiology B **62** (2001) 78.

[60] Ishida M., Ogawa M., Orita K., Imafuji O., Yuri M., Sugino T. and Itoh K., Drastic reduction of threading dislocations in GaN grown on groove stripe structure, Journal of Crystal Growth **221** (2000) 345.

[61] Liu S-S., Li P-W., Lan W. H. and Lin W-J., Improvements of AlGaN/GaN p-i-n UV sensors with graded AlGaN layer for the UV-B (280-320 nm) detection, Material Science and Engineering. B **122** (2005) 196.

[62] Asif-Khan M., Kuznia J. N.,Olson D. T., van Hove J. M. and Blasingame M., High responsivity photoconductive ultraviolet sensors based on insulating single-crystal GaN epilayers, Applied Physics Letters **60** (1992) 2917.

[63] Shur M. S. and Zukauskas A., (Eds) UV Solid State Emitters and Detectors Kluwer, Dordrecht, (2004).

[64] Miyake H., Yasukawa H., Kida Y., Ohta K., Shibata Y., Motogaito A., Hiramatsu K., Ohuchi Y., Tadatomo K., Hamamura Y. and Fukui K., High performance Schottky UV detectors (265-100 nm) using n-Al0.5Ga0.5N on AlN epilayers, Physica Status Solidi (a) **200** (2003) 151.

[65] Wong M. M., Chowdhury U., Collins C. J., Yang B., Denyszyn J. C., Kim K. S., Campbell J. C., and Dupuis R. D., High quantum efficiency AlGaN /GaN solar-blind photodetectors grown by metaorganic chemical vapour deposition, Physica Status Solidi (a) **188** (2001) 333.

[66] Wang C. K., Chang S. J., Su Y. K., Chiou Y. Z., Lin T. K., Liu H. L., and Tang J. J., High detectivity GaN metal-semiconductor-metal UV photodetectors with transparent tungsten electrodes, Semiconductor Science and Technology **20** (2005) 485.

[67] Huang T. Z.,Mott D. B., and Lah A. T., Development of 256x256 GaN ultraviolet imaging arrays, Proceedings SPIE **3764** (1999) 254.

[68] Shen B., Yang K., Zang L., Chen Z-Z., Zhou Y-G., Chen P., Zhang R., Huang Z-C., Zhou H-S and Zheng Y-D., Study of photocurrent properties of GaN ultraviolet photoconductor grown on 6H-SiC Substrate, Japanese. Journal of Applied Physics **38** (1999) 767.

[69] Chung S-J., Hung H., Lin C-Y.,Wu M-H.,Kuan H.and Lin M-R., AlGaN Ultraviolet Metal-Semiconductor-Metal Photodetectors with Low-Temperature-Grown Cap Layers, Japanese. Journal of Applied Physics **46** (2007) 2471.

[70] Tut T, Biyikli N., Kimukin I., Kartaloglu T., Aytur O., Unlu M. S. and Ozbay E., High band-width-efficiency solar-blind AlGaN Schottky photodiodes with low dark current, Solid State Electronics **49** (2005) 117.

[71] Foresi J. S. and Moustakas T. D., Metal contacts to GaN, Applied Physics Letters **62,** (1993) 2859.

[72] Lin M. E., F. Y. Huang, Fan Z, Allen L., and Morkoc H., Low resistance ohmic contacts on wide band-gap GaN, Applied Physics Letters **64** (1994) 1003.

[73] Wu Y., Jiang W., Keller B., Keller S., Kapolneck D., Denbaars S. and Mishra U., Low luminescence ohmic contact to n-GaN with a separate layer method, Solid State Electonics **41** (1997) 75.

[74] Fan Z., Mohammad S. N., Kim W., Aktas O., Botchkarev A. E. and Morkoc H., Very low resistance multilayer Ohmic contact to n-GaN, Applied Physics Letters **68** (1996) 1672.

[75] Davvydov A. V., Motayed A., Boettinger W. J., Gates R. S., Xue Q. Z., Lee H. C. and Yoo Y. K., Combinatorial optimization of Ti/Al/Ti/Au ohmic contacts to n-GaN, Physica Status Solidi (c) **2** (2005) 2551.

[76] Selvanathan D. Zhou L., Kumar V and Adesida I., Low resistance Ti/Al/Mo/Au ohmic contacts for AlGaN/GaN heterostructure field effect transistors, Physica Status Solidi (a) **194** (2002) 583.

CHAPTER 3

Schottky barrier Ultraviolet Photodetectors

3.1 Introduction

The theoretical background of Schottky barrier photodiodes is given in this chapter. Firstly a discussion of the fundamental operation and evaluation of photodiodes is discussed in section 3.2. Section 3.3 discusses the theory of Schottky barrier junctions. The transport mechanisms of Schottky contacts are discussed in section 3.4. This chapter finishes with the applications of Schottky barriers to the photodiodes.

3.2 Ultraviolet (UV) photodetectors

Semiconductor photodiodes work in three fundamental modes:

- Photoconductive detectors
- p-n junction photodiodes
- Schottky barrier diodes.

These are miniature in size, lightweight, and are easily integrated into microelectronic systems. They are very fast and responsive, with relatively little noise. These devices shows high quantum efficiency and low leakage currents; are insensitive to magnetic fields, superior to glass vacuum devices in reliability and have average ability to store charge and integrate detected signal [1]. They can be used in reverse bias mode of photoconductive detector operation or zero bias modes of photovoltaic detector operation and have linear photo-current flux characteristics. The current-voltage (I-V) characteristic of a photodiode follows the standard diode equation [2]:

$$I = I_s\left(\exp[\frac{qV}{kT} - 1]\right) \tag{3.1}$$

where I_s is the saturation current V is the applied voltage q is the electronic charge, T is the temperature, k is Botlzman constant. When a photodiode is illuminated with electromagnetic

radiation, equation 3.1 is modified due to the generation of additional carriers within the device and it becomes [3]:

$$I = I_s\left(\exp\left[\frac{qV}{kT} - 1\right]\right) - qAG \;\; L_p + L_n \tag{3.2}$$

where A is the device area, G is the carrier generation rate; L_p and L_n are diffusion lengths for holes and electrons respectively. When incident electromagnetic radiation is greater than the bandgap of the semiconductor, some of the radiation will be absorbed, creating electron-hole pairs, due to photon-electron scattering. As the photons are absorbed by the semiconductor, they interact with electrons in the valence band, giving them enough energy to be promoted to the conduction band. A hole is left in the valence band, and we have generated an electron hole pair in the semiconductor, which follows the carrier drift process, as shown in figure 3.1.

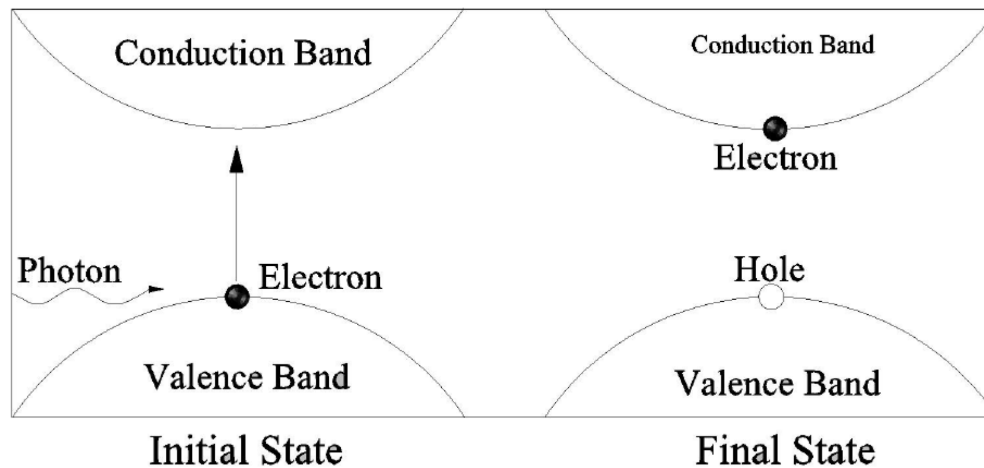

Figure 3.1: Schematics of photon absorption in a direct bandgap semiconductor

The electrons are then swept out by the built-in voltage in the depletion region into the n-type side and holes go to the p-type side of the device. If the absorption occurs within L_n of the depletion region on the p-side of the junction, the electrons may diffuse into the space charge region before recombining and swept out into the n-type region. Similar process occurs for holes

within the L_p of the depletion region. This implies that the total photocurrent is contributed by both the carrier diffusion and drift. The depletion region of the device makes a significant contribution to the device detection efficiency. Some of the parameters of semiconductor photodiodes, which are used in detection mechanisms follows:

3.2.1 Active area of semiconductor diode (A)

The design of photodiodes requires that the device have an area, through which incident radiation can be freely absorbed, called active area, as shown in figure 3.2 [4]. This is accomplished by providing a window between the ohmic and Schottky contact for nitride based semiconductors, ranging from 0.1 to 100 mm [5-6]. The thickness of the metal for Schottky contacts is made sufficiently thin so that it is transparent to incident UV radiation, to optimize photon absorption.

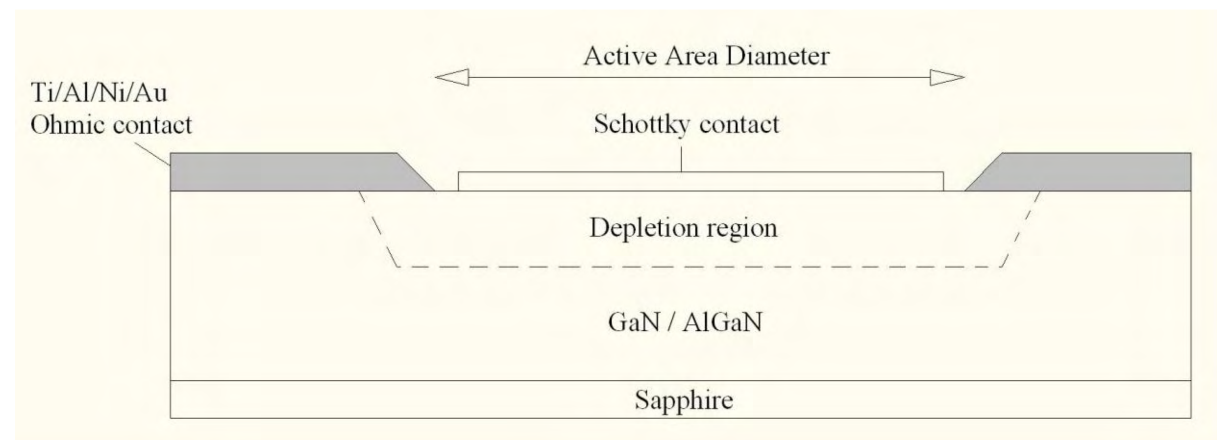

Figure 3.2: Schematics of AlGaN/GaN Schottky barrier photodiode, showing active area.

3.2.2 Responsivity

Responsivity, R_λ of the device is defined as the ratio of the photocurrent I_p to the incident electromagnetic radiation power, *(P)* given by [7]:

$$R_\lambda = \frac{I_p}{P} \tag{3.3}$$

The quantum efficiency is the average number of electron-hole-pairs generated by each incident photon, defined as the fraction of incident photons that contribute to photocurrent, and it is related to responsivity by:

$$Q.E = \frac{R_{\lambda\ observed}}{R_{\lambda\ ideal}} = R_{\lambda}\frac{hc}{\lambda q} = 1240\frac{R_{\lambda}}{\lambda} \tag{3.4}$$

where h is Planck's constant, c is the speed of light and λ is the wavelength of incident radiation. Another parameter, related to responsivity is the R_0A product, where R_0 is the dynamic resistance of the diode at zero bias and A is the diode area. A large R_0A product is necessary for the detector to have large detectivity, D^* meaning that it is able to produce a measurable signal current at very low radiation level. If the detector is limited by thermal noise, then detectivity becomes:

$$D^* = \frac{q\eta}{h\nu}\left(\frac{R_0A}{4kT}\right)^{\frac{1}{2}} \tag{3.5}$$

where η is the quantum efficiency. The detectivity may also be expressed in terms of noise equivalent power (NEP). The NEP is a quantity that signifies the root means square (rms) optical power of an output signal required to generate the noise level present in the detector over a bandwidth of 1 Hz. The detectivity is then expressed as:

$$D^* = \frac{\sqrt{A\Delta f}}{NEP} \tag{3.6}$$

where Δf is the detector bandwidth and f is the noise frequency. Consequently current responsivity may be written as:

$$R_i = \frac{q\lambda}{hc}\eta \tag{3.7}$$

and the voltage responsivity:

$$R_V = \frac{q\lambda}{hc}\eta R \tag{3.8}$$

where $R = (dI/dV)^{-1}$ is the differential resistance of the photodiode.

3.2.3 Operation voltage V_{op}

Metal-semiconductor photodiodes can be used in zero and reverse bias modes of photovoltaic operation, with the operation voltage lower than the breakdown voltage, V_{BR}. This is the maximum reverse voltage that can be safely applied to the photodiode before a breakdown at the junction occurs. The V_{BR} for abrupt p-n junctions and Schottky barriers is given by:

$$V_{BR} = 60\left(\frac{E_g}{1.1}\right)^{3/2}\left(\frac{N_i}{10^{16}}\right)^{-3/4} \tag{3.9}$$

where E_g is the bandgap, N_i is the carrier density (cm^{-3}). If the external reverse bias is increased, the applied voltage increases, thereby increasing the size of the depletion region within the device [8].

3.2.4 Dark Current-Voltage characteristics ($I_d - V_d$)

$I-V$ characteristics of Schottky barrier photodiodes exhibiting a thermionic emission mechanism of current flow is:

$$I_d = I_s\left[\exp\left(\frac{qV_d}{nkT}\right)-1\right] = A^*AT^2\exp\left(-\frac{q\varphi_B}{kT}\right)\left[\exp\left(\frac{qV_d}{nkT}\right)-1\right] \tag{3.10}$$

where I_s is the saturation current, n is the ideality factor, A is the area, V_d is the applied voltage and A^* is the Richardson constant and φ_B is the barrier height. These variables are used in the calculation of the shunt resistance of a photodiode. $R_0 = nkT/qI_s$ is dark resistance and I_d is

dark current at the operation voltage. High temperature annealing is known to reduce the leakage and dark current in a Schottky contact [9].

3.2.5 Response speed

The response speed of a photodiode determines its ability to follow a fast-varying optical signal. For the optical signal to be acceptable, a photodiode must have a speed higher than frequency response. The speed of a photodiode is related to the response time by rise-time, t_τ, or fall-time, t_f, of its response to an impulse signal. The rise-time is defined as the time interval for the response to increase from 10% to 90% of its of peak value, and the fall-time is from 90% to 10% of its decay value [10]. The equation for the response speed is then given by:

$$\varsigma\frac{90}{10} = \varsigma_{cc}^2 + \varsigma_{Diff}^2 + \varsigma_{RC}^2 \;{}^{1/2} \tag{3.11}$$

where ς_{cc} is the time for charge collection from the depleted region, ς_{Diff} the time for photo-generated carriers to diffuse to the depleted region and ς_{RC} is the time constant. We further define ς_{cc} as:

$$\varsigma_{cc} = \frac{W_d}{2\nu_d} \tag{3.12}$$

where W_d is the width of the depletion region and ν_d is the drift velocity of the photo-generated carriers. ς_{Diff} is defined as:

$$\varsigma_{Diff} = \left(\frac{W_0 - W_d}{D_p}\right)^2 \tag{3.13}$$

where W_0 is the thickness of the substrate and D_p is the diffusion constant. Finally, ς_{RC} is given by:

UNIVERSITEIT VAN PRETORIA
UNIVERSITY OF PRETORIA
YUNIBESITHI YA PRETORIA

$$\varsigma_{RC} = 2.2 \ \ R_s + R_L \ \ C_V \tag{3.14}$$

where R_s is the series resistance of the photodiode and C_V is the capacitance at applied voltage V. When a reverse bias is applied to the depletion region, the width thereof increases and collection time for the photo-generated carriers becomes larger.

3.2.6 Capacitance (*C*)

Junction capacitance is the ability of the photodiode to store charge. This value depends on the substrate resistivity, the reverse bias voltage and the active area. In the case of Schottky barriers, C is given by:

$$C = A\left[\frac{\varepsilon_s \varepsilon_0 q N_i}{2 \ \ V_{bi} + V_d - \ \ kT/q}\right]^{1/2} \tag{3.15}$$

where ε_s and ε_0 are the dielectric constants of semiconductor and vacuum respectively, V_{bi} and V_d are built-in and applied voltages. Capacitance is an important parameter that determines the response speed of the photodiode by relating the depletion with mobility of majority carriers and resistivity of the semiconductor. The zero-biased photodiode gives capacitance that is inversely proportional to the substrate resistivity. High resistivity materials yield small capacitance [11].

3.2.7 Series Resistance R_s

Series resistance R_s is the resistance of a detector through which the photodiode current must flow and is the sum of resistances of semiconductor bulk and ohmic contacts. The general expression for series resistance is given by:

$$R_s = \frac{(W_0 - W_d)\rho}{A} + R_c \tag{3.16}$$

The first term is the series resistance of the quasi-neutral region with W_0 and W_d being the thicknesses of the substrate and the depletion region respectively and A is the diode area. R_c is the resistance due to ohmic contact and the semiconductor. Series resistance decreases linearly with increasing carrier concentration.

3.3 Modifications to Schottky-Mott Theory

According to Schottky-Mott theory [12,13] the rectifying property of the metal-semiconductor junction arises from the presence of a barrier between the metal and the semiconductor, resulting from the difference in the work functions, φ_m and φ_s of the metal and the semiconductor [14]. In order for the contact to be rectifying, it is required that $\varphi_m > \varphi_s$ for n-type semiconductor. The barrier heights for n- and p-type semiconductors are given by [11]:

$$\begin{aligned} \varphi_{bn} &= \varphi_m - \chi_s \\ \varphi_{bp} &= \chi_s + E_g - \varphi_m \end{aligned} \tag{3.17}$$

where χ_s is the electron affinity of the semiconductor and E_g is the semiconductor bandgap. Figure 3.3 shows the energy band diagrams of Schottky barrier for n- and p-type semiconductors. The potential barrier, caused by band bending between the bulk of the semiconductor and the metal-semiconductor interface, is given by:

$$\psi_s = \varphi_m - \varphi_s \tag{3.18}$$

where ψ_s is the barrier potential. In practice, however, the built-in potential barrier does not follow such a simple relationship with φ_m, and is effectively reduced as a result of the interface states originating from either surface states or metal-induced gap (MIG) states and to interfacial reactions at the junction. Published results show considerable variations among experimental data on the values of the metal work function, φ_m [15]. Their analysis indicates an empirical relationship of the form [16, 17].

$$\varphi_b = \Upsilon_1 \varphi_m + \Upsilon_2 \qquad (3.19)$$

where Υ_1 and Υ_2 are constants characteristics of the semiconductor. The limits, $\Upsilon_1 = 0$ and $\Upsilon_1 = 1$ indicates that the barrier is due to localized surface states and the ideal Schottky barrier, respectively. The contribution of the surface states to barrier height has been discussed by Bardeen [18]. The slope parameter $\Upsilon_1 = \partial \varphi_b / \partial \varphi_m$ can be used to describe the extent of Fermi level pinning for a given semiconductor. The parameters Υ_1 and Υ_2 have been used by some researchers to estimate the interface states density [16].

Cowley and Sze [19] have shown that, according to Bardeen model, the barrier height, in the case of n-type semiconductor is approximately given by:

$$\varphi_{on} = \Upsilon \;\; \varphi_m - \chi_s \;\; + \;\; 1 - \Upsilon \;\;\; E_g - \varphi_0 \;\; - \Delta\varphi \qquad (3.20)$$

where $\Upsilon = \varepsilon_i \;\; \varepsilon_i + q\delta D_g$ and φ_0 term is the position of the neutral level of the interface states measured from the top of the valence band, $\Delta\varphi$ is the barrier lowering as a result of the image forces, δ is the thickness of the interfacial layer and ε_i is its total permittivity. The surface states are assumed to be uniformly distributed in energy within the bandgap, with density D_g per electron volt per unit area. For very high density of states, Υ becomes very small and φ_{bn} approaches the value $E_g - \varphi_0$. This is because a very small deviation of the Fermi level from the neutral level can produce a large dipole moment, which stabilizes the barrier height. The Fermi level is stabilized or pinned relative to the band edges by the surface states.

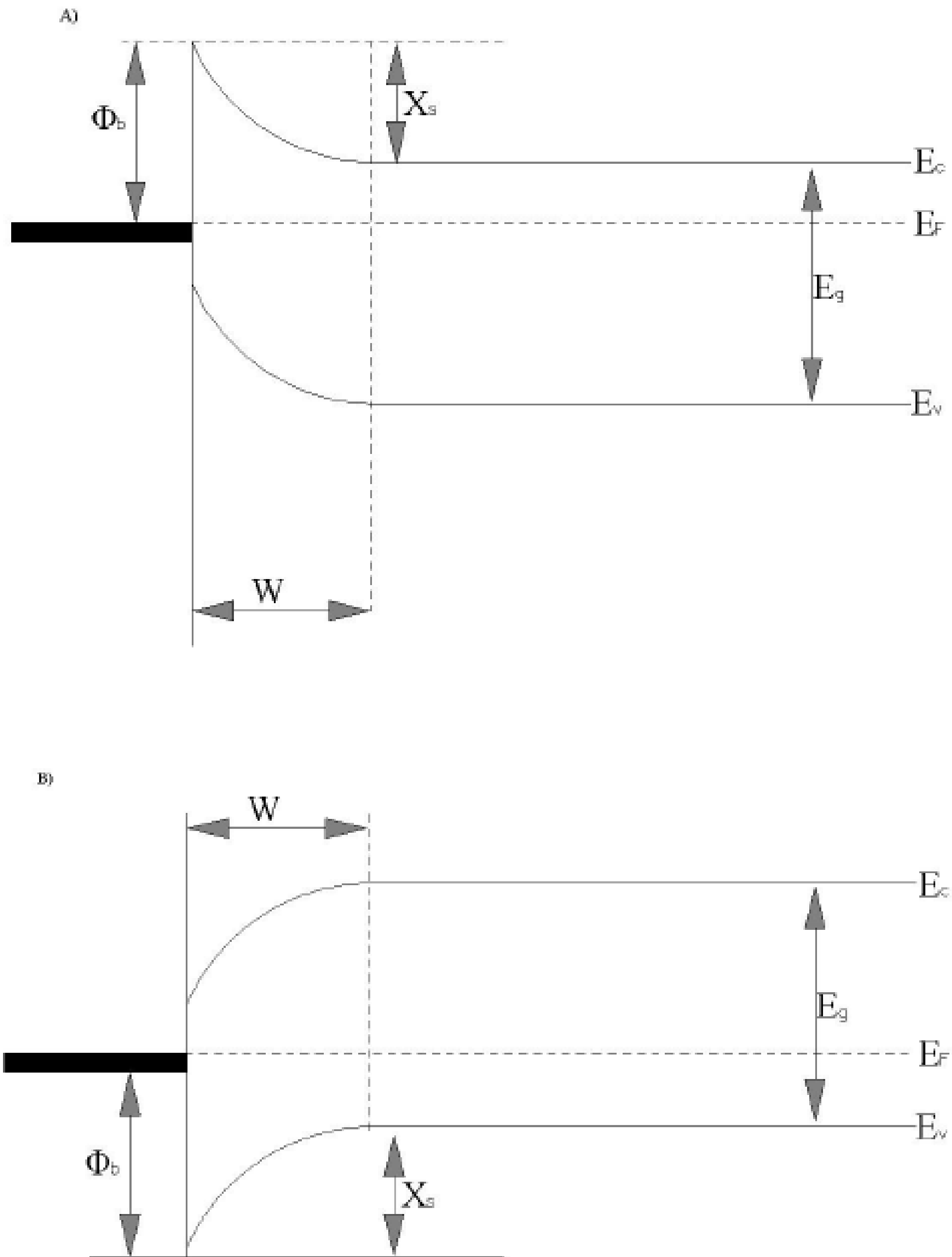

Figure 3.3: Energy band diagrams of Schottky barrier for (A) n- and (B) p-type semiconductors.

3.4 Charge Transport Mechanisms.

The charge transport mechanisms in Schottky barrier diodes, as shown in figure 3.4, are mainly due to majority carriers, the electrons, across the metal-semiconductor junction. These mechanisms are classified as:

- **A.** The emission of electrons from the semiconductor over the top of the potential barrier into the metal,
- **B.** Quantum-mechanical tunneling of electrons through the barrier,
- **C.** Recombination in space-charge region and
- **D.** Recombination in the neutral region (equivalent to hole injection from metal to semiconductor).

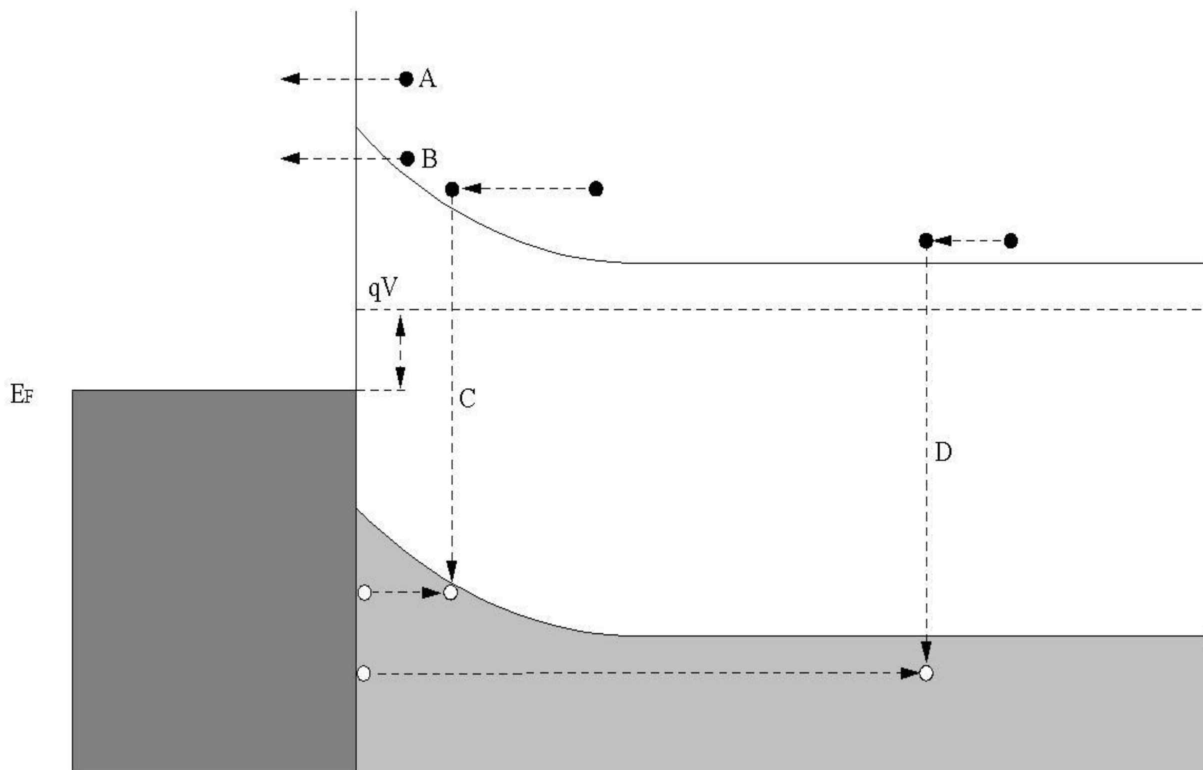

Figure 3.4: Energy band diagram of a forward biased Schottky contact on n-type semiconductor showing different charge transport processes [14]

There may also be edge leakage current due to high electric field at the contact periphery or interface current due to traps at the metal-semiconductor interface. The inverse processes occur under reverse bias. The transports of electrons over the potential barrier have been described by various theories:

- diffusion theory of Schottky and Spenke [20,21],
- Bethe's thermionic emission [22]
- and unified thermionic emission diffusion.

It is now generally accepted that, for high-mobility semiconductors with acceptable impurity concentrations, the thermionic emission theory appears to qualitatively explains the experimentally observed current-voltage ($I-V$) characteristics [23]. Some researchers [24] have also included in the simple thermionic emission theory the effect of quantum-mechanical reflection and tunneling of carriers through the barrier; and have tried to obtain modified analytical expression for ($I-V$) characteristics. Consequently, this has led to a lowering of the barrier height and a rounding off at the top, known as the Schottky effect. The rounding off at the top is the image force lowering of the potential energy for charge carriers' emission due to an applied electric field. Bethe's thermionic emission theory is derived from the following assumptions:

- the barrier height is far larger than kT,
- thermal equilibrium is established at the plane that determines emission,
- and the existence of a net current does not affect this equilibrium.

The barrier height is then extracted from the slope of the linear line resulting from the logarithmic plot of current – voltage ($I-V$) across the Schottky diode. The criterion used by Bethe for the $I-V$ slope of the barrier is that it must decrease by more than kT over a distance equal to the scattering length. The resulting charge flow will depend only on the barrier height, The saturation current is independent of the applied bias.

3.5 Theory of Schottky Barrier ultraviolet photodiodes

The photosensitivity of Schottky barrier diodes is determined by the following:

- Firstly, electrons are generated in the metal and they are injected into the semiconductor at incident photon energies exceeding the height $q\varphi_b$ of the metal-semiconductor potential barrier. When $q\varphi_b < h\nu < E_g$ the short-circuit current I_{p0} varies with the photon energy according to Fowler law [25,26].

$$I_{p0} \sim (h\nu - q\varphi_b)^2 \tag{3.21}$$

- Secondly, electron-hole pairs are generated in the semiconductor, then separated by built in electric field at $h\nu > E_g$. Then, the photocurrent is the sum of the contributions from the charge carriers generated in the space-charge layer of width W and the carriers that reached the layer from the adjoining region of extent L (minority charge diffusion length), given by [27]:

$$I_{p0} = -q\eta(1-R)\Phi\left(\frac{1-\exp(\alpha W)}{1+\alpha L}\right) \tag{3.22}$$

where α is the semiconductor light absorption coefficient and Φ the incident flux.

The energy-band diagrams of a Schottky barrier photodetector are shown in figure 3.5.

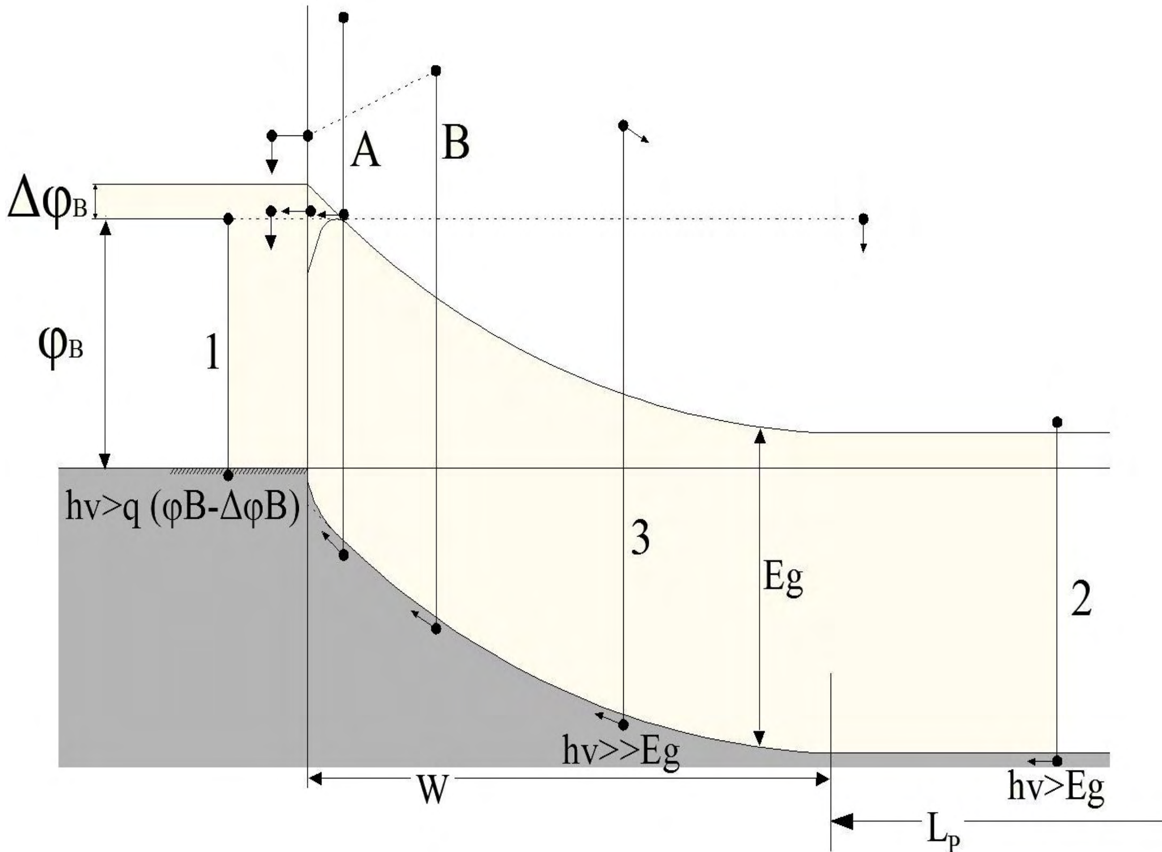

Figure 3.5: Energy band diagrams of a Schottky barrier photodetector

Comparing these mechanisms, the second process is more efficient than the first and therefore the long wavelength limit of the photosensitivity spectrum is close to the bandgap value in direct-band semiconductors and to the threshold energy for direct optical transitions in the indirect bandgap semiconductors. At photon energies far above the bandgap, the photosensitivity is observed to drop, and explained by loss of carriers generated by photons through carrier drift against the built in electric field [28], by thermionic emission, by quasiballistic electron transport or by a drop in internal quantum yield [29].

REFERENCES

[1] Goldberg Y. A., Semiconductor Sciience and Technology **14** (1999) R41.

[2] Schockley W.. Bell Systems Journal **28** (1949) 435.

[3] Streetman B. and Banerjee S., Solid State Electronics, Prentice Hall, New York (2000).

[4] Jiang H. and Egawa T., Electronic Letters **42** (19) (2006) 884.

[5] Collins C.J, Chowdhury U., Wong M. M., Yang B., Beck A. L., Dupuis R. D. and Campbell J. C., Electronic Letters **38** (2002) 824.

[6] Asalm S. .Vest R. E., Franz D., Yan F. and Zhao Y., Electronic Letters **40** (2005) 1080.

[7] Dereniak E. L. and Growe D. G., Optical Radiation Detectors, Wiley, New York (1984).

[8] Sze S. M., Physics of Semiconductors, 2nd Edition, Wiley, New York (1981).

[9] Lee Y. C., Hassan Z., Abdullah M. J., Hashim M. R., and Ibrahim K., Microelectronic Engineering **81** (2005) 262.

[10] Graeme J., Photodiode Amplifiers, McGraw Hill, New York, (1996).

[11] Tyagi M. S., in Metal-Semiconductor Schottky Barrier Junctions and their applications, edited by B. L. Sharma, New York, (1984).

[12] Schottky W. S., Naturwissenschaften **26** (1938) 843.

[13] Mott N. F., Proceedings Cambridge Philosophical Society **34** (1938) 568.

[14] Rhoderick E. H., Metal-Semiconductor Contacts, Oxford, Clarendon, (1978).

[15] Rhoderick E. H., IEEE Proceedings **129** (1982) 1.

[16] Johnson E. O., RCA Review. **26** (1965) 163.

[17] Razeghi M. and Rogalski A. Semiconductor Ultraviolet Photodetectors Journal of Applied Physysics **79** (1996) 7433.

[18] Bardeen J., Physical Reveview **71** (1947) 717.

[19] Cowley A. M. and Sze S. M., Journal Applied Physics **36** (1965) 3212.

[20] Schottky W. and Spenke E., Wiss. Veroff. Siemens-Werken. **18** (1939) 225.

[21] Spenke E., Electronic Semiconductors, McGraw-Hill, New York, (1958).

[22] Bethe H. A., MIT Radiation Laboratory Report **43-12** (1942).

[23] Crowell C. R. and Sze S. M., Solid State Electronics **9** (1966) 1035.

[24] Ottaviani G., Tu K. N. and Mayer J. W., Physical Review Letters **44** (1980) 284.

[25] Fowler R. H., Physical Review **38** (1931) 45.

[26] Anderson C. L., Crowell C. R., and Kao T. W., Solid State Electronics **18** (1975) 705.

[27] Gartner W. W. Physical Review **116** (1959) 84.

[28] Li SS, Lindholm F. A., and Wang C. T., Journal of Applied Physics **43** (1972) 4123.

[29] Goldberg Y. A, Konstantinov O. V., Posse E. A. and Tsarenkov B. V., Semiconductors **29** (1995) 215.

CHAPTER 4

Experimental Techniques

4.1 Introduction

In this chapter, the experimental techniques used in the study are discussed. The performance of Schottky barrier diodes depends on processing issues such as cleaning, the etching of the surface and low surface roughness. Different wet chemicals have been used to reach a stoichiometric GaN surface, characterizing the surface with Auger Electron Spectroscopy (AES) and X-ray Photoelectron Spectroscopy (XPS). The surface topography and roughness were evaluated using a Scanning Electron Microscope (SEM) and an Atomic Force Microscope (AFM). Schottky diodes were fabricated by depositing a metal layer onto the semiconductor using an electron beam and resistive evaporator, depending on the density of the metal. The metals were chosen according to the percentage of UV light transmitted through layers of different thicknesses. The metal was selected with the aid of an in-house computer program

4.2 Sample preparation

n-GaN samples were grown by MOCVD from AIXTRON and HVPE from TDI. As grown samples were degreased in boiling trichloroethylene and isopropanol. HCl:HNO_3 aquaregia was used to remove metal particles and a final rinse in dilute HCl. Each cleaning step was followed by rinsing in deionized water. After cleaning, samples were loaded in AES to evaluate the surface elements and stoichiometry. Morphological studied were done in the SEM and AFM. The samples were then loaded in the electron beam deposition and ohmic contacts were deposited. The contacts were then annealed in the vacuum furnace at 500 °C. Samples were further etched in dilute HCl and then Schottky contacts were deposited. The diodes were then ready for electrical and optical characterization techniques.

4.3 Surface Characterization

4.3.1 Auger Electron Spectroscopy

AES [1] is a suitable technique for surface analysis because it is capable of identifying individual elements. It is a very sensitive surface technique which can measure to a depth of 1 - 3 nm. It can also be used to obtain depth profiling measurements for determining the concentration of surface species. Auger electrons are produced in the ionization process of an atom hit by primary electrons. The process continues with an electron from the higher energy level being attracted to the ionized atom to take it back to a stable state. Auger electrons are then produced from the excess energy resulting from stabilization, which may be absorbed by the sample or detected on the outer monolayers of the surface. The specific energy involved in the transition process is the key to the identification of the elements that produced the Auger electrons. Figure 4.1 shows a picture of the AES. AES has the ability to remove the surface contaminants with the electron beam, in a process called desorption. In this work, it was observed that Cl on the GaN surface was desorbed to the lowest detection limit of the AES during continuous exposure of the surface to the electron beam. The addition of a heater block inside the ultra-high vacuum AES removes surface contaminants, such as those common to the semiconductors, namely O and C. Other elements introduced onto the GaN surface from the chemicals used in the wet cleaning and etching are reduced by exposure to the electron beam and thermal heating inside the AES.

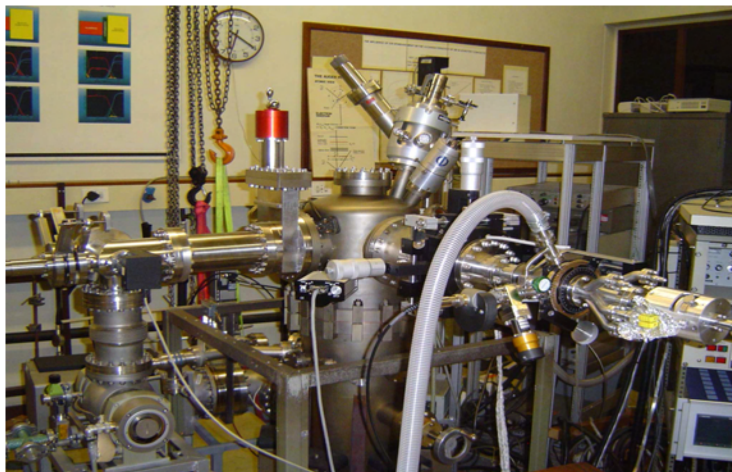

Figure 4.1: Pictorial presentation of the AES at the University of Pretoria.

4.3.2 Scanning Electron Spectroscopy

SEM, as shown in figure 4.2, [2] is a high resolution surface technique suitable for imaging surface defects on conducting materials. It creates a highly focused electron beam which scans in a regular manner over the sample, while the detector measures the resulting scattered electrons. When focused on the surface, the electron beam stimulates the emission of secondary electrons, which are amplified to increase the brightness of the Cathode Ray Tube (CRT) display. A point by point communication exists between the brightness of each point in the CRT and the number of electrons emitted from the sample surface. The energy of the electrons is directly related to the desired image. A high energy electron beam (5 – 50 keV) is used to identify deep structures while making it possible to produce nondestructive images below the surface, up to 20 µm. A useful component of the SEM is the Energy Dispersive X-ray Spectrometer (EDAX) which is characteristic of X-rays produced by primary electrons emitted from the sample, used to identify the elemental species on the surface. The typical pressure of the SEM was about 10^{-6} torr.

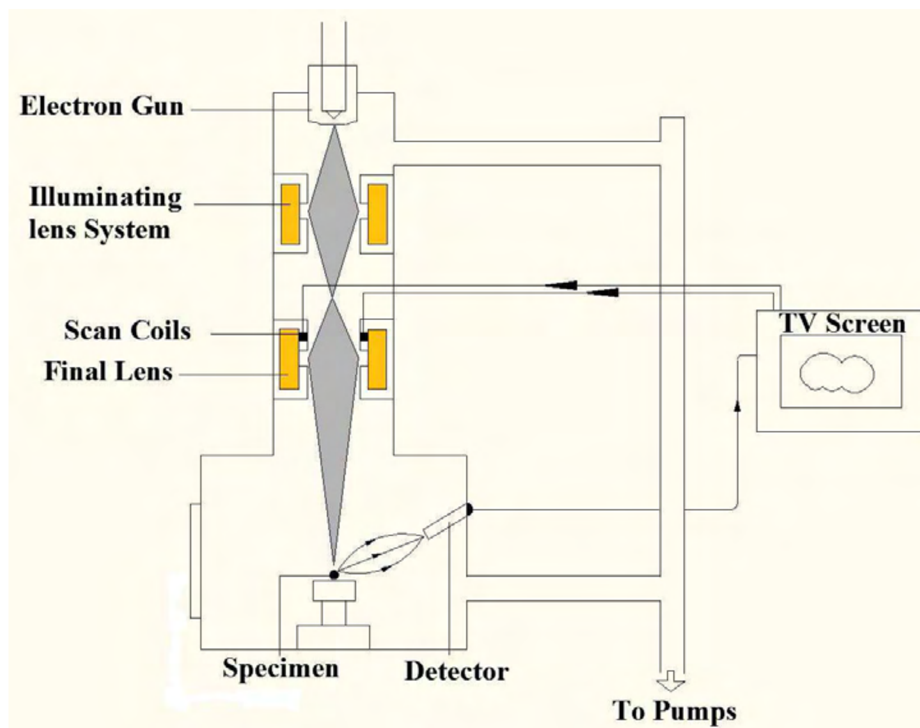

Figure 4.2: Schematics of the SEM operation

4.3.3 Atomic Force Microscopy

AFM [3] is capable of producing three dimensional views of the surface morphology. The advantage of using the AFM is the resolution of the atomic image and ability to measure the force on the nanoscale. The AFM consists of a tip at the end of a flexible cantilever across the sample surface while maintaining a small constant force. Figure 4.3 depicts the schematics of the AFM. The laser, focused on the cantilever, senses the position of the tip relative to the surface, detecting the topography. The laser beam is deflected into a dual element sensor during the scanning. The sensor measures the difference in light intensities registered at the detectors, converting the signals into voltage. The relevant software captures the voltage signals and converts them into an image of the surface. The piezoelectric drive unit monitors the difference in the height sensed from the surface. There are different modes of operating the AFM; the most common is the contact mode where the tip scans the surface in close contact with the surface of the sample. The constant force of about 10^{-9} N at the tip is repulsive, pushing the cantilever against the sample surface with the piezoelectric unit. In this work, the AFM was used in contact mode, employing scanners of 100 X 100 and 7 X 7 μm. The reliability of the results relies on the position of the AFM unit: it should be placed on a stable table.

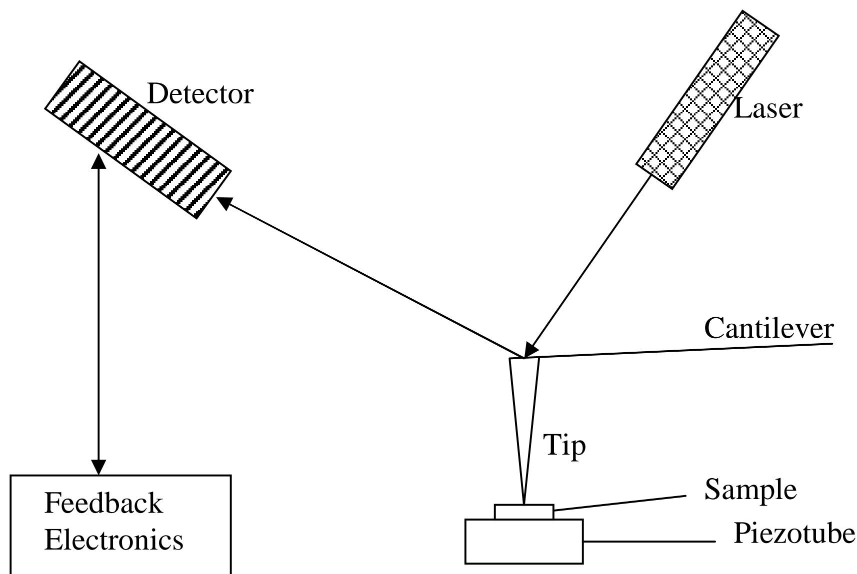

Figure 4.3: Schematics of the AFM operation

4.4 Electrical and Optical Characterization

Current-Voltage *(I-V)* measurements are used to evaluate the rectifying properties of the Schottky barrier diodes (SBD) [4]. The parameters of interest in these measurements are the series resistance (R_s), Schottky barrier height (ϕ_B), saturation current measured at 1 V (I_0) and ideality factor (n). Figure 4.4 illustrates the *I-V* characteristics of an ideal and practical SBD. For an ideal Schottky diode, $n=1$, while practically it is above unity, depending on transport mechanisms. In determining the *I-V* parameters, it is assumed that the current transport is dominated by thermionic emission. The barrier height is then extracted by fitting a straight line in region (b) of the *I-V* plot in figure 4.4. From equation 3.10, the y-intercept of the fit gives the saturation current $I_s = AA^{**}T^2.\exp[-q\varphi_{bo}/kT$ thus the barrier height is given by $\varphi_{b0} = kT/q\ln\left(AA^{**}T^2/I_0\right)$, where A is the diode area, T is the measurements temperature, k is the Boltzmann constant, q is the electronic charge and the modified Richardson plot, A^{**}. This approach requires the knowledge of the modified Richardson plot, A^{**} for a Schottky contact. The more accurate value of the barrier height is extracted using the Arrhenius plot [$\ln\left(I/T^2\right)$ - $1/T$]. The Ideality factor is then extracted from the linear fit of the same region and is expressed as $n = \left(q/kT\right).\left(V_a/\ln\left[I/I_0\right]\right)$. The series resistance is determined form region (c) of figure 4.4, where the voltage is high. The plot assumes a flat state and R_s is extracted from the I-V plot. The leakage current is defined as the current flowing when an ideal current is zero. In particular, leakage occurs when electrons or holes tunnel through an insulator and increases exponentially as the insulating region becomes small [5]. In the case of a Schottky contact, tunneling of carriers occurs between the metal and the semiconductor at the interface. It is of vital importance to measure leakage currents in diodes as they lead to device failure when too high. Figure 4.4 (d) shows the reverse leakage current of a practical diode, and compared with the ideal case, it has to be almost constant and as low as possible.

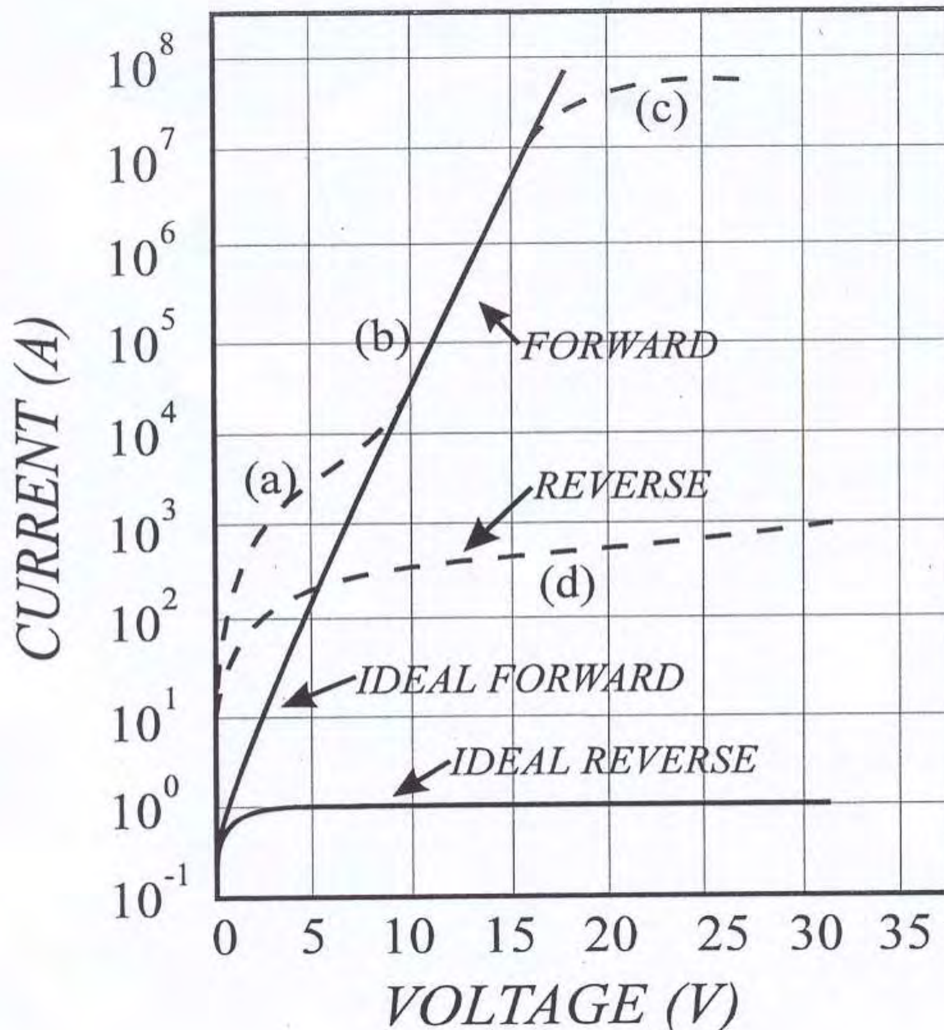

Figure 4.4: Current-Voltage characteristics of an ideal and a practical Schottky barrier diode: (a) generation-recombination current region; (b) diffusion current region; (c) series resistance effect; (d) reverse leakage current due to generation-recombination and surface effects [adapted from [7].

The capacitance-voltage (*C*-*V*) measurements also offer another method for evaluation of the barrier height including the built-in potential (V_{bi}) and the carrier density, N_D. When a metal and a semiconductor come into intimate contact, the conduction and valence bands of the material are lined with the Fermi level at equilibrium. This relationship gives the boundary conditions for the Poisson equation, where the depletion width (*W*) of a reverse biased Schottky contact is given

by $W = \sqrt{2\varepsilon_s / qN_D \left(V_{bi} - V_a - kT/q\right)}$, where ε_s is the permittivity and V_a is the applied voltage. The space charge per unit area is given by $Q_{sc} = qN_d W$ and the depletion region capacitance per unit area at the contact is approximated to that of a parallel plate capacitor given by $C = \varepsilon_s / W$ and can be rewritten as $1/C^2 = 2((V_{bi} - Va - kT/q)/q\varepsilon_s N_D$, and the data from *C-V* measurements can be used to plot $1/C^2$ as a function of applied voltage, where the x-axis intercept yield the built-in potential, V_{bi}. The carrier density can be obtained from $N_D = 2/q\varepsilon_s \left[-1/d/dV\left(1/C^2\right)\right]$. The *C-V* barrier height is obtained from $\varphi_b = V_i + V_n + kT/q - \Delta\varphi$ [6]. Furthermore, the measurements can be used to study the impurity levels in semiconductors.

The optical characterization of the individual diodes is created using a UV light with a monochromator source to select wavelengths. The use of monochromated light makes the measurement of photo-generated current as a function of wavelength and voltage possible. The photocurrent is then used to compute the responsivity, quantum efficiency, detectivity and noise equivalent power of the photodiodes. The responsivity is calculated from equation 3.3. The responsivity value is then used in equation 3.4 to calculate the quantum efficiency. The set-up consists of a probe station, equipped with an HP 4140B meter/dc voltage source for *I-V* measurements and an HP 4192A low frequency impedance analyzer for *C-V* measurements.

This thesis came up with a plan to add optical instruments to the existing I-V and C-V measurements station, to complete an optoelectronic station so that dark current and photocurrents can be measured for optical devices. We used an optical fibre to connect the optical instruments to the probe station. The probe station is housed in a shielded enclosure and the optical instruments are outside as shown in figure 4.5 setup The shielded enclosure is used to reduce the radiation noise from the surroundings. Inside the enclosure is an optical microscope focused on the sample stage for easy selection of miniature diodes. A chopper is used for variation of for light frequencies which is housed inside the shielded enclosure, between the sample and the light. A SiC detector is used to measure the intensity of the light.. The UV monochromator can be replaced by visible range monochromator which is able to measure light

from blue to infra-red. Different light sources are available for the station: Deuterium lamp for deep UV, which has a wavelength range from 100 – 700 nm. The second monochromator is also suitable for UV measurements and is equipped with Xenon lamp for wavelengths ranging from 100 – 1100 nm. When UV light is focused on a diode, a small photocurrent is measured, which can be amplified to a voltage for determination of voltage responsivity, using an operational amplifier. The optical set-up is calibrated with a SiC detector and an AlGaN detector for UV measurements. It has been shown that the station is accurate as the commercial SiC and AlGaN detector factory specification has been reproduced at this station. All these are controlled by a LABVIEW program for dark currents, responsivity and photocurrents measurements as a function of wavelength.

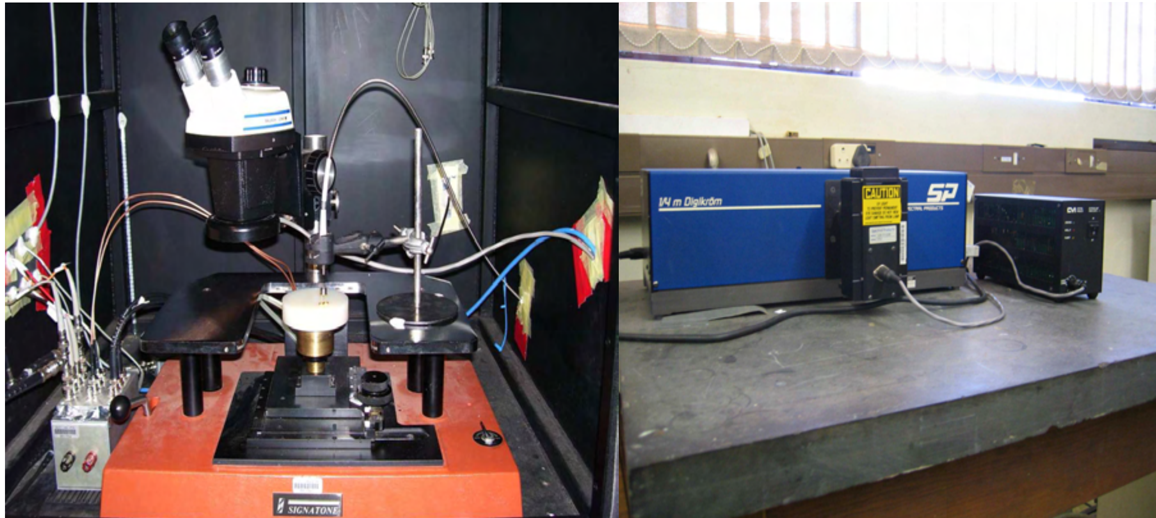

Figure 4.5: Optoelectronic device testing station: Probe stand is housed in a shielded enclosure, where measurements are done. The monochromater and deuterium lamp are connected to the station by a optical fibre.

REFERENCES

[1] Davis L.E., MacDonald N. C, Palmberg P. W., Riach G. E. and Weber R. E., Handbook of Auger Electron Spectroscopy, 2nd Edition Perkin-Elmer, New York (1976) .

[2] Chapman S. K., Working with a Scanning Electron Microscope, Lodgemark, Kent.,(1986).

[3] Binning G and Rohrer, IBM Journal of Research and Development **30** (1986).

[4] Schroder D. K., Semiconductor Material Device and Characterization, 2nd Edition, Interscience, New York-Wiley (1998).

[5] Tsivididi Y., Operation and Modeling of the MOS Transister, 2nd Edition, McGraw Hill, New York (1999).

[6] Sze S. M., Physics of Semiconductor Devices, 2nd Edition, Wiley, New York (1981).

EXPERIMENTAL RESULTS

CHAPTER 5

Analysis of GaN cleaning procedures

5.1 Introduction

A number of groups have investigated GaN cleaning procedures for device fabrication [1-5]. The importance of properly cleaned surfaces for ohmic and Schottky contacts deposition is well known [4-5]. There is currently no standard method of preparing the GaN substrate prior to metallization. Preparation methods differ from one laboratory to the other. Wet and dry etching methods are widely used in surface preparation for removal of surface contaminants. In addition, the morphology of the surface of the substrate prior to metallization has an influence on the continuity of the ultra-thin metals used in fabrication of Schottky barrier diodes for ultraviolet (UV) detection. Wet and dry cleaning of substrates using chemicals have been used on GaN prior to metallization. Dry cleaning methods are known for introducing damage to the surface, usually making the material electrically unsuitable [6]. Various surface analytical techniques such as Auger electron spectroscopy (AES), x-ray photoelectron spectroscopy (XPS), low energy electron diffraction (LEED), and secondary ion mass spectroscopy (SIMS) have been used to identify the surface contaminants, oxides, metal particulate and reconstruction. Atomic force microscopy (AFM) has been used to monitor the surface cleanliness as a function of topography [7, 8].

The work done by Smith et al. in cleaning GaN has shown that the choice of cleaning chemical is of utmost importance [1]. In their work, they used AES to compare HCl and HF based solutions in methanol and in water, to remove contaminants on the GaN surface. The use of UV/O_3 treatment was also done. All the chemical cleaning was followed by thermal desorption at temperatures of up to 800°C to completely produce a contamination free surface. From their results, it was observed that dissolving HCl in deionised water (DI) resulted in cleaner surfaces as compared to dissolving in methanol. HF results showed that C (carbon) and O (oxygen) residues were lower in HF:DI solution than in HF:methanol solution. These results were

influenced by the physiosorption of methanol, thus increasing C content on the surface of GaN. Comparing HCl:DI and HF:DI, it was found that HF based solution was more effective in removing both C and O on the surface. A further observation was the presence of Cl on the surface after treatment with HCl based solution and UV/O_3 increased the surface oxide while decreasing the C. The best cleaning method according to Smith et al. is the final step in which HF was diluted in deionised water as it removed most of the C, O and Cl without leaving any traces of F on the surface. The thermal desorption results showed further reduction of C and O as the temperature is gradually increased up to 800°C, beyond which the decomposition of GaN was observed.

Further work done by King et al. using XPS and AES, on both AlN and GaN showed that different chemicals may be used to yield atomically clean surfaces [2]. They used HCl, HF, NH_4F, HNO_3, H_2SO_4, H_3PO_4, H_2O_2, NH_4OH, NaOH, KOH, RCA SC1 and SC2 (1:1:5NH_3OH: H_2O_2: H_2O at 85°C and 1:1:5 HCl:H_2O_2: H_2O at 85°C) and TCE, acetone, methanol and UV/O_3 treatment. Thermal desorption was done in an integrated UHV system at temperatures of up to 1100°C. As in the previous work by King et al. UV/O_3 was found to be effective in removing C and simultaneously increasing O on the surface. In addition to reducing the C peak, the exposure to UV/O_3 moved the C peak to higher energies, consistent with oxidation of C species on the surface of GaN. It was observed that increasing ozone concentration further reduced C on the surface though it was not completely removed. Further observations of the UV/O_3 exposed surface, showed an increase in the rate of oxidation of GaN surface, as seen in complete disappearance of N KLL and N1s peaks. The observed oxides were found to be in the form of Ga_2O_3 and N-O at binding energies 20.8 and 398.2 eV respectively.

The use of HCl, NH_4OH and HF solutions were found to effectively remove the oxides. A 1:1 HCl:DI solution was found to produce the lowest C/N ratio with a disadvantage of Cl addition to the surface. The O coverage on the HCl sample was found to be inversely proportional to Cl detected on the surface. According to their results, the fact that the N-Cl bond strength is less than that of Ga-Cl gave an explanation why there is Cl residue on GaN surface. The results of using H_2SO_4 and H_3PO_4 were observed residues of SO_4 and PO_4 on the surfaces of GaN, increasing surface oxide coverage after these treatments. The 1:10 HF-based cleaning solutions

were found to increase the O/N ratio with no detection of F on the surface. Stoichiometric GaN surface was produced after annealing the surfaces at 700 – 800°C in NH_3. Using thermal desorption, it was found that HCl cleaned samples showed complete desorption of all contaminant species on the surface after 950°C. AFM was used to investigate the surface roughness of the cleaned surfaces. All samples had surface RMS roughness comparable with the as grown material, while H_3PO_4 resulted in increased surface roughness from as low as 20 Å to as high as 200 Å. On the GaN surface, the RCA SC1 and SC2 reduced the UV/O_3 oxides, though SC2 left more C on the surface relative to SC1.

Lee et al. investigated several methods of cleaning GaN [3]. The methods included different wet chemical procedures, as well as in-situ cleaning in AES at elevated temperatures. The wet chemical methods consisted of acetone, methanol, HF or HCl and UV/O_3 treatments. Thermal cleaning was done in N_2 and H_2/N_2 plasma. UV/O_3 increased the O on the surface while decreasing the C peak. Using AES, it was observed that the surface of the as-grown (as-received) sample contained about 12% C and 13% O and that the Ga/N ratio was 1.08. Applying photoresist and stripping it with acetone reduced the O content slightly, and increased the carbon content to 30%. Treatment in HCl further reduced the O concentration to 7% and the C content to almost the same level as of the as-grown sample. The HCl treatment also left Cl contamination on the surface. Using thermal cleaning after various chemical treatments reduced the C and O surface content to below the detection limit of AES. AFM results showed insignificant change in surface roughness after all the wet chemical cleaning on GaN surface.

The work by Pelto et al. in pre-metallization treatment of GaN for ohmic contacts fabrication showed that the surface cleaning recipes depends on what device is being fabricated [4]. The following etch recipes were used: H_2SO_4: H_3PO_4: DI (1:1:2), HCl:DI (1:2), HNO_3: HCl (1:3), and NH_4OH:DI (1:10). The ohmic contacts' behaviour depended on the etch recipe used, and the expected outcomes. On the other hand, Machuca et al. used a simple cleaning method focusing on the optimization of electron emitters with wide band gap [5]. Using H_2SO_4: H_2O_2 (4:1) to reduce contaminants on GaN surfaces followed by annealing in vacuum at 700°C, they showed that after chemical clean, the vacuum anneal was best for thermal desorption of C and O than

annealing in NH_3. Both these authors do not comment on any remaining surface contaminants on GaN and their effects on electrical properties of the devices made.

Thermal desorption in the vacuum has been recommended as a final step in most cleaning procedures. In particular, thermal desorption done in vacuum have shown that all the surface contaminants can be reduced to less than the AES detection limit. In the above works done, it can be summarized that thermal desorption of contaminants on GaN is independent of what has been used chemically prior to heating. Heating the material to a temperature range from 800°C to 1000°C has shown complete removal of C all contaminants on GaN surface [1, 2, 3].

The above review shows that there is still a gap in GaN cleaning procedures used prior to metallization. There is a need to test the effects of chemical cleaning procedures by evaluating electrical characteristics of devices. In this work, we have investigated chemical cleaning of GaN surfaces and evaluating the results with AFM and AES. A variety of wet chemistries for O and C removal were investigated. We particularly report on the effects of HCl, KOH and $(NH_4)_2S$ on GaN surfaces. In addition we give thermal cleaning results.

5.2 Experimental

n-GaN samples of orientation (1000) and unintentional doping of $1.6 \times 10^{16} cm^{-3}$ were obtained from AIXTRON, grown by metal organic chemical vapor deposition (MOCVD) on sapphire (Al_2O_3) substrate. The thickness of the GaN layer was 1μm. The cleaning methods used are summarized in Table 5.1. All samples were finally blown dry with compressed nitrogen gas of ultra-high pure quality. Only analytical grade quality chemicals were used and all water rinses were done in deionised water ($\rho > 18$ MΩ.cm). All samples used in this study were cut from the same wafer for compatibility . Ultrasonic rinse was employed to ensure the removal of all loose debris on the surface. All cleaning equipments used were made of pure quarts glass and Teflon. Samples were loaded into the AES immediately after wet chemical cleaning. AES analysis was carried out on Physical Electronics Model 545 Spectrometer, using a cylindrical mirror analyzer with 5 keV electron beam incident on samples mounted on a sample holder of which the angle with the electron beam is 30°. The percentage surface concentration was calculated from the peak-to-peak heights and relative sensitivity factors for different elements.

Thermal cleaning was done by mounting the degreased sample onto a heater block and loaded into the AES, PHI model 549. The analysis was carried out from room temperature of 23°C, continually monitoring the surface up to a temperature of 1100°C. The heating process was stopped at this stage to avoid any decomposition of GaN into the AES system. The scanning probe microscope used in this study was a commercial instrument model, Topometrix 2000 Discoverer. The topographical features of GaN crystals were studied by means of AFM in contact mode. The 130 µm and 7 µm scanner and standard Topometrix Si_2N_3 tips were applied. All scans were applied under ambient conditions. Several images were taken at different positions on the sample to gain better understanding of the surface topography. The same scan parameters (set point, proportional gain, integral gain and derivative gain) were used, however, in each scan optimizations were performed. The topography of the surfaces were analysed from obtained images, using the surface roughness parameters: the root mean square (RMS) roughness, maximum peak height from the mean line, $R_{p;}$ the maximum peak to valley height in the profile, R_t,

Table 5. 1

Outline of cleaning procedures

Number	Method	Procedure
1	Degrease	Boil in Trichloroethelyne for 3 min Boil in Isopropanol for 3 min 3 rinses in DI for 20 sec each Blow dry with N_2
2	Aqua Regia (AR)	Degrease Boil in $HCl:HNO_3$ = 3:1 for 8-10 min 3 rinses in DI for 20 sec each Blow dry in N_2
3	HCl	Degrease Aquaregia $HCl:H_2O$ = 1:1 dip for 60 sec 2 rinses in DI for 20 sec each Blow dry with N_2
4	KOH	Degrease Aquaregia 1mol KOH boil for 3 min 3 rinses in DI for 60 sec each Blow dry with N_2
5	$(NH_4)_2S$	Degrease Aquaregia $(NH_4)_2S$ for 1 min 3 rinses in DI for 60 sec each. Blow dry with N_2

5.3 Results and Discussion

5.3.1 Atomic Force Microscope

AFM images from randomly selected 5 X 5 μm^2 areas of degrease to $(NH_2)_4S$ cleaned surfaces and corresponding line profiles are presented in Figure 5.1- 5.5. The images, together with corresponding line profiles, indicate difference in topography of investigated GaN surfaces after every cleaning method. The as grown surface has been degreased to deal with packaging contaminants.

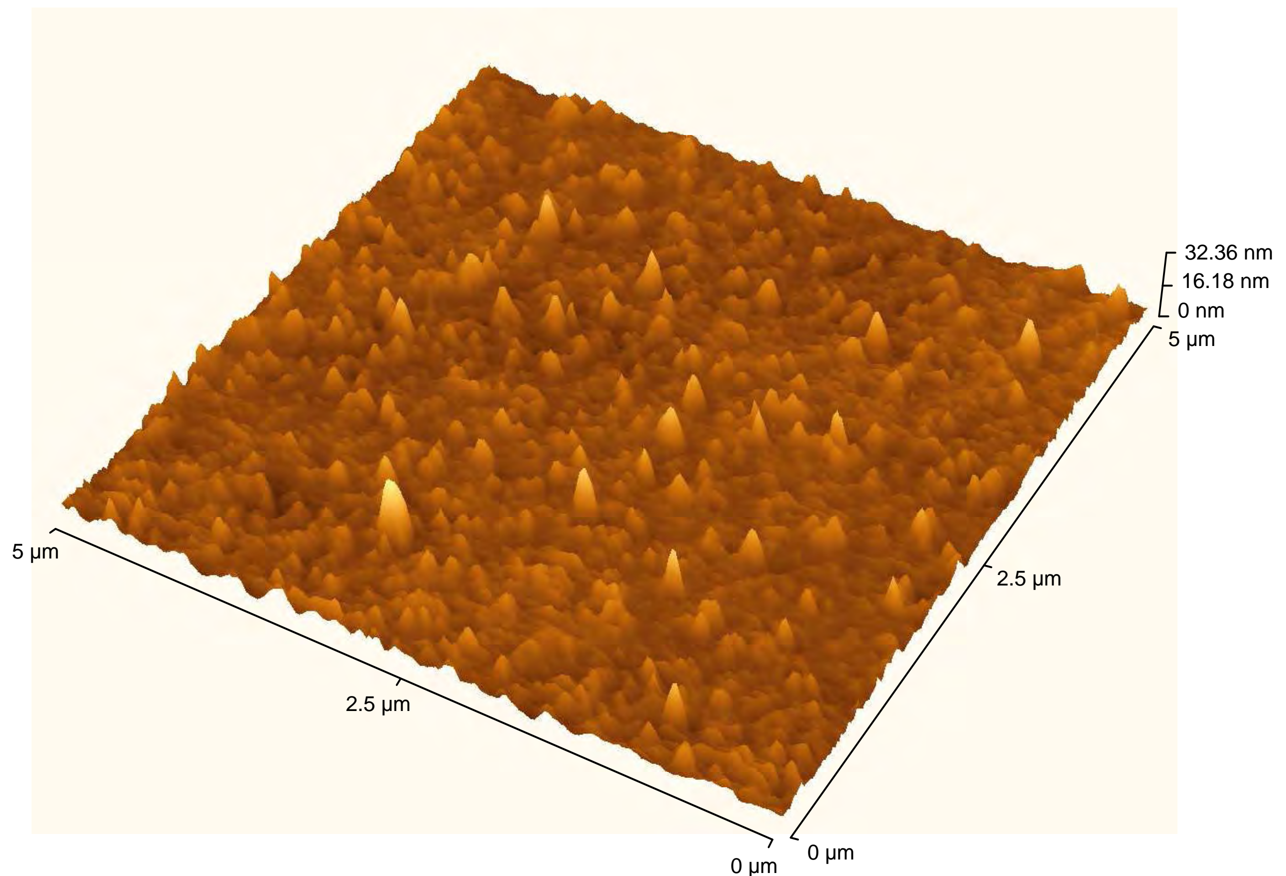

Figure 5.1 (a): AFM images taken from selected degreased 5 µm x 5 µm areas of GaN.

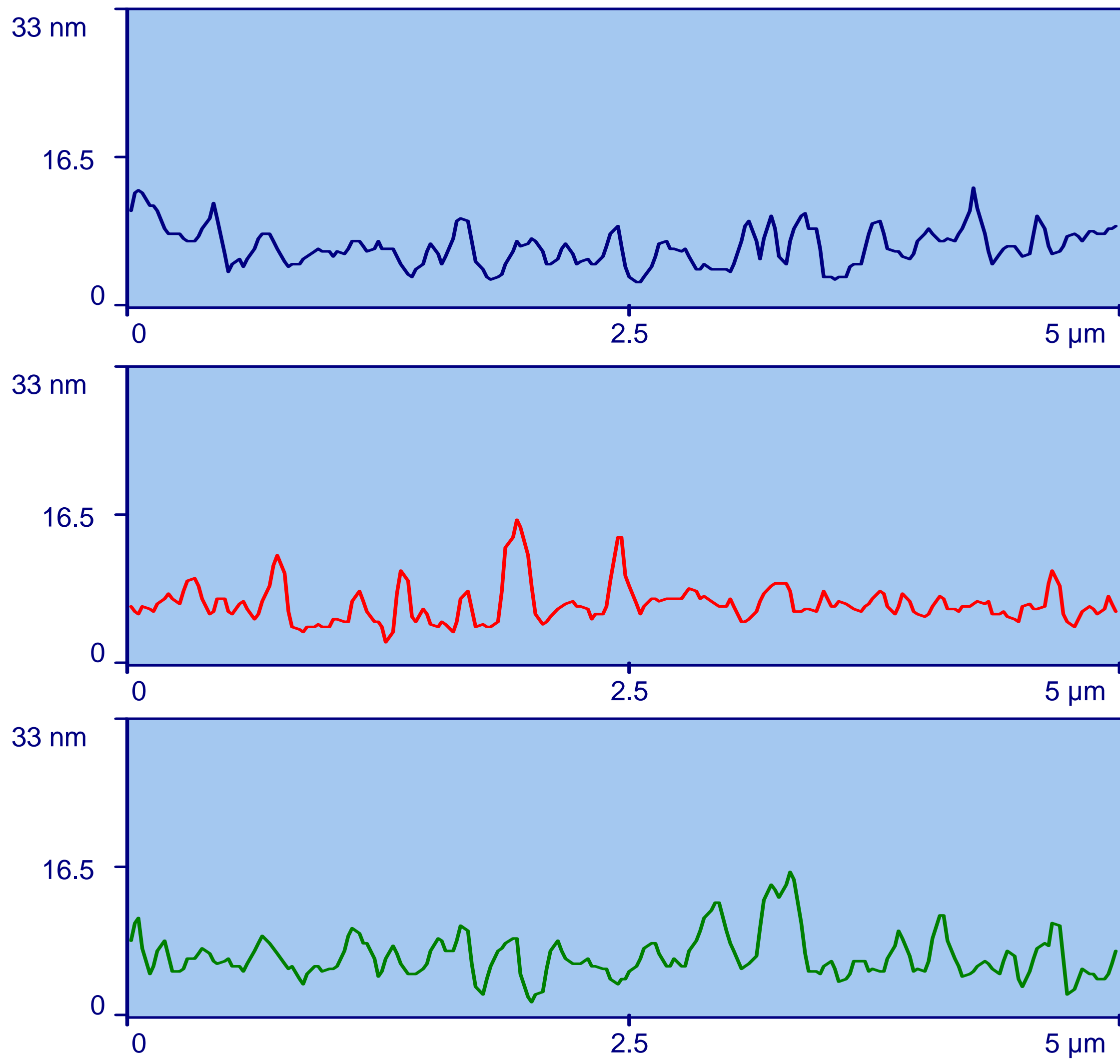

Figure 5.1(b): The corresponding line profiles of AFM images taken from selected degreased 5 µm x 5 µm areas of GaN surfaces cleaned.

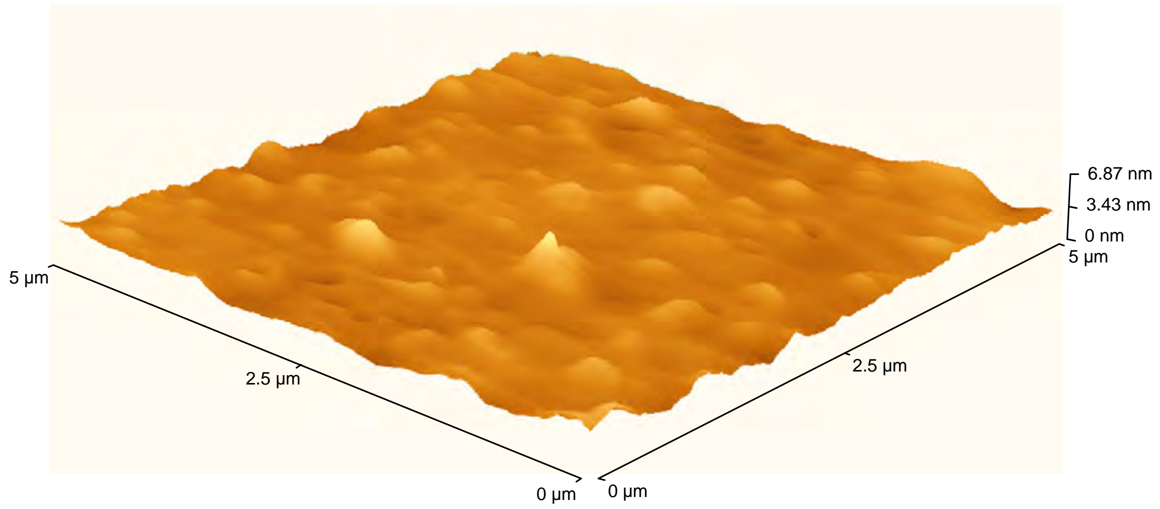

Figure 5.2 (a): AFM images taken from selected aquaregia cleaned 5 µm x 5 µm areas of GaN.

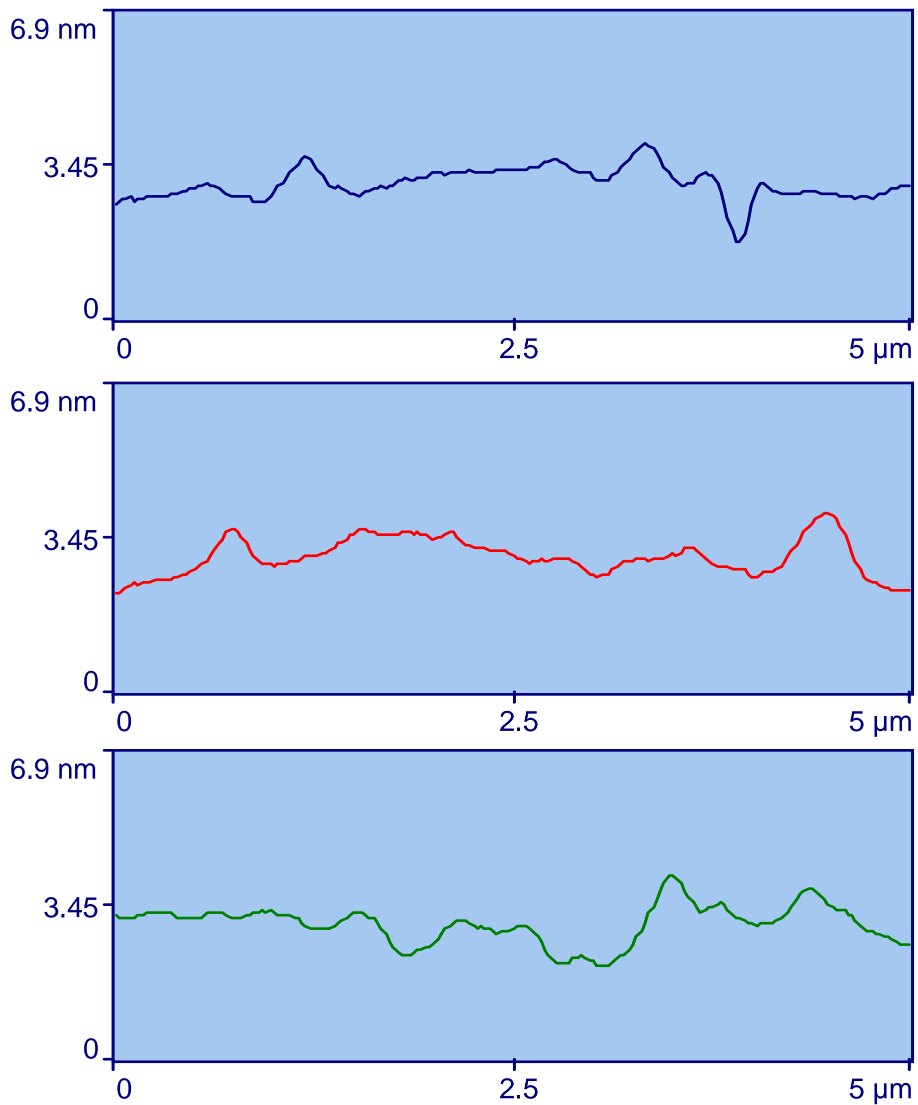

Figure 5.2(b): The corresponding line profiles of AFM images taken from selected aquaregia cleaned 5 µm x 5 µm areas of GaN.

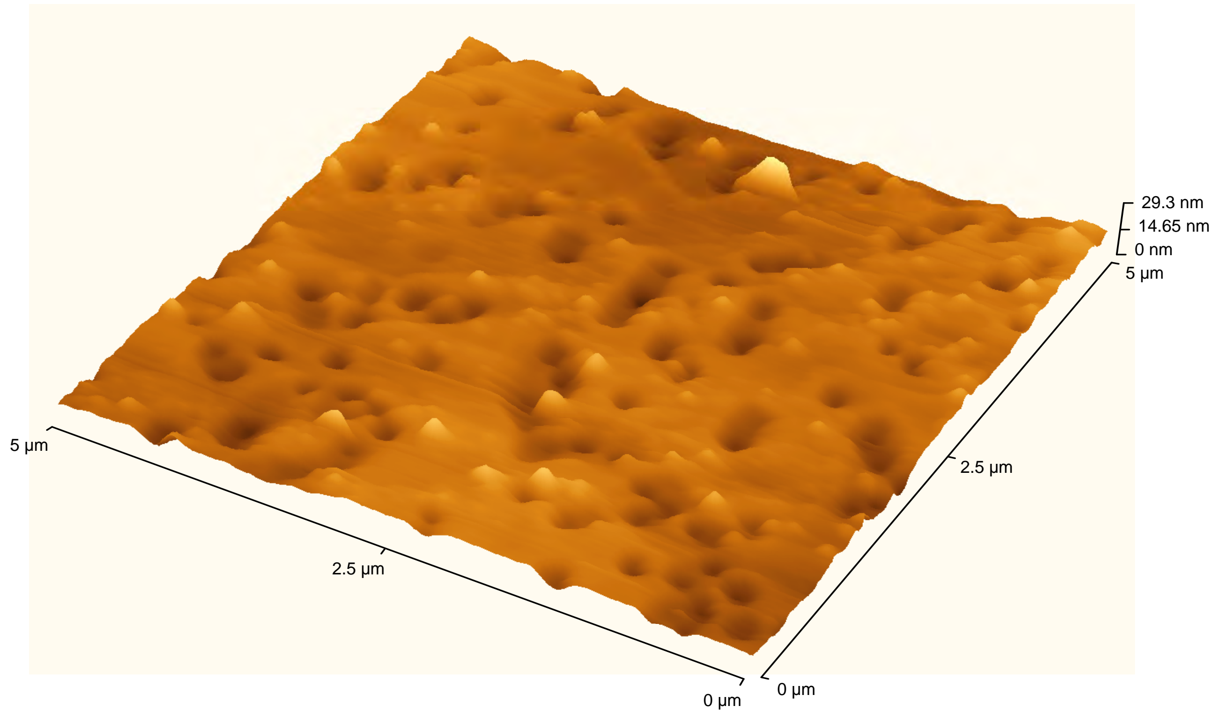

Figure 5.3 (a): AFM images taken from selected HCl cleaned 5 µm x 5 µm areas of GaN.

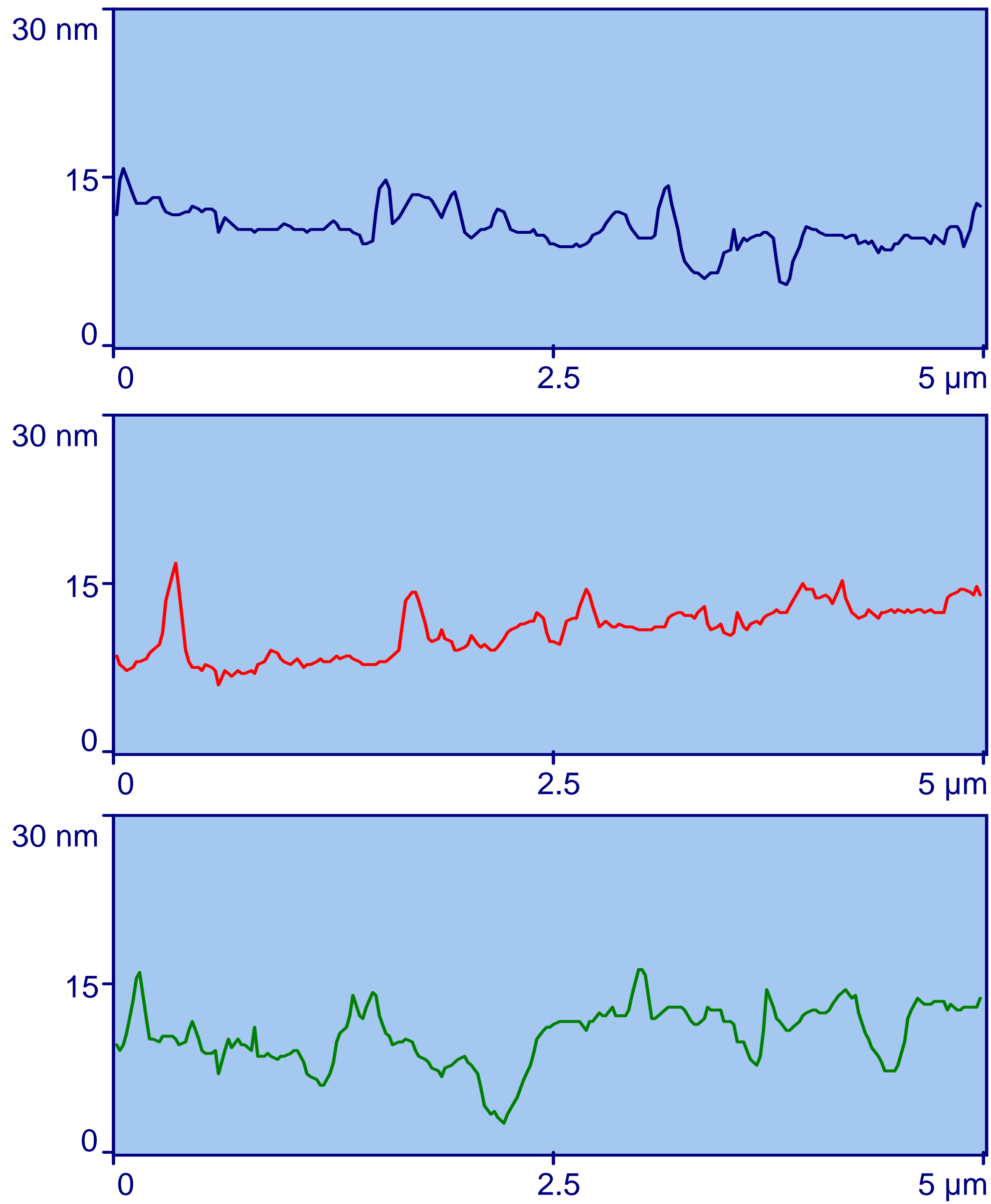

Figure 5.3(b): The corresponding line profiles of AFM images taken from selected HCl cleaned 5 µm x 5 µm areas of GaN.

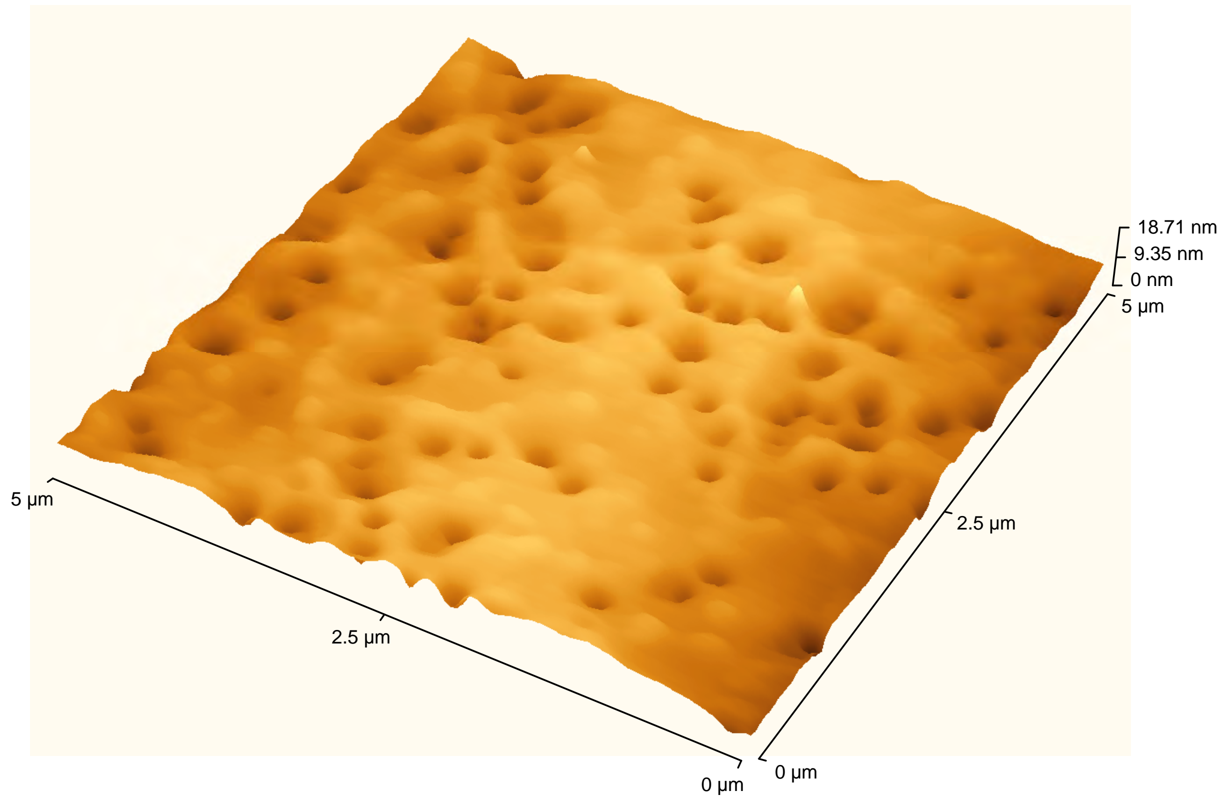

Figure 5.4 (a): AFM images taken from selected KOH etched 5 µm x 5 µm areas of GaN.

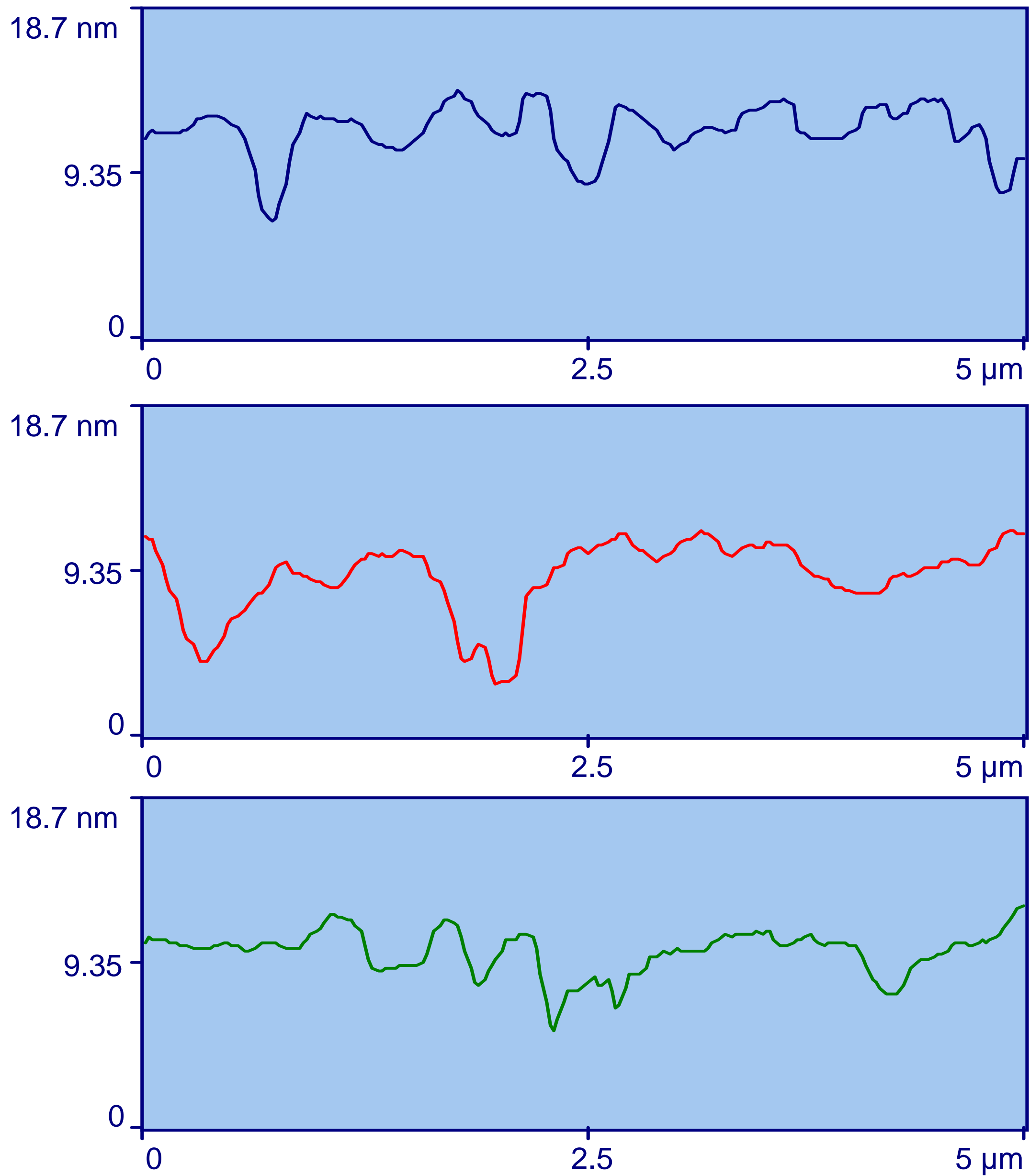

Figure 5.4(b): The corresponding line profiles of AFM images taken from selected KOH etched 5 µm x 5 µm areas of GaN.

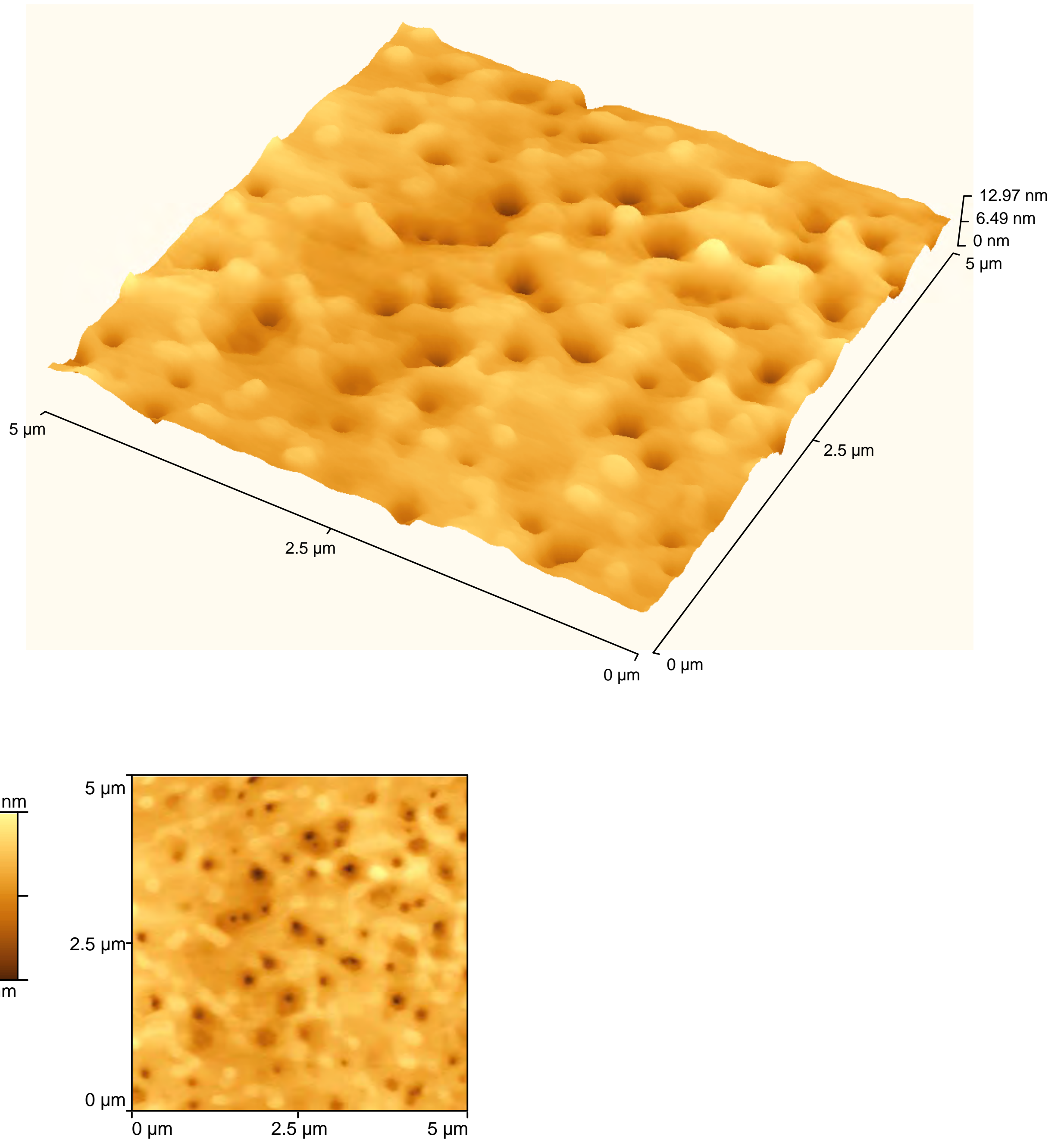

Figure 5.5 (a): AFM images taken from selected $(NH_4)_2S$ etched 5 µm x 5 µm areas of GaN and the corresponding flat image.

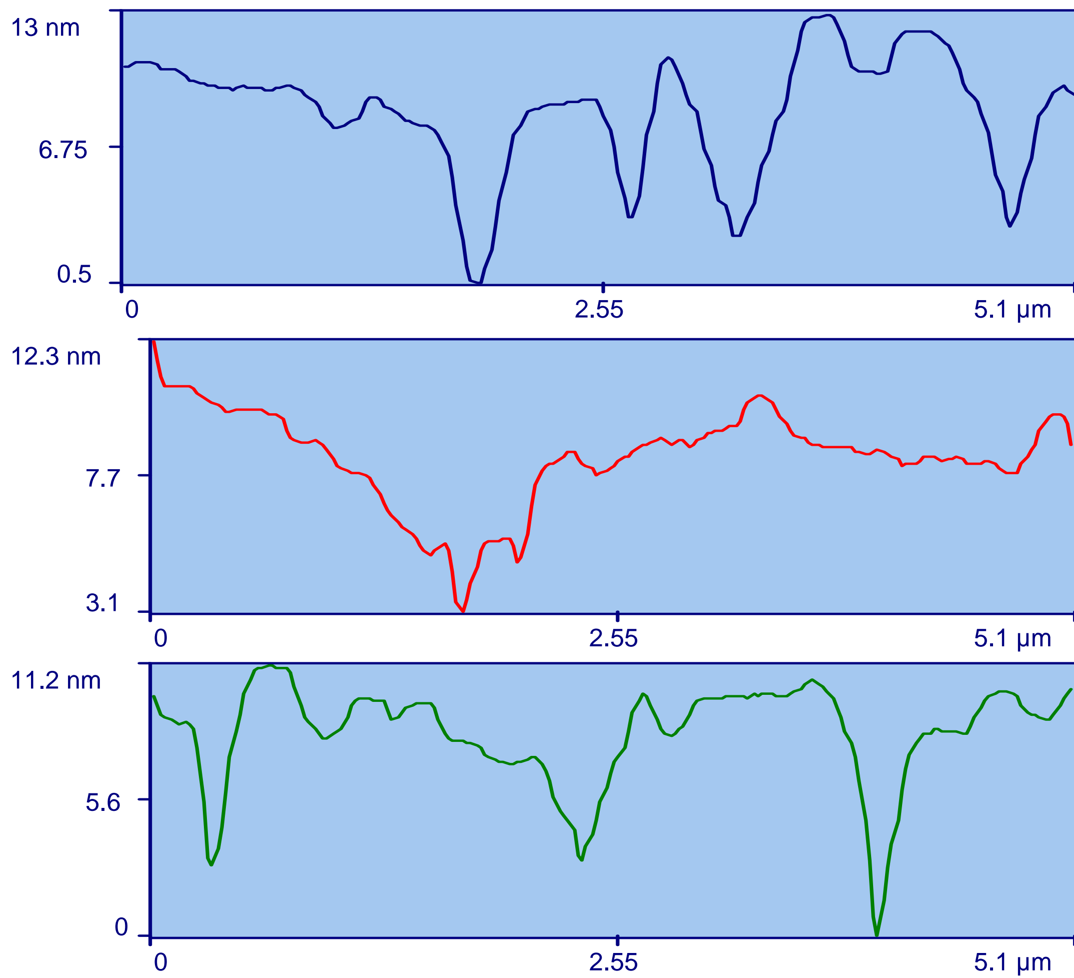

Figure 5.5(b): The corresponding line profiles of AFM images taken from selected $(NH_4)_2S$ etched 5 µm x 5 µm areas of GaN.

The as grown surface has needle-shaped protrusion as shown in Figure 5.1(a) and (b) is the corresponding line profile. Using R_t, we compared the difference in features, ranging from protrusions to craters. From R_t measurements, the average height of the protrusions on the surface of the degreased samples was found to be 20.05 nm, as shown in Table 5.2. The second surface, represented in Figure 5.2(a) and (b), was cleaned in aqua regia and shows a disappearance of the protrusions and the emergence of craters, which are hexagonal in shape, with R_t value decreasing to 2.5 nm. This observation implies that the chemicals used thus far, were able to act on the protrusions on the as degreased surface, characterizing GaN by showing hexagonal structure of the crystal.

Table 5.2: Statistical Characterization of GaN samples by AFM.

Cleaning Procedure	Maximum topography variation (R_t-nm)	Mean topography variation (R_p-nm)	RMS surface roughness	Roughness factor
degrease	20.05	11.27	1.74	1.006
aquaregia	2.5	1.55	0.4	1.060
HCl	13.36	7	2.02	1.010
KOH	11.03	4.03	2.1	1.077
$(NH_4)_2S$	8.74	2.74	1.2	1.098

The next step is etching the surface in HCl, and it is observed that protrusions are disappearing from the surface and craters are increasing, as shown in Figure 5.3(a) and (b). These craters are either isolated or joint to form a bigger crater on the surface and the value of R_t increasing to 13.36 nm, indicating deeper craters as protrusions are removed. The surface protrusions seem to have changed shape, from needles to rounded protrusions. The use of KOH on the surface, as shown in Figure 5.4(a) and (b), shows that the protrusions appeared to be white and flat shaped. In Figure 5.5(a) and (b) the surface of the samples cleaned in $(NH_4)_2S$ are shown. The protrusions on this surface are quite similar to the ones on the KOH etched surface. A two

dimensional (2D) image of the sample cleaned in $(NH_4)_2S$ is shown in Figure 5.5 (a), confirming that the observed protrusions on the surface are part of the crystal.

The density of craters on each of the three last cleaning processes is similar, particularly for the HCl and KOH surfaces at approximately 6.2 x 10^8cm^{-2}. The $(NH_4)_2S$ surface has a little lower density of craters at approximately 5.3 x 10^8 cm^{-2}. The approximated density of craters is similar to the dislocation density of the GaN used in this experiment, which is approximated to be 10^7 to 10^8 cm^{-2}. Comparing the cleaning procedures, it was found that GaN was etched along the threading dislocation. Threading dislocations have been found to be dominant defects in GaN from TEM studies. In addition, the observed decrease in the density of the craters shows that a new surface has appeared. It has been observed from TEM studies that threading dislocation decrease gradually away from the interface [9]. KOH has been used to characterize defects in GaN, and the defects density was found to be 2 x 10^9 cm^{-2}. Different values of defect densities have been recorded as 3 x 10^7 cm^{-2} and 4 x 10^7 cm^{-2} on N-face, and 1 x 10^7 cm^{-2} and 5 x 10^5 cm^{-2} on Ga-face. The understanding of the mechanisms for the formation thereof, will lead to the reduction of these defects [10].

Using line profiles, statistical parameters were deduced from the AFM for each of the cleaning procedures and are shown in Table 5.2 [11]. From the analysis of these data, the morphologies of differently cleaned surfaces differ from one cleaning method to the other. The value of R_t changed from 20.5 nm for degreased sample to 2.5 nm after aqua regia treated, implying a removal of surface protrusions. The last three etch processes also differ in the value of R_t, indicating how one chemical is able to etch the GaN surface. KOH and $(NH_4)_2S$ each were able to produce new surfaces as compared to HCl, which was not able at producing a new surface. The other parameters, R_p, RMS roughness and the roughness factor all confirm the R_t values. The highest RMS roughness is from the KOH etched surface and the lowest is from the aqua regia cleaned surface. Furthermore, using RMS roughness parameter, we have compared the stoichiometries on each of the cleaned surfaces, and stoichiometry and RMS roughness are compared as shown in Figure 5.6.

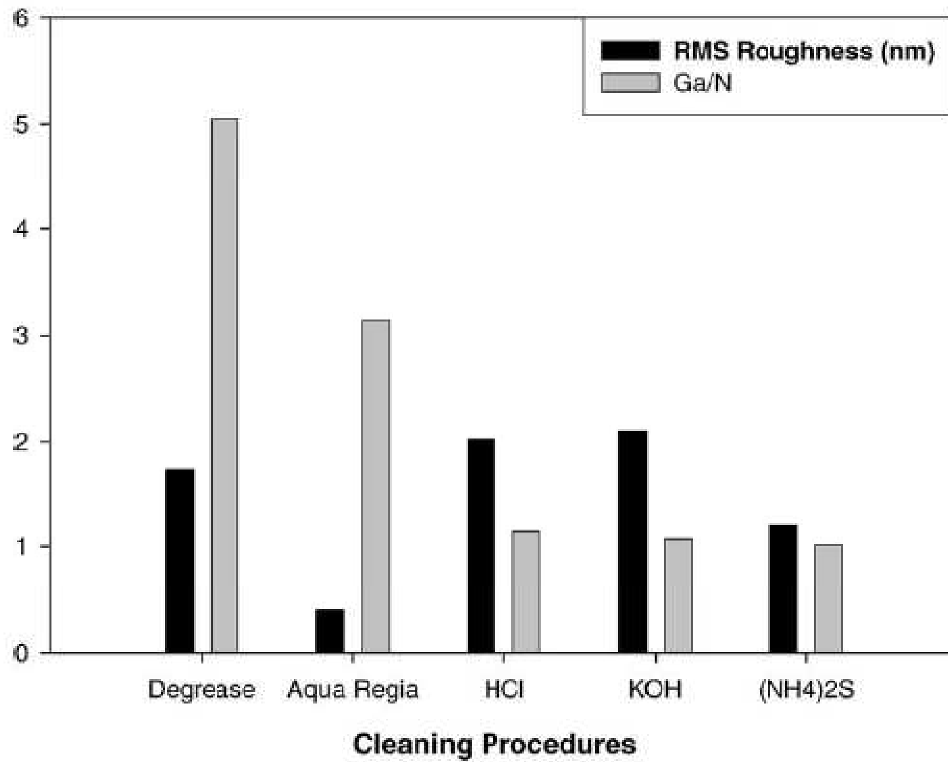

Figure 5.6: Graph of root mean square (RMS) surface roughness and Ga/N ratio from AES elemental surface concentrations.

5.3.2 Auger Electron Spectroscopy

AES was used to analyze the surface contaminants and the results are shown in Figure 5.7. The effect of the cleaning procedure is seen in the reduction of O and C peaks. In addition to reducing C and O peaks, HCl in aqua regia and $(NH_4)_2S$, respectively, added Cl and S to the surface. The atomic percentage of surface elements present on every surface after wet chemical cleaning procedures was calculated from the relative sensitivity factors. These contaminants may be of advantage to the metal contact formation on the GaN surface as bonding with Au may be enhanced and adhesion improved. Furthermore the use of sulfurants, alkenoids and halogens has proved to enhance adhesion of metals such as Au, Ag, Pt, Pd and Ni to semiconductor surfaces [12,13].

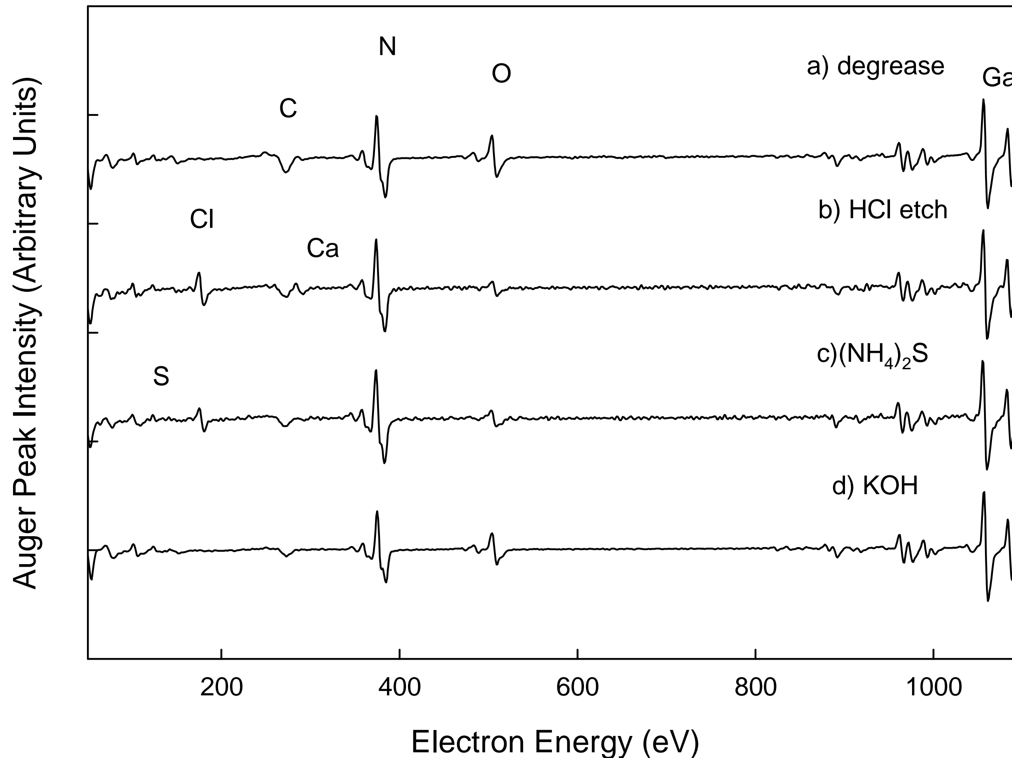

Figure 5.7: AES surface scans of GaN surface cleaned as indicated.

Comparing the AES surface scans of HCl and $(NH_4)_2S$, it is found that using HCl on the GaN surface reduced the O peak, added Cl, and the use of $(NH_4)_2S$ prevents re-oxidation of the surface, adding insignificant amount of S, and reducing the Cl contaminant. This result further confirms the importance of using $(NH_4)_2S$ as a chemical that prevents re-oxidation of surfaces. KOH removed all the Cl from the surface, and reduced the C significantly.

There had been reports of improved electrical characteristics of metals/GaN contacts after treatments in HF, HCl, and NaOH. E. J. Miller et al has reported the reduction of reverse bias leakage current in GaN Schottky diodes after treatment in NaOH. The high concentration of OH-ion on the GaN surface is attributed to the reduction of reverse bias leakage in their Schottky contacts [14]. In another report, Y-J Lin et al has reported the reduction of surface

states on InGaN using $(NH_4)_2S$ [15]. Electrically, $(NH_4)_2S$ was reported to reduce the Schottky barrier height. In particular, it was reported that Ga-O, In-O and C-O bonds were removed from the InGaN surface after $(NH_4)_2S$ treatment. Furthermore, repeated exposure of the surface that has a Cl peak to the electron beam in the AES system has resulted in desorption of the surface contaminants, and consequently, complete removal of the Cl peak.

To further analyse the cleaned surfaces, the ratio of Ga/N, and RMS surface roughness are plotted as a function of cleaning method, as shown in Figure 5 above. There is a relationship between the RMS surface roughness and the contaminants on the surfaces, which consequently affects the Ga/N ratio. The as grown surface shows a very high surface roughness and Ga/N ratio and the cleanest surface shows lowest surface roughness and Ga/N ratio. Therefore as the surface is cleaned, the surface roughness reduces as the Ga/N ratio improves, implying that the chemicals used has etch GaN surface to removes contaminants. The RMS surface roughness of KOH etched surface, differ from the as grown surface by about 0.4 nm. Different wet chemicals used previously in removing contaminants on GaN have shown no effect on the surface roughness of the material [2,3]. The work done previously to etch and remove surface GaN to form etch steps were not achieved by using HCl and KOH [15]. Ultraviolet light illumination and addition of ions were used to etch GaN successfully in KOH [16].

Previous results have recommended the use of thermal desorption after every chemical clean, to completely remove surface contaminants [1,2,3]. In this work, we have found that thermal cleaning of the degreased GaN surface resulted in almost complete removal of surface contaminants. Figure 5.8 is a typical temperature profile of a sample cleaned in UHV under high temperatures. This profile may be divided into two regions: region 1 from 23°C to 500°C and region II from 500°C to 1010°C. In region I the carbon peak first decreases and then increases as temperature increases. In region II, the carbon coverage on the surface of GaN decreases until it drops to below AES detection limit, where average peak-to-peak height is less than 1.5. In the case of oxygen, the surface coverage starts increasing and quickly decreases sharply until the temperature of about 500ºC. At this temperature, all oxides are removed from the surface according to AES sensitivity, in which average peak-to-peak height is less than 0.5. The increase in O from 23°C to 50°C may be attributed to the removal of common surface water that had been

covering the surface prior to thermal heating. This water is very sticky and is usually removed at temperatures above 220 °C. On the other hand, the increase in C may be due to segregation from the bulk, which needs further study to confirm.

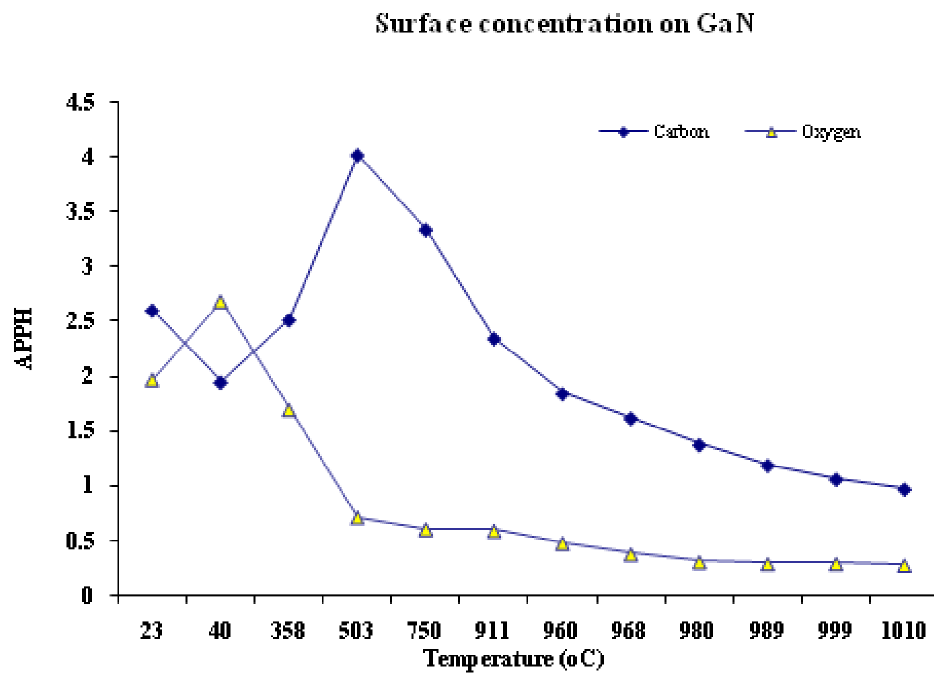

Figure 5.8: Surface concentration profiles of O and C on GaN surface during thermal anneal in the AES.

5.4 Conclusions

In conclusion, the effectiveness of wet chemical cleaning of GaN with different solutions, have been characterized by AFM and AES. AFM results have shown that GaN surface roughness is affected by the cleaning method used on the surface. Surface defects were characterized by different etch chemicals, with $(NH_4)_2S$ producing a defects free interface. AES has shown the contaminant as C and O and that using HCl and $(NH_4)_2S$, will leave Cl and S on the surface. This result has given sufficient information on removal of surface contamination; stoichiometry; surface roughness and chemical etch. Using $(NH_4)_2S$ prevented re-oxidation of the surface, and further removes Cl from the surface of the GaN. KOH effectively removes the C on the surface. The effects of S and Cl on the surface may enhance adhesion of metals to GaN surface, thus improving device quality. Further work is necessary in finding the effects of different cleaning procedures on the optical properties of the material and electrical properties of devices.

REFERENCES

[1] Smith L. L, King S. W, Nemanich R. J, Davis R. F, Journal Electronic Materials **25** (1996) 805.

[2] King S. W., Barnak J. P., Bremster M. D., Tracey K. M., Ronning C., Davis R. F., Nemanich R. J., Journal of Applied Physics **84** (1998) 5248.

[3] Lee K. N., Donovan S. M., Gila B., Overberg M., Mackenzie J. D., Abernathy C. R., Wilson R. G., J. Electrochemical Society **147** (2000) 3087.

[4] Pelto C. M., Chang Y. A., Chen Y., Williams R. S., Solid State Electronics **45** (2001) 1597.

[5] Machuca F., Liu Z., Sun Y., Pianetta P., Spicer W. E., Pease R. F., Journal of Vacuum Science and Technology A **20** (2002) 1784.

[6] Shul R. J., Vawter G. A.., Willison C. G., Lee J. W., Pearton S. J., Abernathy C. R., Solid State Electronics **42** (1998) 2259.

[7] Nel J. M., Demanet C. M., Hillie K. T., Auret F. D., Gaiger H. L., Applied Surface Science **134** (1998) 22.

[8] Deenapanray P. N. K., Auret F. D., Myburg G., Hillie K. T., Demanet C. M., Surface and Interface Analysis, **26** (1998) 748.

[9] Jasinki J., Swider W., Liliental-Werber Z., Visconti P., Jones K. M., Reshchikov M. A., Yun F., Morkoc H., Park S. S., Lee K. Y., Applied Physics Letters **78** (2001) 2297.

[10] Morkoc H., Materials Science and Engineering **R33** (2001) 135.

[11] Zymierska D., Auleytner J., Kobiela T., Dus R., Physica Status Solidi(a) **180** (2000) 479.

[12] Wang J., Zeng B., Fang C., Zhou X., Journal of Electroanalytical Chemistry **484** (2000) 88.

[13] Shalish I., Shapira Y., Burstein L. and Salzan J., Journal of Applied Physics **89** (2001) 390.

CHAPTER 6

Experimental Results

Study of metal contacts on GaN for transmission of UV light

6.1 Introduction

Schottky barrier metal-semiconductor contacts are a choice device for the fabrication of ultraviolet [1]. They have simple fabrication technology; suffer lower breakdown voltages, have larger leakage currents at lower voltages as compared with p-n structures of the same semiconductor material. Thus the formation of Schottky contact with high barrier height, low leakage current [2], and good thermal stability [3] to withstand high temperature processing and operation are some of the most important factors in improving the performance of Schottky barrier photodiodes to be used for ultraviolet detection.

Different metals have been used for the formation of such contacts, including Au, Ni and Ni/Au. Sheu et. al. have discovered the high transparency of Ni/Au contacts to GaN, using the metal structure for ohmic contacts to p-GaN. After annealing the contacts at 550 °C, they recorded a transmittance of above 80 %, after forming NiO [4]. NiO is a transparent wide bandgap semiconductor which is very easy to fabricate by annealing Ni in air or in oxygen. This semiconductor is p-type with a bandgap of 4.3 eV [5]. NiO has been used to study the electrical properties of oxidized Au/NiO_x/p-GaN ohmic contact and found that annealing this structure is the main mechanisms that is responsible for the ohmic contact nature of the system [6]. Furthermore, NiO/ZnO structure has been used to study the defects in ZnO [7]. The optical transmittance of 5 nm Au and Ni ultra-thin films is less than 40 % [8]. In this work, we report on the study of Au, Ni, and Ni/Au contacts onto GaN for the fabrication of ultraviolet detectors.

6.2 Choice of metal for transparent contacts

In fabricating UV detectors of Schottky type to GaN, the metal contact must be transparent to UV light. Published works have used a metal layer of high work function and 10 nm thickness onto GaN [2]. A computer modeling program was used, employing the knowledge of the absorption coefficient of GaN and the metal thickness. UV light was focused onto metal/GaN structure and the transmission percent of the structure as a function of UV wavelength range from 240 to 400 nm was recorded. The choice of the metals was due to high work function and availability. Metals with high work function produce high barrier height for Schottky diodes onto semiconductors. Figure 6.1 show the simulation results of the designed metal/GaN photodiodes using different metals. The result of the model made Ag, Au, Ni suitable candidates for fabrication of UV detectors. Ag was abandoned as it was oxidizing easily.

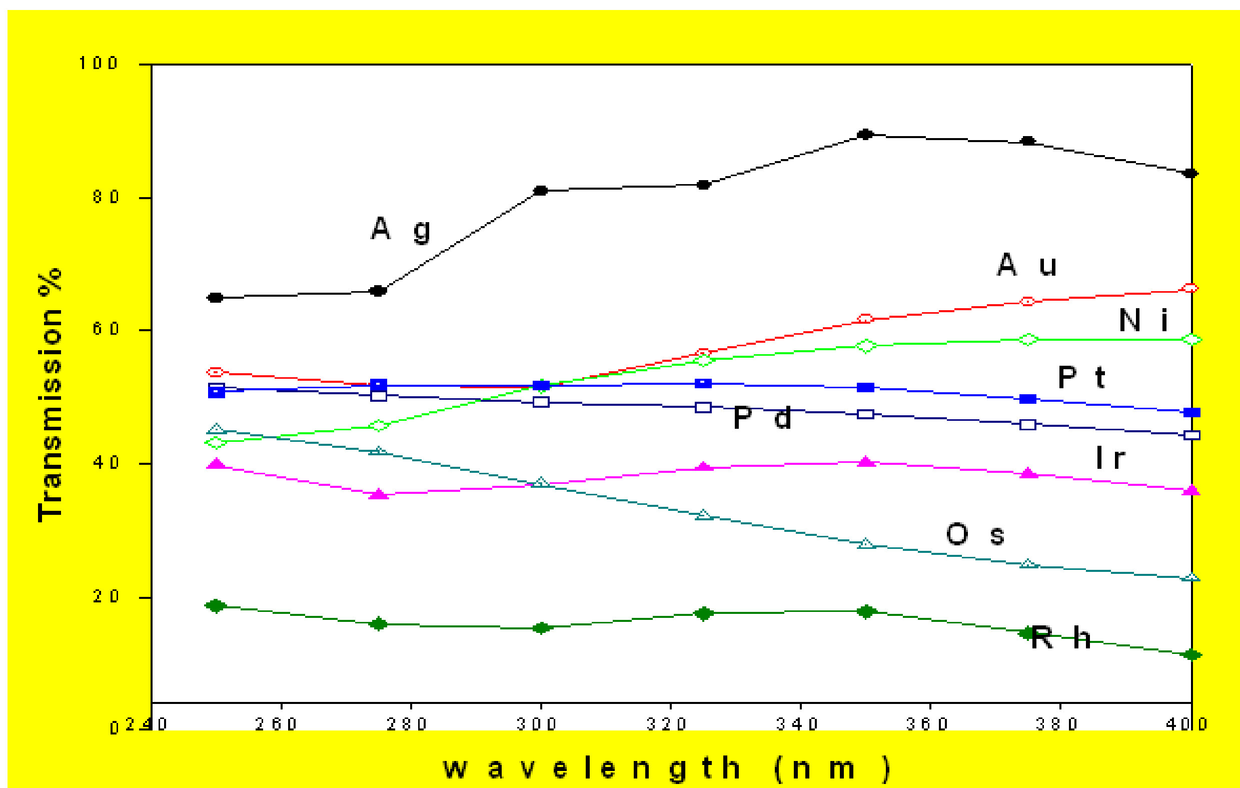

Figure 6.1: Simulation results for the designed metal/GaN photodetector, with Au being highly transparent.

6.3 Experimental

GaN samples were degreased in trichloroethylene and isopropanol; then boiled in aquaregia and finally etched in HCl: H_20 (1:1). Ti/Al/Ni/Au (15 nm /220 nm /40 nm /50 nm) ohmic contacts were electron-beam deposited onto samples and annealed at 500 °C for 5 minutes in air. Circular Au, Ni and Ni/Au Schottky contacts of diameter 0.6 mm were resistively evaporated onto GaN through a metal mask at room temperature. To ensure temperature stability during deposition, the glass dome was cleaned of all metal residues before loading the samples for metallization. The thickness of the Au and Ni layers was 10 nm, and that of Ni/Au was 5/5 nm. Atomic Force Microscope (AFM) was used to study the morphology of Ni and Au onto GaN. Auger Electron Spectroscopy (AES) was used to characterize the Ni/Au layer after annealing in air for 5 minutes at 550 °C. Current voltage (I-V) measurements were taken using an HP4140B pA meter/DC source for all metal contacts.

6.4 Results and Discussion

Analysis of the metal films for continuity using AFM is presented in figure 6.2. The surface structure of all particles, even inside the etch pits, was found to be the same, indicating that the 10 nm metal film is continuous. Comparing Au and Ni, it is found that their surface structures on GaN differ. Ni films present smooth morphology and Au shows grained structures. The RMS roughness of the 10 nm Au and Ni are 25.6 and 22.7 nm respectively. Choosing an area without any etch pits, it was found that the peak-to-valley surface roughness of Ni films was approximately 9,0 Å and RMS roughness of 1.5 Å shows that the Ni films are relatively smooth. The Au peak to valley roughness was recorded as 11 nm and the RMS roughness 2.3 nm.

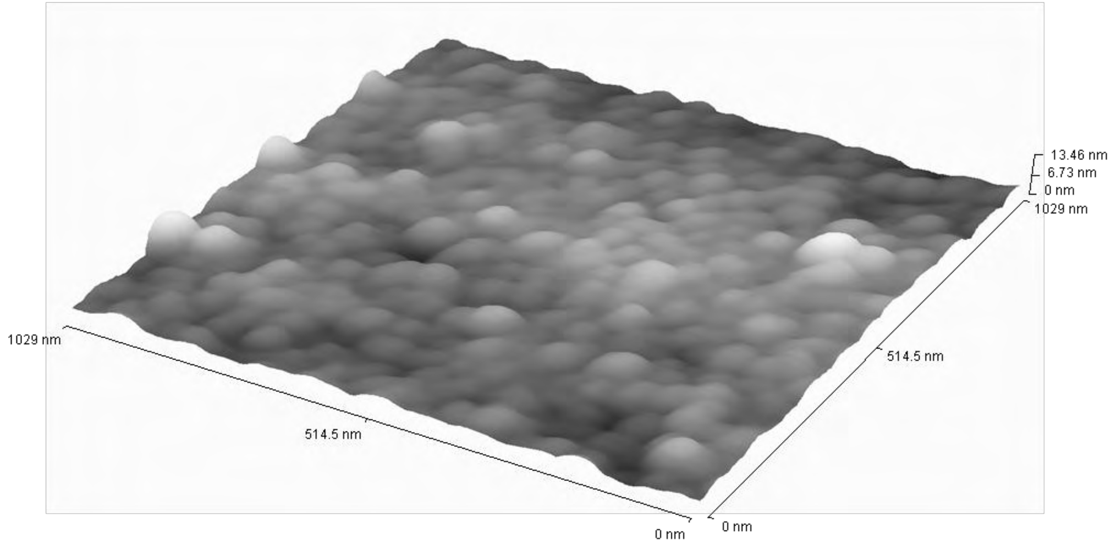

a) 10 nm Au layer

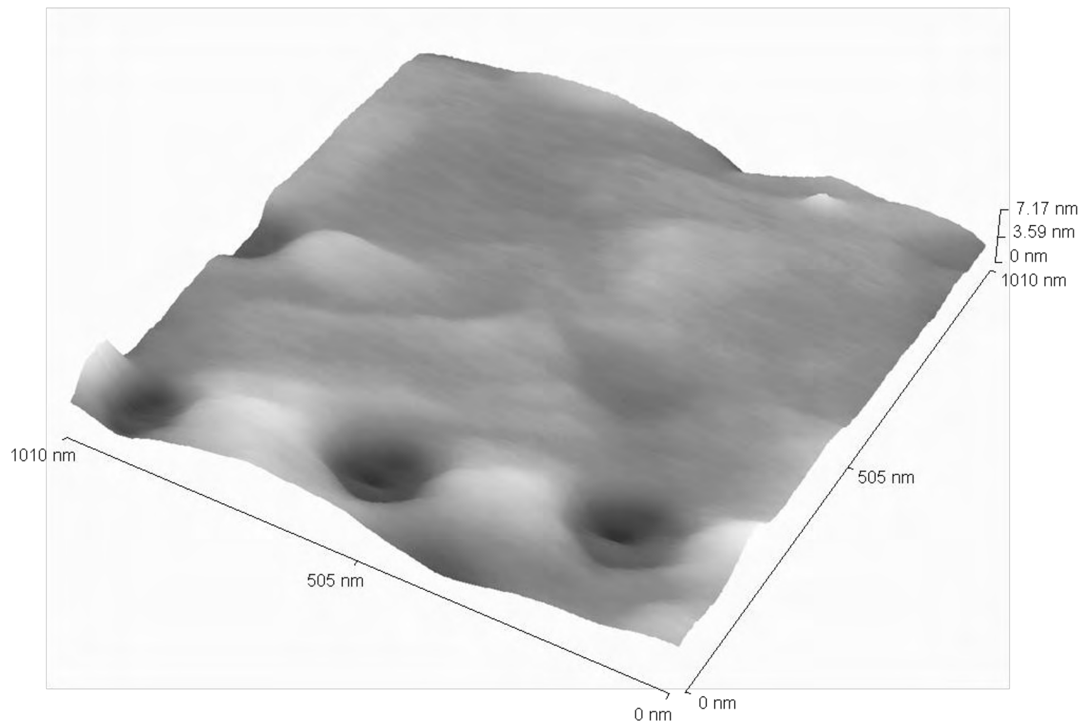

b) 10 nm Ni layer

Figure 6.2: The AFM images of 10 nm Au and Ni.

Figure 6.3 shows the Auger peak to peak heights (APPH) depth profiles as a function of sputtering time for as deposited (a) and annealed (b) at 500°C Au/Ni/GaN in air. The elements presented on the surface before anneal are Au, Ni, Ga, N and O as indicated. Figure 6.3(b) shows the formation of sandwiched layers after anneal. At highest APPH, we identify Au layer, presenting a compound as a result of annealing. The compound may be due to diffusion of elements during annealing. O and Ni compounds are also identified, followed by Ga and N compound. A diffused layer of Ni and Ga is seen at the beginning, showing a possible diffusion of Ni into GaN. At the end of sputtering, the depth profiles show that there exists a 1:1 ratio of Ni and O, indicating possible formation of NiO.

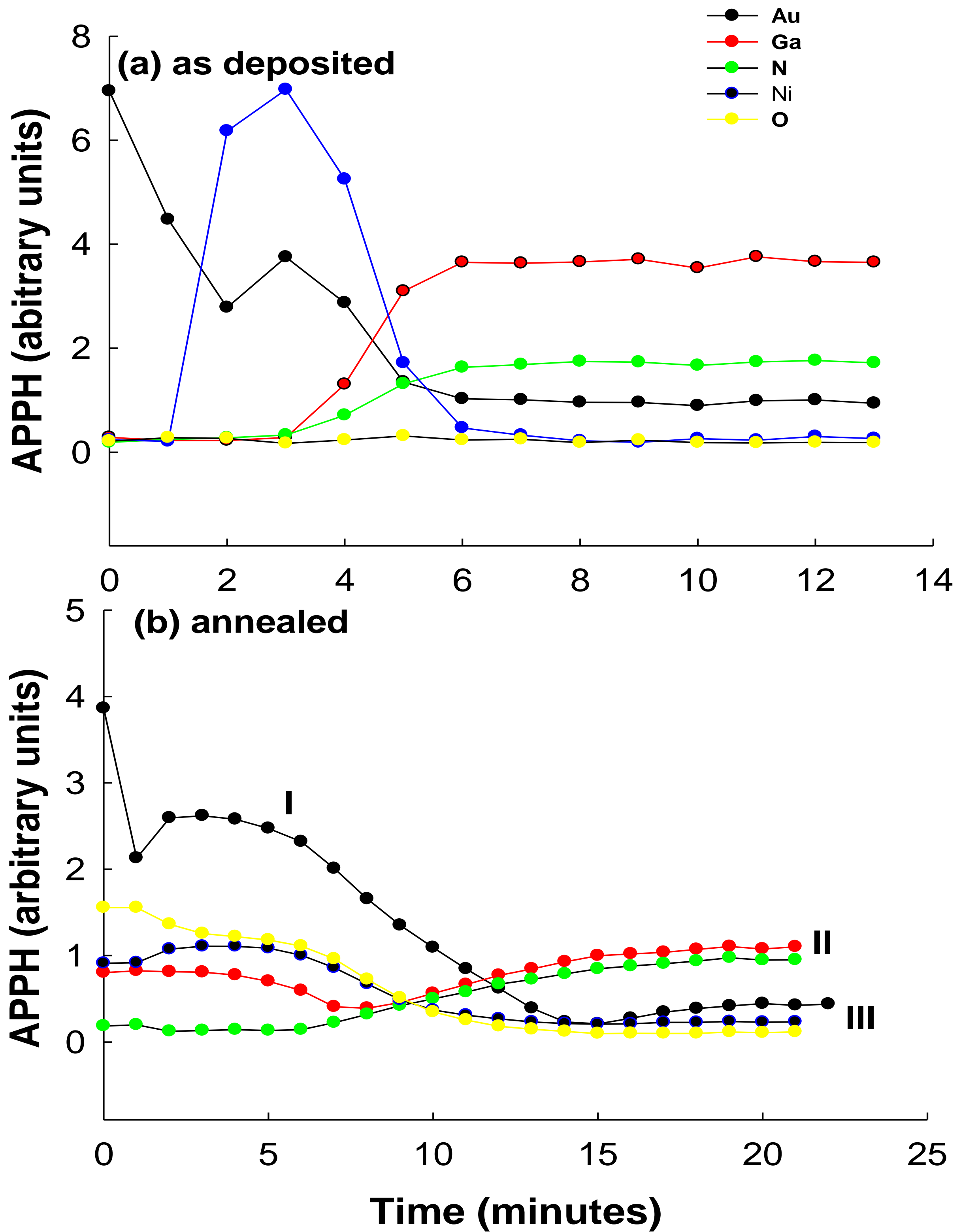

Figure 6.3: AES profiles of sputtered GaN/Ni/Au surface, (a) as deposited and (b) annealed.

Figure 6.4 is the RBS peak of Au, showing that Au has diffused into the Au/Ni/GaN structure during annealing so that we have a stack of compounds on GaN in agreement with AES results. In figure 6.3 (b), region I indicate the compound of Au, possibly with Ni as Au diffuses into the sample. A study of correlation of contact resistance with metal diffusion was done by Hu et. al. [9], using RBS. It was found that annealing Au/Ni/p-GaN for 10 minutes in air, Au diffused into the sample towards Ni and an out diffusion of Ni to the surface, resulting in the formation of NiO. Region II shows GaN compound and region III shows the formation of NiO.

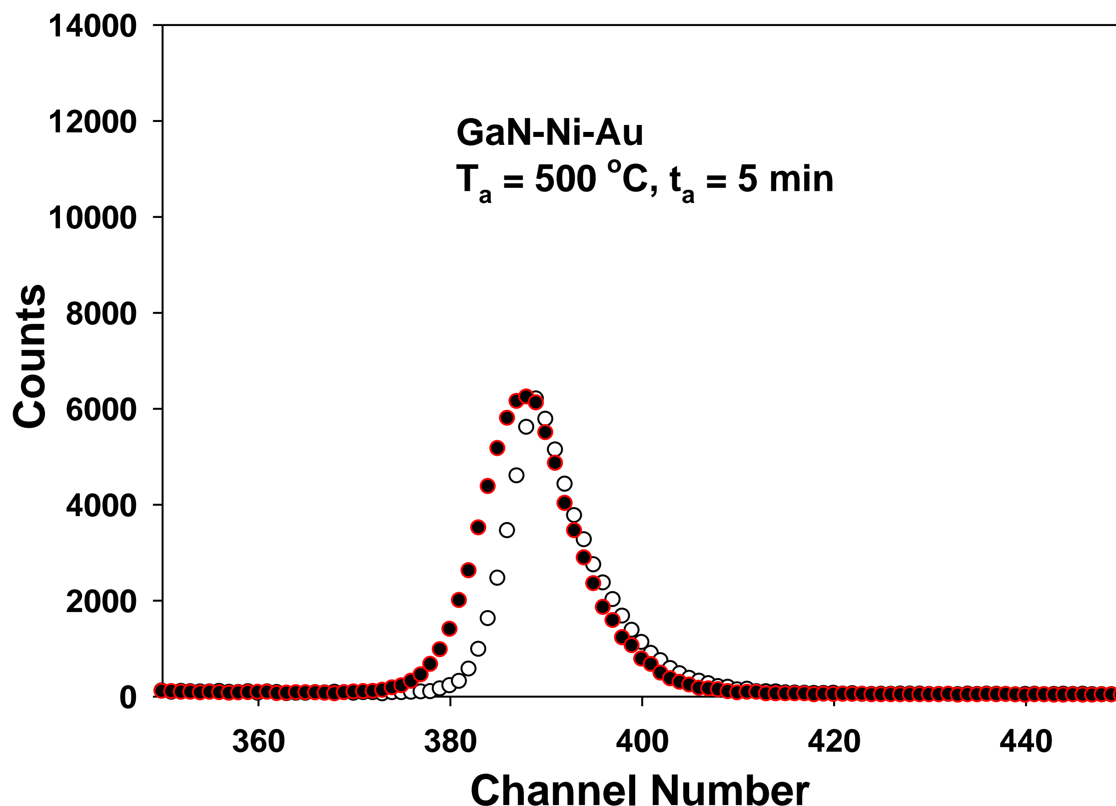

Figure 6.4: RBS spectra of Au profile, showing the as grown and annealed at 500 °C, where Au is seen to diffuse towards the interface.

A further study was done with 100 nm Ni onto GaN, annealed in air for one hour, to understand the compound formed at the Ni/GaN interface. In this study, XRD and SEM were used to analyse the samples. Figure 6.5 gives the XRD results indicating the formation of NiO and residual Ni onto GaN after 1 hour anneal. Electron Diffraction Spectroscopy (EDS) analysis of the annealed sample confirmed the observation, with ratio of Ni and O as almost 1:1. This is in agreement with work done by Nel et. Al., where it was shown that NiO formed at 500°C with no evidence of Ni_2O_3 phase [10].

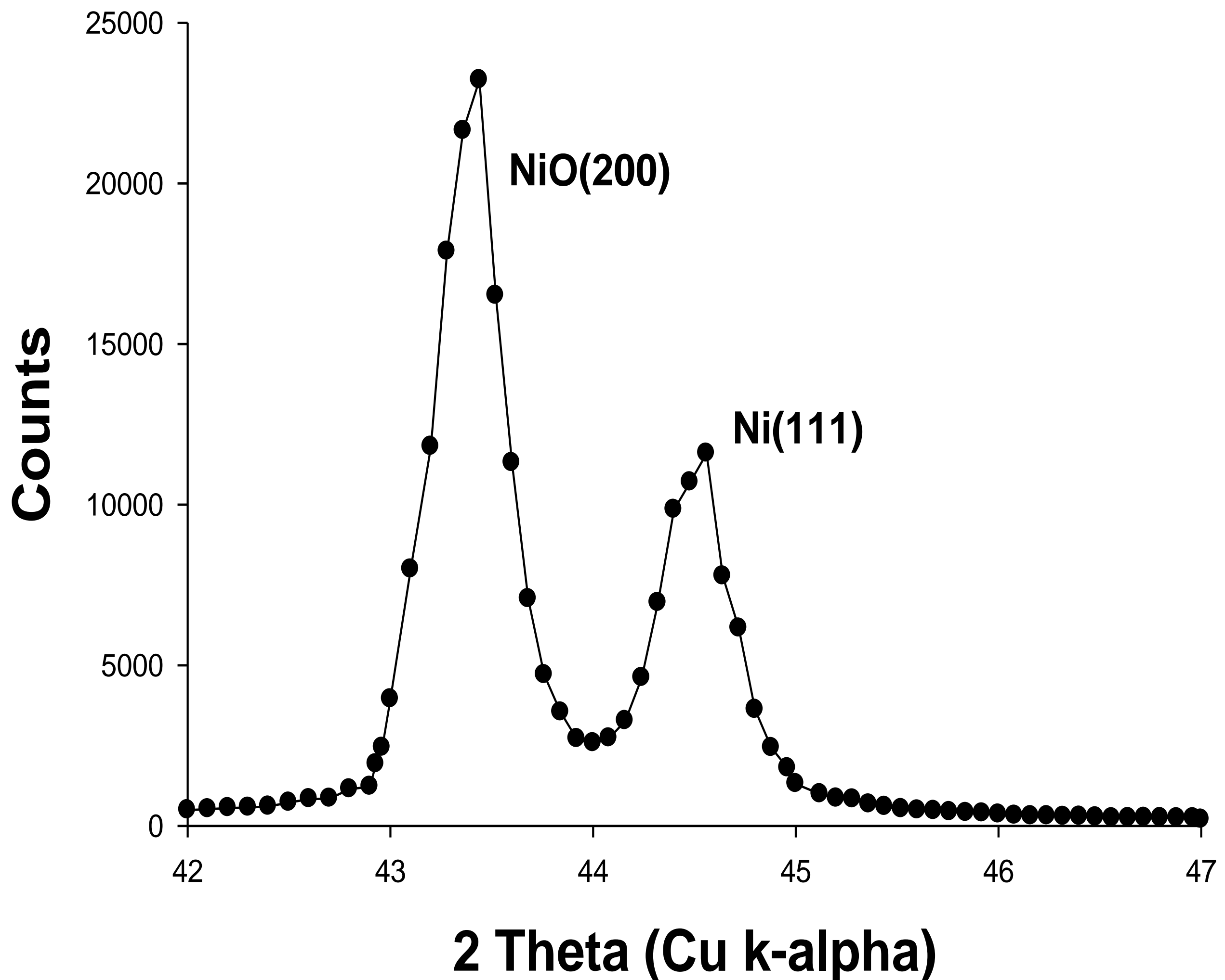

Figure 6.5: XRD patterns of oxidised Ni at 500°C showing the formation of NiO.

Figure 6.6 shows the current voltage mechanism of Au, Ni and Ni/Au contacts onto GaN. The Schottky barrier height of Au contacts was obtained as 0.81 ± 0.02 eV. Series resistance for these contacts was about 481 ± 4 Ω. The current-transport mechanisms are dominated by thermionic emission at lower voltages and series resistance effect depicted clearly at higher voltages. Generally Au contacts age very quick due to the problem of adhesion to GaN. The Schottky barrier height of Ni contacts was obtained as 0.78 ± 0.04 eV Series resistance for these contacts was about 38 ± 1 Ω, far less than that of Au contacts. Ni/Au contacts are annealed at 500 °C for transparency. The leakage current of Ni/Au is two orders of magnitude lower than that of Ni, and the Schottky barrier height was averaged at 0.92 ± 0.01 eV. Current transport mechanisms are clearly displayed with generation-recombination dominating the lower voltage region. In the high voltage region, the diode characteristics are affected by series resistance. The presence of NiO onto GaN reduced the leakage current by two orders of magnitude.

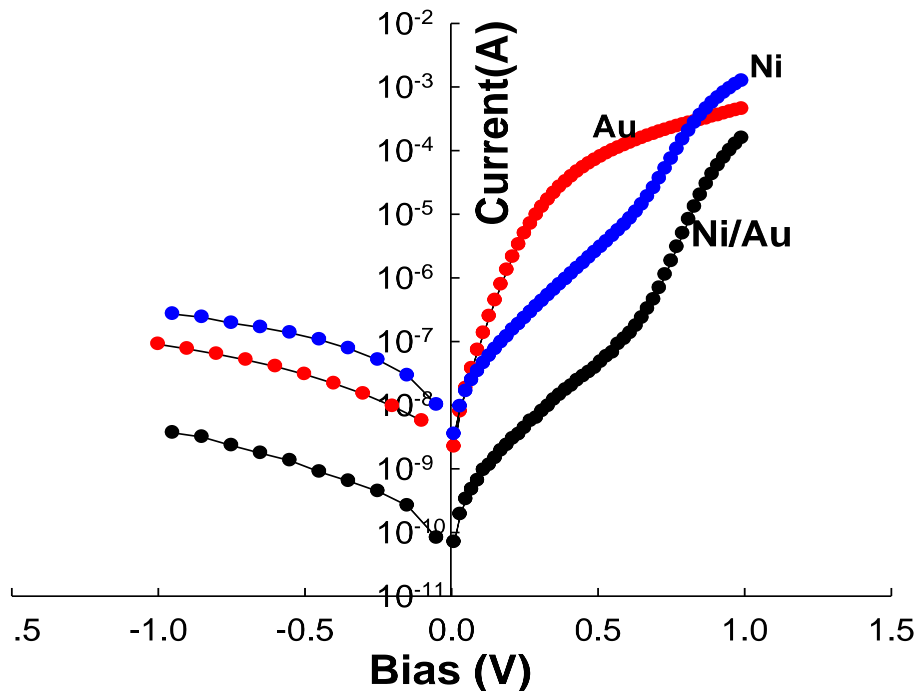

Figure 6.6: Curent-Voltage plots of Au, Ni and Ni/Au contact on n-GaN. Ni/Au was annealed at 500 °C while Ni and Au are 10 nm each thick are not annealed.

6.5 Conclusions

In conclusion, Au, Ni and Ni/Au contacts onto GaN were fabricated and characterized. AFM showed that 10 nm thick Au and Ni contacts onto GaN were continuous with peak-to-valley surface roughness of Ni films approximately 9.0 Å and RMS roughness of 1.5 Å while Au peak to valley roughness was recorded as 11 nm and the RMS roughness 2.3 nm. Annealing Ni/Au onto GaN produced a highly transparent and conductive NiO, as confirmed by XRD, SEM, AES sputtering profiles and EDS analysis. *I-V* characteristics showed that Ni/Au contacts had the lowest reverse leakage current, two orders of magnitude below that of Au contacts. The barrier heights of the diodes were 0.81, 0.78 and 0,92 for Au, Ni and Ni/Au respectively.

REFERENCES

[1] Monroy E., Calle F., Munoz E., Omnes F., Gibart P. and Munoz J. A., Applied Physics Letters **73** (1998) 2146.

[2] Osinsky A., Gangopadhyay V, Lim B. W., Anwar A. Z., Asif-Khan M., Kuksenkov D. V. and Temkin H., Applied Physics Letters **72** (1998) 742.

[3] Luther B. P, Wolter S. D. and Mahoney S. E., Sensors and Actuators B, **56** (1999) 164.

[4] Sheu L. K., Su Y. K., Chi G. C., Koh P. L., Jou M. J., Chang C. M., Liu C. C. and. Hung W. C., Applied Physics Letters **74** (1999) 2340.

[5] .Sawatzky G. A and Allen J. W., Physisical Review Letters **53** (1984) 2339.

[6] Liday J., Hotovy I., Sitter H., Vogrincic P., Vincze A, Vavra I, Satka A., Ecke G., Bonnani A., Breza J., Simbrunner C. and Plchberger B., Journal Materials Science **19** (2008) 855.

[7] Auret F. D., Wu L., Meyer W. E., Nel J. M., Legodi M. J. and Hayes M., Physica Status Solidi (c) **1** (2004) 674.

[8] Su Y. K, Chang S. J, Chen C. H, Chen J. F., Chi G. C, Sheu J. K., Lai W. C. and Tsai J. M., IEE Sensors Journal **2** (2002) 7361

[9] Hu C. Y., Ding Z. B., Qin Z. X., Chen Z. Z., Yang Z. J., Yu T. J., Hu X. D., Yao S. D. and Zhang G. Y., Semiconductor Science and Technology **21** (2006) 1261.

[10] Nel J. M., Auret F. D., Wu L., Legodi M. J. and Hayes M., Sensors and Actuators B: Chemical **100** (2004) 270.

CHAPTER 7

Chemical treatment effect on Au/GaN diodes

7.1 Introduction

Rectifying contacts with low leakage currents and high barrier height are required for the successful fabrication of GaN-based devices. Schottky barrier diodes (SBD) are the choice structure for many semiconductor devices, including microwave diodes, field-effect transistors and photodiodes [1,2,3]. Their technological importance requires a full understanding of the nature of the electrical characteristics of SBDs. It is well known that SBD has a thin layer of an oxide between the metal and the semiconductor, which cannot be removed by conventional chemical cleaning. Such an oxide converts the diode to metal-insulator-semiconductor (MIS) and usually influences the electrical characteristics of the diode, causing a change in the interfacial charge with bias, giving rise to an electric field at the interfacial layer between the metal and the semiconductor [4,5]. The oxide layer reduces the barrier height and consequently increases the series resistance.

Generally, the forward biased current-voltage (I-V) characteristics are linear in the semi-logarithmic scale at low voltages, but deviate considerably from linearity due to the effects of series resistance, R_s resulting from the presence of the thin oxide layer and other surface contaminants. The series resistance is only effective in the curvature downward region or non-linear region of the forward I-V characteristics at sufficiently high voltages. The concavity of the current-voltage characteristics at higher voltages increases with increasing series resistance. Increasing series resistance decreases the barrier height and this result in non-ideal current-voltage characteristics. Other parameters such as the ideality factor, n(V) and zero biases-barrier height, $\Phi_{b,0}$ are effective in both the linear and the non-linear regions of the I-V curve, accompanying the changes in the Schottky barrier height (SBH) [6]. The effect of the series resistance between the depletion region and the ohmic contact of the neutral region of the

semiconductor bulk causes the I-V characteristics of the metal-semiconductor contact to deviate from the expected [7].

The interface states at the metal-semiconductor junction play a vital role in evaluating the Schottky barrier height and the ideality factor. These manifest themselves as deviations from the ideal Schottky barrier formation and are localized within a few atomic layers of the intimate metal-semiconductor contact with energies which fall inside the forbidden gap. Bardeen showed that such charge accumulated at the metal-semiconductor contact reduces the effective potential difference between the semiconductor and the metal contact [8]. Interface states arises from semiconductor surface states due to discontinuity in the lattice potential, metal-induced-gap sates due to wave-function tunneling from the metal into the semiconductor, surface states due to contamination and defects; and any new compounds formed as a result of the interaction of the metal and the semiconductor.

A study of the importance of series resistance in calculating the characteristics parameters of Si Schottky contacts was done by Aydin et al [7], obtaining their estimations from determination of interface states density distribution from the analysis of the current voltage measurements. Kampen and Monch studied the barrier heights of different metals on GaN using metal-induced gap states (MIGS) and the electronegativity model, concluding that the experimental values of the barrier height are excellently reproduced by the theoretical predictions, which follow from physical MIGS and the electronegativity concept [9]. A review of metal-contact technology has revealed the importance of surface preparation prior to metal deposition [10].In this study, two different surface chemicals were used to treat GaN surface prior to metal deposition. The effects of chemical treatments on Schottky characteristics were investigated using capacitance-voltage (*C-V*) and current-voltage (*I-V*) characteristics. The average barrier height for the diodes was 1.43 and 1.20 eV for *C-V*; and 0.81 and 0.89 for *I-V* measurements respectively.

7.2 Experimental.

For this investigation, we have used GaN samples with carrier density of 1 x 10^{17} cm^{-3}, obtained from TDI. Before contact fabrication, samples were cleaned using trichloroethylyne (TEC), Isopropanol and HCl:HNO_3 aquaregia. Each of the samples was finally etched in 1:1 HCl:H_2O (sample 1) and $(NH_4)_2S$ (sample 2) respectively. Using patterned surface, Ti/Al/Ni/Au (150/2200/400/500 Å) ohmic contacts were deposited by electron-beam and annealed in ultra pure Ar for 5 minutes at 500 °C. Thereafter, Au Schottky contacts, 0.25 mm thick, were deposited in the resistive evaporator at room temperature. The values of zero-biased barrier height and ideality factor were determined from *I*-*V* and *C*-*V* measurements at room temperature and corrected afterwards for the effect of series resistance.

7.3 Results and Discussion

7.3.1 Capacitance-Voltage

In Schottky diodes, the depletion layer capacitance can be expressed as [1]

$$C^{-2} = \frac{2(V_{bi} - V_A)}{q\varepsilon_s A^2 N_D} \quad (1)$$

where A is the area of the diode, V_{bi} the diffusion potential at zero bias and is determined from the extrapolation of the linear $C^{-2} - V$ plot to the V axis, and V_A is the applied voltage. The value of the barrier height can be obtained from the relation:

$$\Phi_{b,0}(C-V) = V_{bi} + V_0 \quad (2)$$

where V_0 is the potential difference between the bottom of the conduction band and the Fermi level; and can be calculated knowing the donor concentration N_D obtained from the following relation:

(3)

where $N_C = 4.6 \times 10^{16} cm^{-3}$ is the effective density of states in the conduction band [2].

Nine dots with the same diameter (0.25 mm) on each sample were evaluated. Figure 7.1 shows the reverse bias $C^{-2} - V$ characteristics for one diode from sample 1 and sample 2 respectively. For these particular diodes on samples 1 and 2, the C-V barrier heights are 1.43 and 1.20 eV respectively. The carrier concentration of 1.9 x 10^{16} and 2.4 x 10^{16} cm^{-3} from the reverse bias $C^{-2} - V$ plots were obtained for sample 1 and sample 2. The C-V barrier heights ranged from 1.28 to 1.50 eV for sample 1 and from 1.14 to 1.25 eV for sample 2. The statistical analysis for the C-V data yielded SBH mean value of 1.35 ± 0.04 eV for t sample 1 dots and SBH mean value of 1.20 ± 0.03 eV for sample 2.

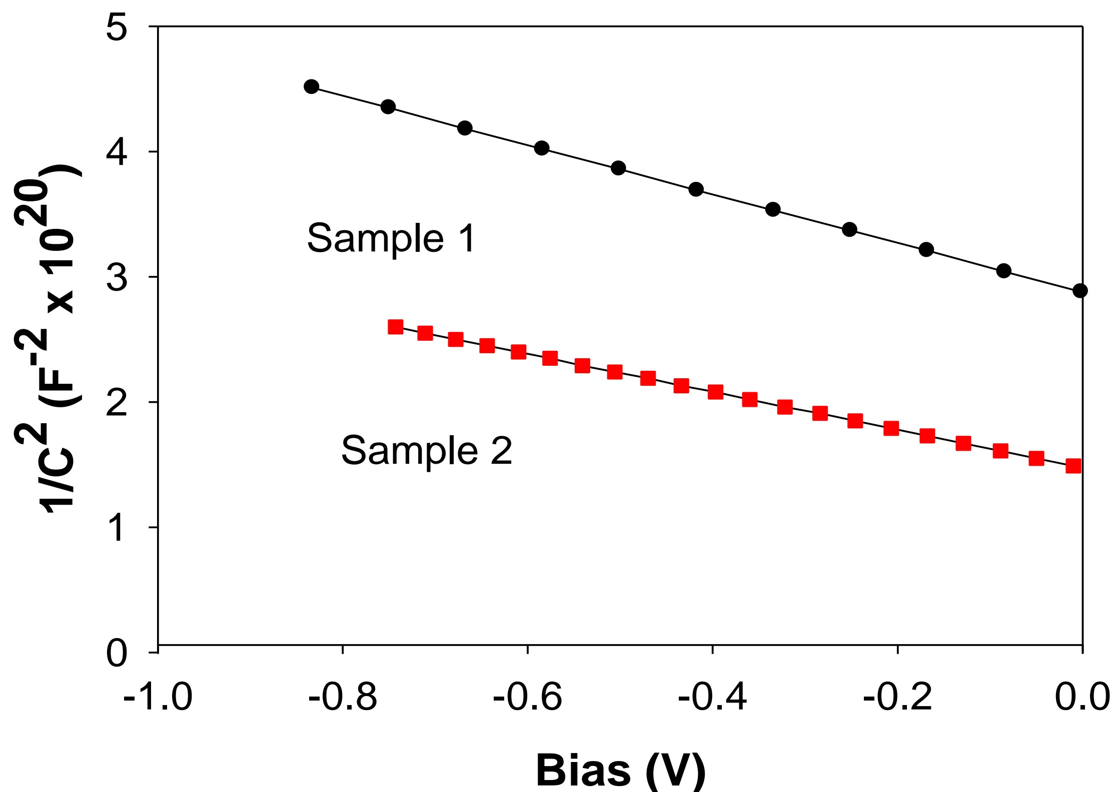

Figure 7.1: Reverse Bias C^2-V curves of the HCl and $(NH_4)_2S$ samples. For these particular diodes on samples 1 and 2, the C-V barrier heights are 1.43 and 1.20 eV respectively.

7.3.2 Current-Voltage

In Schottky barrier diodes, the barrier height depends on the voltage and surface conditions prior to metal deposition. The surface condition includes the thickness of the interfacial oxide, which affects the current-transport mechanisms. These include the thermionic emission, which is characterized by ideality close to unity and thermionic field emission and field emission. These mechanisms are affected by series resistance, tunneling and generation recombination in the depletion region. Table 1 gives the summary of the electrical characteristics of the diodes.

Table 7.1: Values obtained experimentally from the current-voltage characteristics of the Au/GaN Schottky diodes. The difference in series resistance for the sample 1 and 2 is due to the surface state after different chemical treatment.

Sample 1	n	1.17
	$R_s\,(\Omega)$	22.3
	$\Phi_{b,c}$ (eV), C-V	1.43
	$\Phi_{b,0}$ (eV), I-V	0.82
Sample 2	n	1.89
	$R_s\,(\Omega)$	17.1
	$\Phi_{b,c}$ (eV), C-V	1.20
	$\Phi_{b,0}$ (eV), I-V	0.71

For a Schottky contact with series resistance, the net current of the device is due to thermionic emission and it is written as [1]:

$$I = I_0 \exp\left(-\frac{q(V_A - IR_s)}{nkT} \right) \qquad (4)$$

where the saturation current I_0 is expressed as

$$I_0 = AA^* T^2 \exp\left(-\frac{q\Phi_{b,0}}{kT} \right) \qquad (5)$$

where q is the electron charge, A^* is the effective Richardson constant and is equal to $26 A/cm^2K^2$ for n-type GaN [11], A is the diode area, T is the absolute temperature, k Boltzmann

constant, n the ideality factor of the SBD and $\Phi_{b,0}$ the zero bias barrier height. When $V_A \geq 3kT/q$, the extrapolated current, I_0,and the zero bias barrier height can be expressed as

$$\Phi_{b,0} = \frac{kT}{q} \ln\left(\frac{A^{*}AT^{2}}{I_0}\right) \tag{6}$$

and the ideality factor from equation 4 can be written as

$$n = \frac{q}{kT} \frac{dV}{d \ \ln I} \tag{7}$$

The ideality factor of the SBD, n is a measure of the conformity of the diode to pure thermionic emission. From figure 7.2, current-transport mechanisms displayed are thermionic emission and the series resistance effect at high voltages. The values of the ideality factor, n, and the barrier height Φ_b were calculated from the forward *I-V* characteristics according to (6) and (7). For sample 1 the barrier height, $\Phi_{b,0}$ ranged from 0.79 to 0.89 eV and the ideality factor n ranged from 1.02 to 1.17. Sample 2 $\Phi_{b,0}$ values ranged from 0.71 to 0.85 eV and the n from 1.31 to 1.36. The statistical analysis yielded mean values of 0.84 ± 0.05 eV for the 1.06 ± 0.50 for barrier height and ideality factor of sample 1 (9 dots) respectively and the mean values of 0.80 ± 0.01 eV and 1.34 ± 0.20 (9 dots) for sample 2 diodes. Ideality factors above unity has been attributed to: interface states due to thin oxide layer between the metal and the semiconductor, including other contaminants, tunneling currents in highly doped semiconductors, image-force lowering of the Schottky barrier in electric field at the interface, and generation-recombination currents within the depletion region [1]. Our previous results have shown S and Cl residues onto GaN after cleaning in HCl and $(NH_4)_2S$ using Auger Electron Spectroscopy (AES) and X-ray Photoemission Spectroscopy (XPS) [12]. The work done on GaAs and GaP nitrididation has shown anion exchange where a thin layer of Ga-N was formed on each of the materials [13]. Surface Ga-N in turn passivates the GaAs and GaP, affecting the I-V and C-V characteristics of these materials. In addition, the work done by Liu et al has shown that the Ga peak becomes larger when samples are cleaned in $(NH_4)_2S$ than in HF/HCl [14]. Furthermore, $(NH_4)_2S$ has been found to reduce the barrier height on GaN, and preventing re-oxidation of the surface [15]. We suggest that there exist Ga-Cl and Ga-S on sample 1 and sample 2, respectively. Previous

XPS results have shown that as-grown GaN surface has oxides in the form of Ga_2O_3 and GaOH [12]. In addition, while rinsing GaN in water, addition of OH to GaN to form the GaOH, may occur, and be part of sticking surface water that may contribute to interface states [16].

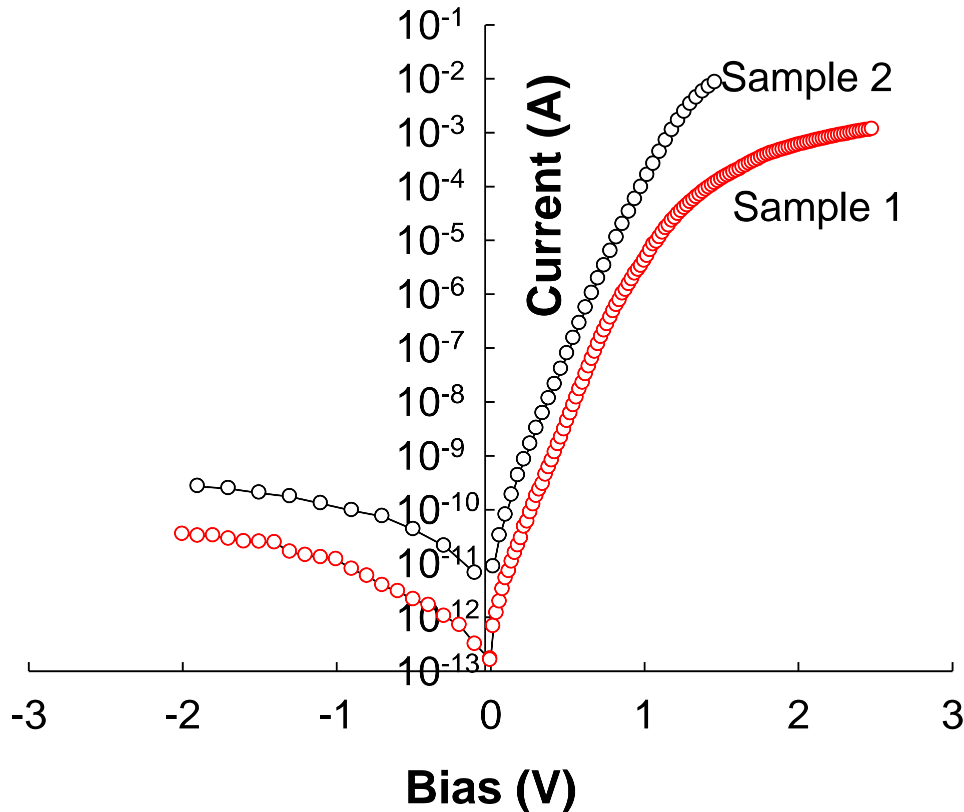

Figure 7.2: *I-V* curves of the treated samples. The series resistance values of HCl samples are generally higher than those treated in $(NH_4)_2S$, which presented less oxide and reduced barrier height

The values of R_s and $\Phi_{b,0}$ for both sample 1 and 2 were obtained as 0.82 eV and 22.3 Ω; and 0.71 eV and 17.0 Ω respectively. As mentioned above, the barrier height values of 1.43 and 1.20 eV for sample 1 and 2 were obtained from the C^{-2}-V plots, respectively. These barrier height values obtained from the C^{-2}-V (1.43 eV) and *I-V* characteristics (0.89 eV) are different from each other by 0.54 eV. We attribute the difference between the *I-V* and *C-V* barrier height in the metal-semiconductor to SBH inhomogeneity. This is the fact that the barrier heights of the

diodes on the same sample differs from diode to diode and at different positions on the same diode. The measured *I-V* barrier height is significantly lower than the weighted arithmetic average of the SBHs. On the other hand, the *C-V* measured barrier height is influenced by the distribution of charge at the depletion region follows the weighted arithmetic average of the barrier height inhomogeneity; hence the BH determined by *C-V* is close to the weighted arithmetic average of the barrier heights. Therefore, the barrier height determined from zero bias intercept assuming thermionic emission as current transport mechanism is well below the measured BH and the weighted arithmetic average of the barrier heights [17,18]. Furthermore, the surface damage at the metal-semiconductor-interface affects the I-V measurements because defects may act as recombination centers for trap-assisted tunneling currents. C-V measurements are generally less prone to interface states, so that the determined barrier height is considered more reliable, though the depletion width can be altered by the interface defects if they are deeper into the space charge region [19].

7.4 Conclusions

In conclusion, we have fabricated Au/n-GaN SBDs using different cleaning procedures. From the current-voltage characteristics, we obtained the values of ideality factor, SBH, and R_s for the samples. *I-V* characteristics are near ideal with thermionic emission as the dominant current transport mechanism. Furthermore, HCl treated samples behave like a MIS diode due to the amount of oxide remaining on the surface after treatment. The series resistance values of HCl samples are generally higher than those treated in $(NH_4)_2S$, which presented less oxide and reduced barrier height, in agreement with published results. Most published results on GaN have only reported their findings without specifics on current transport mechanism. Thus further work is needed for the investigation ideality factor far above unity, which will need the knowledge of the oxide layer thickness on GaN, effects of passivation of GaN surface on electrical characteristics, and analysis of barrier height inhomogeneities on the rectifying diode characteristics on GaN.

REFERENCES

[1] Rhoderick E. H. and Williams R. H., Metal-Semiconductor Contacts, Oxford, Clarendon, (1988).

[2] Sze S. M., Physics of Semiconductor Devices, 2nd Edition, New York, Wiley (1981).

[3] Wang L., Nathan M. I., Lim T-H, Asif Khan M. and Chen Q, Applied Physics Letters **68** (1996) 1267.

[4] Hanselaer P., Laflere W.H., Meirhaeghe R. L. and Cardon F., Applied Physics Letters **56** (1984) 2309.

[5] Monroy E., Calle F., Pau J.L., Mućoz E. and Omnes F., Electronic Letters **36** (2000) 2096.

[6] Card J. C. and Rhoderick E. H., Journal of Applied Physics: D **4** (1971) 1589.

[7] Aydin M. E., Akkiliç K. and Kiliçoğlu T., Applied Surface Science **225** (2004)1304.

[8] Bardeen J., Physical Review, **71** (1947) 771.

[9] Kampen T. U. and Monch W., Applied Surface Science 117/118 (1997) 388.

[10] Liu Q. Z. and Lau S . S., Solid State Electronic **42** (1998) 677.

[11] Schmidt A. C., Ping A. T., Asif Khan M., Chen Q., Yang J. W. and Adesida I., Semiconductor Science and Technology, **11** (1996) 1464.

[12] Diale M., Auret F. D., Van der Berg N. G., Odendaal R. Q. and Roos W. D., Applied Surface Science **246** (2005) 279.

[13] Bruno G., Applied Surface Science **235** (2004) 239.

[14] Liu J., Shen B., Zhou Y. G., Zhou H. M., Wang M. J.,. Zheng Z. W, Zhang B., Shi Y. and Zheng Y. D., Optical Materials **23** (2003) 133

[15] Cao X. A., Pearton S. J., Dang G., Zhang A. P., Ren F. and Van Hove J. M., Applied Physics Letters,**75** (1999) 4130.

[16] Diale M., Auret F. D., Van der Berg N. G., Odendaal R. Q. and Roos W. D., Surface and Interface Analysis **37** (2005) 1158.

[17] Werner J. H. and. Guttler H. H, Journal of Applied Physics, **69** (3) (1991) 1552.

[18] Tung R. T., Levi A. F. J., Sullivan J. P. and Schrey F., Physical Review Letters **66** (1971) 72.

[19] Fontaine C., Okumura T. and Tu K. N., Journal of Applied Physics **54** (1983) 1404.

CHAPTER 8

Fabrication and characterization of GaN and AlGaN Schottky barrier photodiodes

8.1 Introduction

GaN is a wide bandgap semiconductor that has been explored for the fabrication of ultraviolet photodiodes suitable for operations in chemically harsh and high temperature environments [1]. Alloying of Al with GaN to form AlGaN has a very important property called solar-blindness, which makes the material insensitive to visible light [2]. Intrinsic solar-blindness is a bandgap dependent property of the semiconductors [3]. The bandgap of GaN and AlN are 3.4 and 6.2 eV respectively, which makes AlGaN bandgap to lie between the two extremes for the specified Al content. [4]. Similar to GaN, the growth of AlGaN had issues such as lack of suitable substrate, resulting in cracks in the thin film [5]. AlGaN grown on sapphire has high densities of threading dislocation which increases with increasing Al content [6]. Threading dislocations are detrimental to devices as they are a major reason for high leakage currents and reduced spectral responsivity in semiconductor photodiodes [7]. There has been much progress in the growth of AlGaN, with the use of AlN nucleation layer to reduce cracks in the AlGaN film [8].

Schottky barrier photodiodes are used in applications such as missile warning and guidance, flame monitoring and prevention of skin cancer [9]. Thus far, various types of GaN-based photodetectors have been reported, with low dark current, high response speed, and high detectivity [10]. They have reported low capacitance, which is an important component of large bandwidth and low noise performance in photodetectors. Another important parameter is high transparency of the metal used for Schottky barriers, which determines the number of photons entering the semiconductor [11]. In this work, we have fabricated GaN and AlGaN Schottky barrier photodiodes, using Ni/Au metallization system. The photodiodes were characterized in our in-house electro-optical measurement station. The photodiodes gave zero biased dark

currents as small as 10^{-9}A (35.8 μA/cm^2) for GaN and 2.8 x 10 $^{-9}$ A (21.6 nA/cm^2) for AlGaN (55% Al). The recorded reverse biased peak responsivity was 31.8 A/W with quantum efficiency of 11 % when the wavelength of light is 369 nm in the case of GaN. AlGaN results have shown a peak responsivity of 3.8 mA/W at 280 nm, with quantum efficiency of 1.7 %.

8.2 Experimental

GaN samples used in the experiment were 5.6 μm thick, grown by HVPE. AlGaN epitaxial structures were grown by HVPE with 55 % Al content. This structure consist of 30 nm GaN grown on sapphire followed by Si doped GaN film for the fabrication of ohmic contacts. The following layer was 0.1 μm AlN, which is believed to reduce threading dislocations in AlGaN film. The active layer was a thin film of 0.5 μm layer of $Al_{0.55}Ga_{0.45}N$. Samples were cleaned in organic solvents, boiled in HCl:HNO_3 aquaregia and a final etch in HCl, prior to loading in the electron-beam deposition system for ohmic contacts consisting of Ti/Al/Ni/Au onto the top layer. All rinsing was done in methanol. The ohmic contacts were then annealed in Ar ambient for 5 minutes at 500 °C.

The samples were then etched in HCl before loaded for the deposition of Schottky contacts in the resistive evaporator, consisting of Ni/Au with thickness 5 nm each. Similarly, GaN photodiodes were fabricated, using the same cleaning procedure and the same metals as with AlGaN for both ohmic and Schottky contacts. For device characterization, current-voltage (*I-V*) measurements were carried out. *I-V* measurements were taken using an HP4140B pA meter/DC source. Dark- and photocurrent were measured from annealed samples. Wavelength dependent measurements were done at the same *I-V* station with a deuterium lamp connected to the monochromator by optical fibre. All measurements were performed at room temperature. Using the commercial SiC and AlGaN photodiodes' data sheets and the quantum efficiencies specified therein, the irradiance was determined, which was then used to calculate the responsivities and quantum efficiencies of the fabricated diodes.

8.3 Results and Discussion

The GaN photodiodes have recorded a zero biased dark current as low as 6.48 x 10^{-9} A (35.8 μA/cm^2) while that of AlGaN was 2.8 x 10^{-9} A (21.6 μA/cm^2). Figure 8.1 (a) and (b) shows the I-V characteristics of GaN and AlGaN photodiodes respectively. The barrier height of 0.67 eV was recorded for *I-V* measurements and the corresponding ideality factor of 2.48. The series resistance of the diodes was 381 Ω. In the case AlGaN the *I-V* barrier height was 1.09. The ideality factor for Schottky diodes fabricated on AlGaN was 1.35 with series resistance in 1090 Ω. Schottky diodes on GaN and AlGaN suffer from high series resistance. Series resistance in AlGaN/GaN structures increases with increasing Al content and thickness of thin film. High series resistance contributes to slow response and thermal noise of the photodiodes.

Schottky barrier GaN photodiodes with dark currents densities as low as 10^{-10} A/cm^2 have been reported [12]. The reported low current densities were measured at higher voltages of up to 50 V when device active areas were differing from one device to the other. From the work done by Jhou et al [13], in annealing the Ni/Au contacts in oxygen, low dark currents were observed. Our Ni/Au contacts were annealed in air. Su et al [14], have compared GaN and AlGaN photodetectors, where high quantum efficiencies and low noise levels in AlGaN were reported. The fact that the ideality factors of the diodes are all far above unity, indicates that the total current is a combination of current mechanisms, other than thermionic emission [15]. The low values of barrier height show that we have fabricated GaN photodiodes which alows majority carriers to easily cross from the metal to the semiconductor. Consequently, such diodes have long cut-off wavelength, so that GaN-Ni/Au pair are correctly selected for UV detection. The dark current can be further lowered by cooling the photodiodes.

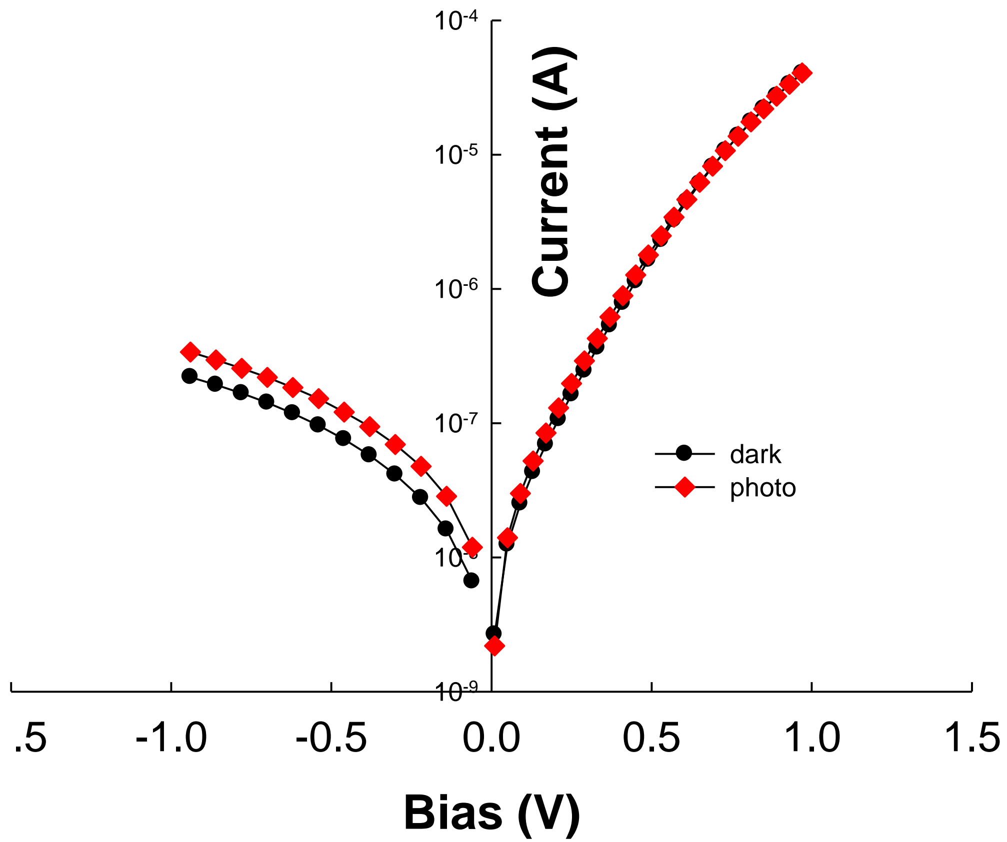

Figure 8.1 (a): ***I-V*** **characteristics of GaN photodiodes.**

UNIVERSITEIT VAN PRETORIA
UNIVERSITY OF PRETORIA
YUNIBESITHI YA PRETORIA

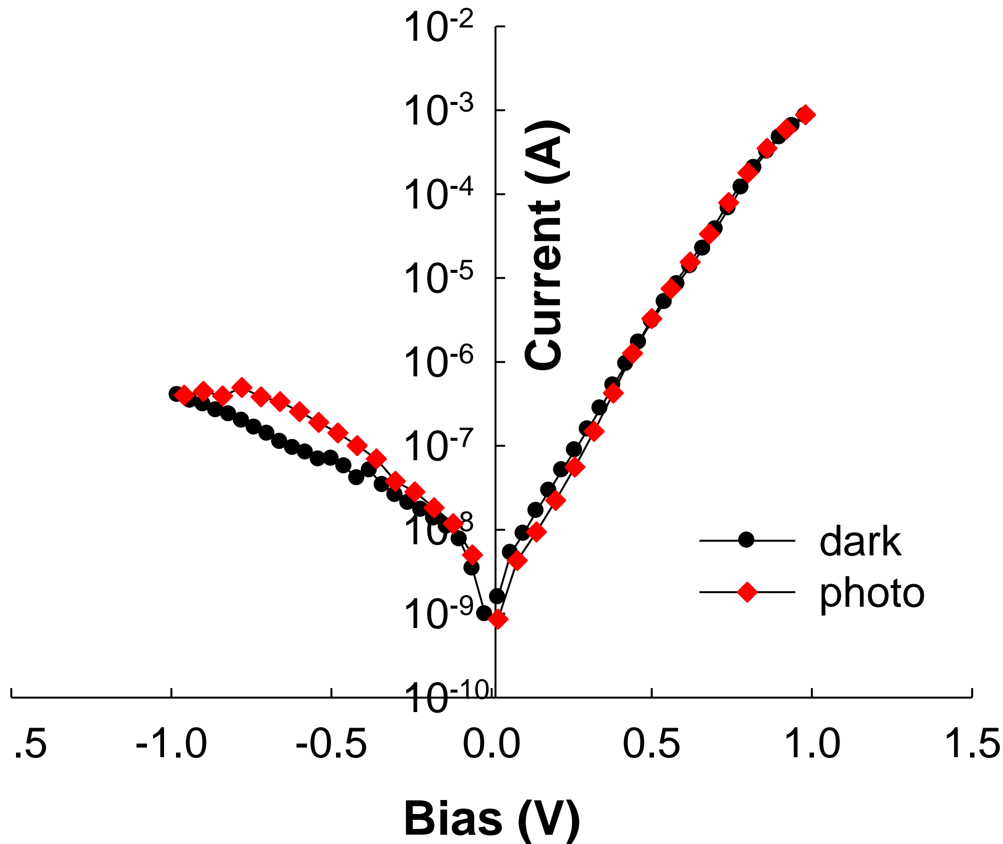

Figure 8.1 (b): ***I-V*** **characteristics of AlGaN photodiodes.**

Spectral responsivity measurements were done in the 150-450 nm range, using Deuterium lamp, a single-pass monochromator and a calibrated SiC or AlGaN photodetector. The response curves of commercial AlGaN and laboratory AlGaN are presented in figure 8.2, confirming the optoelectronic station accuracy. The peak responsivity of the commercial AlGaN photodiode occurred at 45.8 at 270 nm, with 21 % quantum efficiency. During the measurements, applied voltage on the photodetector was varied from 0.1 – 0.5 V. The responsivity of a photodiode is a measure of the effectiveness of the conversion of incident radiation into current or voltage and can be expressed as [16]:

$$R_{\lambda} = \frac{I_p}{P_{opt}} = \frac{\eta q}{h\nu} = \frac{\eta\lambda \ \mu m}{1.24} \ AW^{-1} \qquad (1)$$

where $I_p, P_{opt}, \eta, q, h, \nu$ and λ are the photocurrent, optical power, quantum efficiency, electron charge, Plank's constant, frequency and wavelength respectively. The irradiance of the lamp was estimated from the factory settings of the detector; using the calibration values to evaluate the optical power. Using equation (1) the peak responsivity, R_λ of 31.8 mA/W was recorded for GaN and 3.8 mA/W for AlGaN respectively. The maximum photo response occurred at 369 nm and 280 nm wavelengths for GaN and AlGaN photodiodes, as shown in Figure 8.3 (a) and (b) respectively. Since $\lambda_c < 280$ nm was satisfied, true solar-blind detection was successfully demonstrated for AlGaN photodiodes, while GaN satisfied the condition for visible-blind photodiodes at $\lambda_c < 380$ nm [17]. The quantum efficiency (Q.E), defined as the percentage of incident photons that contribute to the photocurrent, follows from equation (1) and is given by:

$$\eta = \frac{R_{observed}}{R_{ideal}(100\%)} = R_\lambda \frac{hc}{q} = 1240 \frac{R_\lambda}{\lambda(nm)} \qquad (2)$$

Maximum quantum efficiency of GaN and AlGaN photodetector determined from the responsivity value was about 11 % and 1.7% respectively. The low Q.E of AlGaN photodiodes shows that very little light was absorbed.

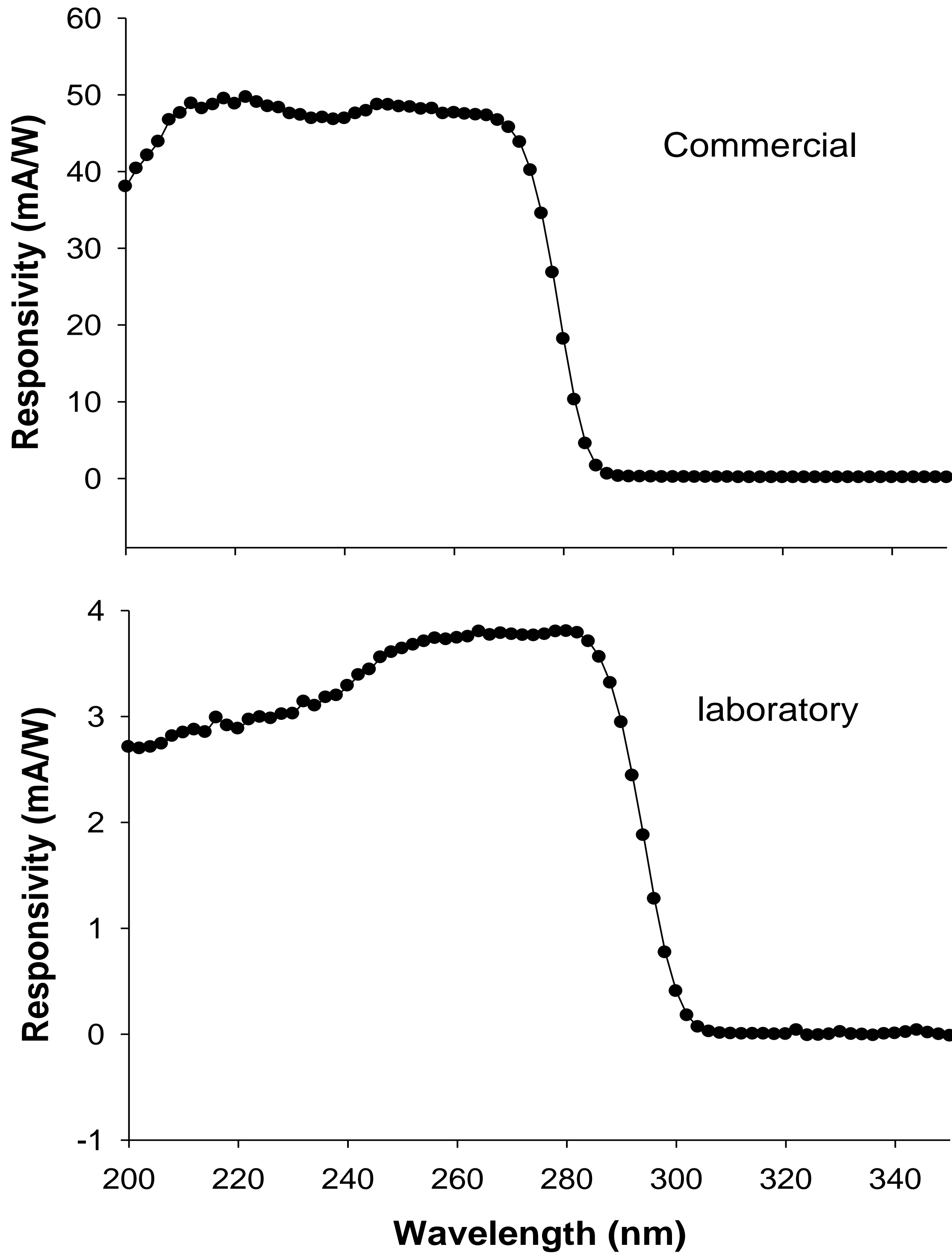

Figure 8.2: Photocurrent density response curves as a function of wavelength for AlGaN UV detectors.

Figure 8.3 (a): Photocurrent density response curves as a function of wavelength for GaN UV detectors

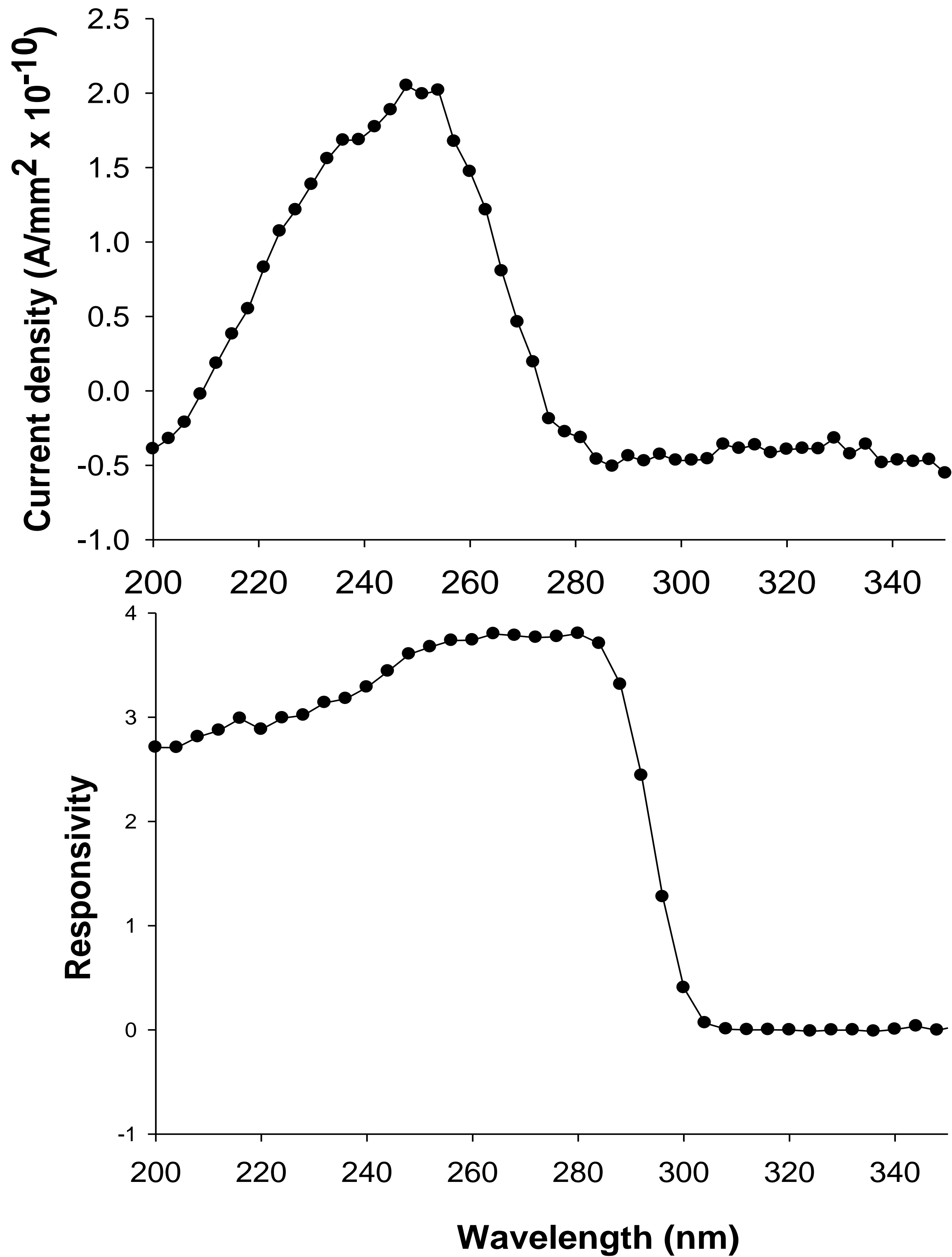

Figure 8.3 (b): AlGaN photocurrent density response curves as a function of wavelength.

8.4 Conclusions

In conclusion, we have demonstrated the fabrication of visible-blind GaN and solar-blind AlGaN Schottky photodiodes with low zero biased dark currents. Device responsivity as high as 31.8 mA/W for GaN and 3.8 mA/W for AlGaN were recorded. The calculated quantum efficiencies of the photodiodes were 11 % for GaN and 1.7 % for AlGaN respectively. The barrier heights of 0.67 eV and 1.09 were recorded, for GaN and AlGaN photodiodes. The series resistance of GaN was 178 Ω and that of AlGaN 1090 Ω. Ideality factors of 2.48 and 1.35 were recorded for GaN and AlGaN respectively. The commercial and fabricated AlGaN photodiodes have photocurrent density and responsivity maximum peaks occurring in the range of 270 - 280 nm. Further work will be done to improve the performance of AlGaN photodiodes. For the structure studied here, there is a need to etch away the AlGaN and AlN layers so that ohmic contacts are deposited onto GaN.

REFERENCE

[1] Razeghi M. and Rogalski A., Journal of Applied Physics, **79** (1996) 7433.

[2] Schreiber P., Dang T., Smith G., Pickenpaugh T., Gehred P. and Litton C., Proceedings SPIE, **3629** (1999) 230.

[3] Carrano J. C., Li T., Grudowski P. A., Dupuis R. D. and Campbell J. C., IEEE Circuit Devices Magazine, **15** (1999) 15.

[4] Asif Khan M., Shatalov M., Maruska H. P., Wang H. M and Koukstis E., Japanese Journal of Applied Physics **44** (7191) 2005.

[5] Kida Y., Shibata T., Naoi H., Miyake H., Hiramatsu K., and Tanaka M., Physica Status Solidi (a) **194** (2002) 498.

[6] Wang H-M., Zhang J-P., Chen C-Q., Fareed Q., Yang J-W., and Asif Khan M., Applied Physics Letters **81** (2002) 604.

[7] McCarthy L., Smorchkova I., Xing H., Fini P., Keller S., Speck J., Denbaars S. P., Rodwell M. J. W. and Mishra U. K., Applied Physics Letters **78** (2001) 2235.

[8] Biyikli N., Aytur O., Kimukin I., Tut T. and Ozbay E., Applied Physics Letters **81** (2002) 3272.

[9] Biyikli N., Kartaloglu T., Aytur O., Kimukin I. and Ozbay E., Applied Physics Letters **79** (2001) 2838.

[10] Jiang H., Egawa T., Ishikawa I., Dou Y. B., Shao C. L. and Jimbo T., Electronic Letters **39** (2003) 148.

[11] Motayed A., Davydov A. V., Bendersky A. L., Wood M. C., Derenge M. A., Wang D. F., Jones K. A. and Mohammad S. N., Journal of Applied Physics **92** (2002) 5218.

[12] Butun S., Gokkavas M., Hongbo Y. and Ozbay E., Applied Physics Letters **89** (2006) 73503.

[13] Jhou Y. D., Chen C. H., Chang S. J., Su Y. K., Chang P. C., Chen P. C., Hung H., Yu C. L., Wang S. M. and Wu M. H., Microelectronic Journal **37** (2006) 328.

[14] Su Y. K., Chang P. C., Chen C. H., Chang S. j., Yu C. L., Lee C. T., Lee H. Y., Gong J., Chen P. C. and Wang C. H., Solid-State Electronics **49** (2005) 459.

[15] Sze S. M., Physics of Semiconductor Devices, 2nd Edition, 1981.

[16] Dereniak E. L. and Growe D. G., Optical Radiation Detectors, Wiley, New York (1984).

[17] Ozbay E., Biyikli N., Kimukin I., Kartaloglu T., Tut T. and Aytur O., IEEE Journal of Selected Topics in Quantum Electronic **10** (2004) 742.

CHAPTER 9

Conclusions and Future Work

For the past two decades, GaN-based semiconductors have been researched extensively due to their applications in blue-UV regions of the electromagnetic spectrum. The work done thus far has witnessed improvements in crystal quality, where dislocation densities are reduced from 10^{14} to 10^{4} cm^{-2}. With the GaN-based materials and device technology being in the advanced stage, the studies presented in this thesis have resulted in advances in the characterization of the material and the fabrication of Schottky devices. Continued work and recommendations detailed at the end of this chapter will lead to further advancement and improvement in the blue/UV devices.

Various surface cleaning techniques and chemicals for the removal of contaminants from the GaN surface were investigated. Auger electron spectroscopy (AES) analysis was used to monitor the presence of surface contaminants while atomic force microscopy (AFM) was used to monitor surface roughness. AES analysis revealed that KOH was effective in removing carbon (C). When comparing the topographies of GaN surfaces cleaned in HCl, KOH and $(NH_4)_2S$ in aqueous solutions, it was found that surfaces treated in $(NH_4)_2S$ were most effectively cleaned with the lowest values of both C and O, RMS roughness and Ga/N ratio. This was as a result of $(NH_4)_2S$ preventing the re-oxidation of the GaN surface. The nearly complete removal of C and O was achieved by heating the samples in AES in ultra-high vacuum where contaminants on the GaN surface were removed by thermal desorption Using AES, it was found that carbon was purely a surface issue and, consequently, it was completely removed from the surface of GaN by thermal heating in a vacuum in AES.

GaN samples used in this study were grown on sapphire, requiring that both ohmic and Schottky contacts be fabricated on the same side of the material. This method of fabrication greatly reduces the active area of the Schottky barrier photodiode where UV light can be transmitted through to the semiconductor material. Thus the metals used must be transparent to UV radiation. A computer program was used to choose these metals, and it was found that

Ag, Ni and Au were most suitable, with modelled transparency of above 50% for a 10 nm thick layer. After extensive review, we chose to focus on Ni and Au, due to their high work function and barrier height. From literature, the transmission of Au was found to be higher than that of Ni with the same thickness, while that of annealed Ni/Au was 30% greater than that of Au and Ni. XRD analysis of GaN/Ni indicated that the transparent material on the surface is NiO, with SEM showing the surface mirror-like.

The effects of chemical cleaning on the electrical characteristics of Au Schottky contacts fabricated on n-GaN treated in HCl and $(NH_4)_2S$ have been investigated using current-voltage (I-V) and capacitance voltage (C-V) techniques. The reduction of surface oxide yielded a low series resistance. Current transport mechanisms of the diodes were dominated by thermionic emission with series resistance dominating higher voltages. $(NH_4)_2S$ was found to reduce barrier heights. It was found that the ideality factors of all diodes on GaN are above unity, requiring further studies of the interface states, which are believed to influence the values of both the ideality factors and Schottky barrier heights, which were found to have different values on the same diode at different positions. The best photodiodes were 0.25 mm in diameter, where the transport mechanism was almost purely themionic at lower voltages and series resistance at higher voltages.

Finally, the study was completed with the setting- up of an optoelectronic station for the evaluation of photonic devices. The setup consisted of a monochromator, an optical fibre and a deuterium light source, incorporated into the existing *I-V* station so that the measurements of dark and photocurrent could be carried out in the same system. GaN and AlGaN Schottky barrier photodiodes were fabricated using the Ti/Al/Ni/ Au ohmic contacts. Ni/Au was used to fabricate Schottky contacts. The photocurrent densities of GaN and AlGaN photodiodes recorded were 35.8 $\mu A/cm^2$ and 21.6 $\mu A/cm^2$ respectively. Device responsivity as high as 31.8 mA/W for GaN and 3.8 mA/W for AlGaN were recorded. The corresponding quantum efficiencies of the photodiodes were 11 % for GaN and 1.7 % for AlGaN respectively. The barrier heights of 0.67 eV and 1.09 were recorded, for GaN and AlGaN photodiodes. The commercial and fabricated AlGaN photodiodes have photocurrent density and responsivity maximum peaks occurring in the range of 270 - 280 nm.

The current-transport mechanisms of Schottky barrier diodes on GaN need to be explored in the same manner that Si has been researched. It is important to review the current-transport mechanisms on GaN, both experimentally and theoretically, in order to explain some anomalous behaviour such as the ideality factor far above unity, very high series resistance and barrier height inhomogeneity. The results of this thesis have shown that there is a problem with barrier height values and ideality factors reported in literature on new materials like GaN and AlGaN. The values are often scattered and an inconsistency is evident in the methods of preparation, growth of samples and metals used. Although Si has been used to lay a foundation for all semiconductor materials, it does not necessarily mean that the results concerning Si can be assumed for other materials. The optoelectronic station could be improved by extending its use to visible and infrared regions of electromagnetic radiation so that the research spreads out to all photonic devices.

From this thesis, several issues in the fabrication and characterization of Al(GaN) remain unresolved and deserve further investigations. Future work should focus on:

- The improve heterostructure should have AlN layer thickness reduced to some few nanometres so that series resistance should be lowered.
- Establishing wet etch rates for (Al)GaN heterostructures so that ohmic contacts can be fabricated onto the GaN layer.
- Fabrication of (Al)GaN ohmic contacts.
- Determination of more parameters for the evaluation of UV photodiodes:
    - Detectivity
    - Noise equivalent power and
    - Response speed

List of Publications

1. **M. Diale**, C. Challens, E. C. Zingu, Applied Physics Letters **62** (1993) p943, **Cobalt self diffusion during cobalt silicide formation.**
2. T. L. Alford, D. Adams, **M. Diale**, J. Li, S. A. Rafalski, R. L. Spreitzer, S. Q. Hong, S. W. Russel, N. D. Theodore, and J. W. Mayer, In: D. P. Fayreau, Y. Shacham-Diamand and Y. Horiike, Editors, MRS Pittsburg, PA(1993) p49, **Advanced metallization of USLI Applications.**
3. T.L. Alford, E.J. Jaquez, N.D. Theodore, S.W. Russell, **M. Diale**, D. Adams and S. Anders, J. Appl. Phys **79** (1996), p2074, **Influence of interfacial copper on the room temperature oxidation of silicon.**
4. H. W. Kunert, D. J. Brink, M. Hayes, J. Malherbe, L. Prinsloo, J. Barnas, AGJ Machatine, and **M. Diale**, Physica Status Solidi C 1(2) (2004) p223,**Optical characterization of GaN doping superlattices: As grown, hydrogen implanted, and annealed.**
5. **M. Diale,** F. D. Auret, N. G. van der Berg, R. Q. Odendaal, W. D. Roos, Applied Surface Science 246 (2005) p279, **Analysis of GaN Cleaning procedures.**
6. **M. Diale,** F. D. Auret, N. G. van der Berg, R. Q. Odendaal, W. D. Roos, Surface and Interface Analysis 37 (2005) p115, **Study of Carbon behaviour on GaN surface in ultra-high vacuum (UHV).**
7. G. H. Kassier, M. Hayes, F. D. Auret, **M. Diale**, B. G. Svensson, Physica Status Solidi C 1(5) (2008) p569, **Hall effects study of donors and acceptors in different types of bulk ZnO modified by annealing and hydrogen implantation.**
8. W. Mtangi, F. D. Auret, C. Nyamhere, P. J. Janse van Rensburg, **M. Diale**, A. Chawanda, Physica B **404** (2009) p1092, **Analysis of temperature dependent I-V measurements on Pd/ZnO Schottky barrier diodes and the determination of the Richardson constant.**
9. **M. Diale** and F. D. Auret, **Effects of chemical treatment on Au-GaN Schottky barrier diodes**, accepted by Physica B, 2009.
10. W. Mtangi, F. D. Auret, C. Nyamhere, P. J. Janse van Rensburg, **M. Diale**, J. M. Nel and W. E. Meyer, Physica B **404** (2009) p4402, **The dependence of**

barrier height on temperature for Pd Schottky contacts on ZnO.

11. L. van Schalkwyk, **M. Diale**, W. E. Meyer and F. D. Auret, SMEOS 2009, South African Journal of Science, 2009, **Optoelectronic study of Schottky photodiodes on AlGaN.**
12. A. Chawanda, C. Nyamhere, F. D. Auret, W. Mtangi, T Hlatswayo, **M. Diale**, and J. M. Nel, Physica B **404** (2009) p4482, **Thermal stability study of palladium and cobalt Schottky contacts on n-Ge(100) and defects introduced during contacts fabrication and anneal.**
13. A. Chawanda, C. Nyamhere, F. D. Auret, W. Mtangi **M. Diale**, J. M. Nel, Physica Status Solidi C 1-4 (2010), **Comparison of metal Schottky contacts on n-Ge (100) at different annealing tempreratures.**
14. A. Chawanda, C. Nyamhere, F. D. Auret, W. Mtangi **M. Diale**, J. M. Nel, Journal of Alloys and Compounds 491 (2010), **Thermal annealing behaviour of platinum, nickel and titanium Schottky barrier diodes on n-Ge(100)**.

Available online at www.sciencedirect.com

SCIENCE DIRECT®

Applied Surface Science 246 (2005) 279–289

applied surface science

www.elsevier.com/locate/apsusc

Analysis of GaN cleaning procedures

M. Diale[a,*], F.D. Auret[a], N.G. van der Berg[a], R.Q. Odendaal[a], W.D. Roos[b]

[a]*University of Pretoria, Department of Physics, Lynnwood Road, Pretoria 0001, South Africa*
[b]*University of Free State, Bloemfontein, South Africa*

Received 5 August 2004; accepted 12 November 2004
Available online 30 December 2004

Abstract

In this study, various surface cleaning techniques for the removal of contaminants from GaN were investigated. Auger electron spectroscopy (AES) analysis was used to monitor the presence of surface contaminants and atomic force microscopy (AFM) was used to monitor surface roughness. AES analysis showed that KOH was effective in removing carbon (C). Comparing the topographies of GaN surfaces cleaned in HCl, KOH and $(NH_4)_2S$ in aqueous solutions; it has been found that surfaces cleaned in $(NH_4)_2S$ is the best cleaned, have the lowest values of both C and O, RMS roughness and Ga/N ratio. The nearly complete removal of C and O were achieved by heating the samples in AES in vacuum.
© 2004 Elsevier B.V. All rights reserved.

PACS: 73.61

Keywords: Morphology; Wet chemical; Cleaning; GaN

1. Introduction

A number of groups have investigated GaN cleaning procedures for device fabrication [1–5]. The importance of properly cleaned surfaces for ohmic and Schottky contacts deposition is well known [4,5]. There is currently no standard method of preparing the GaN substrate prior to metallization. Preparation methods differ from one laboratory to the other. Wet and dry etching methods are widely used in surface preparation for removal of surface contaminants. In addition, the morphology of the surface of the substrate prior to metallization has an influence on the continuity of the ultra-thin metals used in fabrication of Schottky barrier diodes for UV detection. Wet and dry cleaning of substrates using chemicals have been used on GaN prior to metallization. Dry cleaning methods are known for introducing damage to the surface, usually making the material electrically unsuitable [6]. Various surface analytical techniques such as Auger electron spectroscopy (AES), X-ray photoelectron spectroscopy (XPS), low energy electron diffraction (LEED), and secondary ion mass spectroscopy (SIMS) have been used to identify the

* Corresponding author. Tel.: +27 12 420 4418;
fax: +27 12 362 5288.
E-mail address: mdiale@postino.up.ac.za (M. Diale).

0169-4332/$ – see front matter © 2004 Elsevier B.V. All rights reserved.
doi:10.1016/j.apsusc.2004.11.024

surface contaminants, oxides, metal particulate and reconstruction. Atomic force microscopy (AFM) has been used to monitor the surface cleanliness as a function of topography [7,8].

The work done by Smith et al. in cleaning GaN has shown that the choice of cleaning chemical is of utmost importance [1]. In their work, they used AES to compare HCl- and HF-based solutions in methanol and in water, to remove contaminants on the GaN surface. The use of UV/O_3 treatment was also done. All the chemical cleaning was followed by thermal desorption at temperatures of up to 800 °C to completely produce a contamination-free surface. From their results, it was observed that dissolving HCl in deionised water (DI) resulted in cleaner surfaces as compared to dissolving in methanol. HF results showed that C (carbon) and O (oxygen) residues were lower in HF:DI solution than in HF:methanol solution. These results were influenced by the physiosorption of methanol, thus increasing C content on the surface of GaN. Comparing HCl:DI and HF:DI, it was found that HF-based solution was more effective in removing both C and O on the surface. A further observation was the presence of Cl on the surface after treatment with HCl-based solution and UV/O_3 increased the surface oxide while decreasing the C. The best cleaning method according to Smith et al. is the final step, in which HF was diluted in deionised water as it removed most of the C, O and Cl without leaving any traces of F on the surface. The thermal desorption results showed further reduction of C and O as the temperature is gradually increased up to 800 °C, beyond which the decomposition of GaN was observed.

Further work done by King et al. using XPS and AES, on both AlN and GaN showed that different chemicals may be used to yield atomically clean surfaces [2]. They used HCl, HF, NH_4F, HNO_3, H_2SO_4, H_3PO_4, H_2O_2, NH_4OH, NaOH, KOH, RCA SC1 and SC2 (1:1:5 NH_3OH:H_2O_2:H_2O at 85 °C and 1:1:5 HCl:H_2O_2:H_2O at 85 °C) and TCE, acetone, methanol and UV/O_3 treatment. Thermal desorption was done in an integrated UHV system at temperatures of up to 1100 °C. As in the previous work by King et al., UV/O_3 was found to be effective in removing C and simultaneously increasing O on the surface. In addition to reducing the C peak, the exposure to UV/O_3 moved the C peak to higher energies, consistent with oxidation of C species on the surface of GaN. It was observed that increasing ozone concentration further reduced C on the surface though it was not completely removed. Further observations of the UV/O_3 exposed surface, showed an increase in the rate of oxidation of GaN surface, as seen in complete disappearance of N KLL and N1s peaks. The observed oxides were found to be in the form of Ga_2O_3 and N–O at binding energies 20.8 and 398.2 eV, respectively.

The use of HCl, NH_4OH and HF solutions were found to remove the oxides effectively. A 1:1 HCl:DI solution was found to produce the lowest C/N ratio with a disadvantage of Cl addition to the surface. The O coverage on the HCl sample was found to be inversely proportional to Cl detected on the surface. According to their results, the fact that the N–Cl bond strength is less than that of Ga–Cl gave an explanation why there is Cl residue on GaN surface. The results of using H_2SO_4 and H_3PO_4 were observed residues of SO_4 and PO_4 on the surfaces of GaN, increasing surface oxide coverage after these treatments. The 1:10 HF-based cleaning solutions were found to increase the O/N ratio with no detection of F on the surface. Stoichiometric GaN surface was produced after annealing the surfaces at 700–800 °C in NH_3. Using thermal desorption, it was found that HCl cleaned samples showed complete desorption of all contaminant species on the surface after 950 °C. AFM was used to investigate the surface roughness of the cleaned surfaces. All samples had surface RMS roughness comparable with the as-grown material, while H_3PO_4 resulted in increased surface roughness from as low as 20 Å to as high as 200 Å. On the GaN surface, the RCA SC1 and SC2 reduced the UV/O_3 oxides, though SC2 left more C on the surface relative to SC1.

Lee et al. investigated several methods of cleaning GaN [3]. The methods included different wet chemical procedures, as well as in situ cleaning in AES at elevated temperatures. The wet chemical methods consisted of acetone, methanol, HF or HCl and UV/O_3 treatments. Thermal cleaning was done in N_2 and H_2/N_2 plasma. UV/O_3 increased the O on the surface while decreasing the C peak. Using AES, it was observed that the surface of the as-grown (as-received) sample contained about 12% C and 13% O and that the Ga/N ratio was 1.08. Applying photoresist and stripping it with acetone reduced the O content

UNIVERSITEIT VAN PRETORIA
UNIVERSITY OF PRETORIA
YUNIBESITHI YA PRETORIA

slightly, and increased the carbon content to 30%. Treatment in HCl further reduced the O concentration to 7% and the C content to almost the same level as of the as-grown sample. The HCl treatment also left Cl contamination on the surface. Using thermal cleaning after various chemical treatments reduced the C and O surface content to below the detection limit of AES. AFM results showed insignificant change in surface roughness after all the wet chemical cleaning on GaN surface.

The work by Pelto et al. in pre-metallization treatment of GaN for ohmic contacts fabrication showed that the surface cleaning recipes depends on what device is being fabricated [4]. The following etch recipes were used: H_2SO_4:H_3PO_4:DI (1:1:2), HCl:DI (1:2), HNO_3:HCl (1:3), and NH_4OH:DI (1:10). The ohmic contacts' behaviour depended on the etch recipe used, and the expected outcomes. On the other hand, Machuca et al. used a simple cleaning method focusing on the optimization of electron emitters with wide bandgap [5]. Using H_2SO_4:H_2O_2 (4:1) to reduce contaminants on GaN surfaces followed by annealing in vacuum at 700 °C, they showed that after chemical clean, the vacuum anneal was best for thermal desorption of C and O than annealing in NH_3. Both these authors do not comment on any remaining surface contaminants on GaN and their effects on electrical properties of the devices made.

Thermal desorption in the vacuum has been recommended as a final step in most cleaning procedures. In particular, thermal desorption done in vacuum have shown that all the surface contaminants can be reduced to less than the AES detection limit. In the above works done, it can be summarized that thermal desorption of contaminants on GaN is independent of what has been used chemically prior to heating. Heating the material to a temperature range from 800 to 1000 °C has shown complete removal of C all contaminants on GaN surface [1–3].

The above review shows that there is still a gap in GaN cleaning procedures used prior to metallization. There is need to test the effects of chemical cleaning procedures by evaluating electrical characteristics of devices. In this work, we have investigated chemical cleaning of GaN surfaces and evaluating the results with AFM and AES. A variety of wet chemistries for O and C removal were investigated. We particularly report on the effects of HCl, KOH and $(NH_4)_2S$ on GaN surfaces. In addition, we give thermal cleaning results.

2. Experimental

n-GaN samples of orientation (1 0 0 0) and unintentional doping of 1.6×10^{16} cm^{-3} were obtained from AIXTRON, grown by metal organic chemical vapor deposition (MOCVD) on sapphire (Al_2O_3) substrate. The thickness of the GaN layer was 1 μm. The cleaning methods used are summarized in Table 1. All samples were finally blown dry with compressed nitrogen gas of ultra-high pure quality. Only analytical grade quality chemicals were used and all water rinses were done in deionised water ($\rho > 18$ MΩ cm). All samples used in this study were cut from the same wafer as GaN growth techniques are not yet well established as compared to other semiconductors. Ultrasonic rinse was employed to ensure the removal of all loose debris on the surface. All cleaning

Table 1
Outline of cleaning procedures

Number	Procedure
Degrease	Boil in trichloroethelyne for 3 min Boil in isopropanol for 3 min Three rinses in DI for 20 s each Blow dry with N_2
Aqua regia (AR)	Degrease Boil in HCl:HNO_3 = 3:1 for 8–10 min Three rinses in DI for 20 s each Blow dry in N_2
HCl	Degrease Aqua regia HCl:H_2O = 1:1 dip for 60 s Two rinses in DI for 20 s each Blow dry with N_2
KOH	Degrease Aqua regia 1 mol KOH boil for 3 min Three rinses in DI for 60 s each Blow dry with N_2
$(NH_4)_2S$	Degrease Aqua regia $(NH_4)_2S$ for 1 min Three rinses in DI for 60 s each. Blow dry with N_2

UNIVERSITEIT VAN PRETORIA
UNIVERSITY OF PRETORIA
YUNIBESITHI YA PRETORIA

equipments used were made of pure quarts glass and Teflon. Samples were loaded into the AES immediately after wet chemical cleaning.

Thermal cleaning was done by mounting the degreased sample onto a heater block and loaded into the AES, PHI model 549. The analysis was carried out from room temperature of 23 °C, continually monitoring the surface up to a temperature of 1100 °C. The heating process was stopped at this stage to avoid any decomposition of GaN into the AES system.

The scanning probe microscope used in this study was a commercial instrument model, Topometrix 2000 Discoverer. The topographical features of GaN crystals were studied by means of AFM in contact mode. The 130 and 7 μm scanner and standard Topometrix Si_2N_3 tips were applied. All scans were applied under ambient conditions. Several images were taken at different positions on the sample to gain better understanding of the surface topography. The same scan parameters (set point, proportional gain, integral gain and derivative gain) were used; however, in each scan, optimizations were performed. The topography of the surfaces was analysed from obtained images, using the surface roughness parameters: the root mean square (RMS) roughness, maximum peak height from the mean line, R_p; the maximum peak to valley height in the profile, R_t.

The AES study was carried out on Physical Electronics Model 545 Spectrometer, using a cylindrical mirror analyzer with 5 keV electron beam incident on samples mounted on a sample holder of which the angle with the electron beam is 30°. The percentage surface concentration was calculated from the peak-to-peak heights and relative sensitivity factors for different elements.

3. Results and discussion

3.1. AFM

AFM images from randomly selected 5 μm × 5 μm areas of degrease to $(NH_4)_2S$ cleaned surfaces are presented in Figs. 1–3. The images, together with corresponding line profiles, indicate difference in topography of investigated GaN surfaces after every cleaning method. The as-grown surface has been degreased to deal with packaging contaminants.

The as-grown surface has needle-shaped protrusion as shown in Fig. 1(a). Using R_t, we compared the difference in features, ranging from protrusions to craters. From R_t measurements, the average height of the protrusions on the surface of the degreased samples was found to be 20.05 nm, as shown in Table 2. The second surface, represented in Fig. 1(b), was cleaned in aqua regia and shows a disappearance of the protrusions and the emergence of craters, which are hexagonal in shape, with R_t value decreasing to 2.5 nm. This observation implies that the chemicals used thus far, were able to act on the protrusions on the as degreased surface, characterizing GaN by showing hexagonal structure of the crystal.

The next step is etching the surface in HCl, and it is observed that protrusions are disappearing from the surface and craters are increasing, as shown in Fig. 2(a). These craters are either isolated or joint to form a bigger crater on the surface and the value of R_t increasing to 13.36 nm, indicating deeper craters as protrusions are removed. The surface protrusions seem to have changed shape, from needles to rounded protrusions. The use of KOH on the surface, as shown in Fig. 2(b), shows that the protrusions appeared to be white and flat-shaped. In Fig. 3, the surfaces of the samples cleaned in $(NH_4)_2S$ are shown. The protrusions on this surface are quite similar to the ones on the KOH etched surface. A two-dimensional (2D) image of the sample cleaned in $(NH_4)_2S$ is shown in Fig. 3, confirming that the observed protrusions on the surface are part of the crystal.

The density of craters on each of the three last cleaning processes is similar, particularly for the HCl and KOH surfaces at approximately $6.2 \times 10^8\ cm^{-2}$. The $(NH_4)_2S$ surface has a little lower density of craters at approximately $5.3 \times 10^8\ cm^{-2}$. The approximated density of craters is similar to the dislocation density of the GaN used in this experiment, which is approximated to be 10^7 to $10^8\ cm^{-2}$. Comparing the cleaning procedures, it was found that GaN was etched along the threading dislocation. Threading dislocations have been found to be dominant defects in GaN from TEM studies. In addition, the observed decrease in the density of the craters shows that a new surface has appeared. It has been observed from TEM studies that threading dislocation decrease gradually away from the interface [9].

UNIVERSITEIT VAN PRETORIA
UNIVERSITY OF PRETORIA
YUNIBESITHI YA PRETORIA

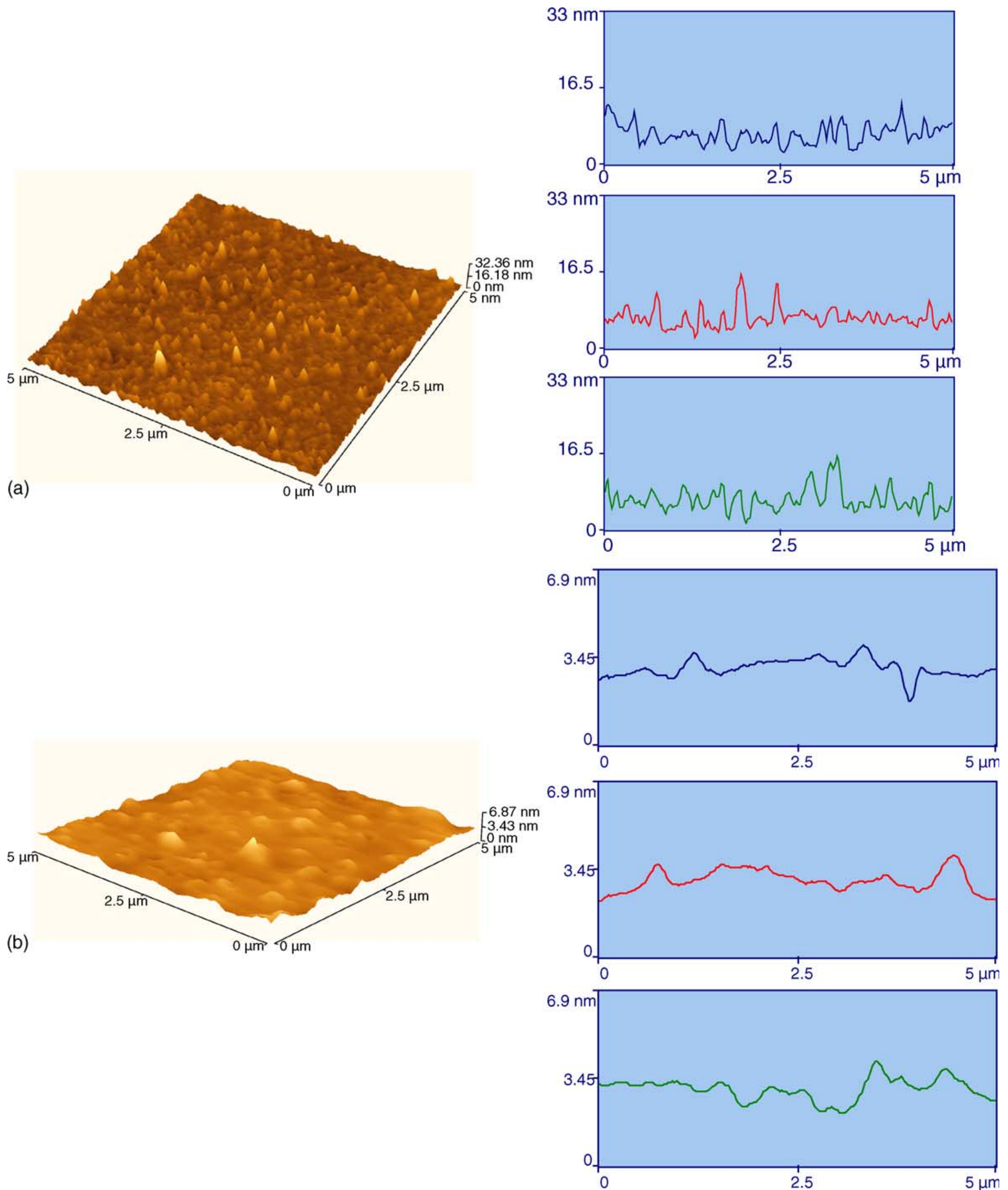

Fig. 1. AFM images taken from selected 5 μm × 5 μm areas of GaN surfaces cleaned by (a) degrease and (b) aqua regia, and the corresponding line profiles.

UNIVERSITEIT VAN PRETORIA
UNIVERSITY OF PRETORIA
YUNIBESITHI YA PRETORIA

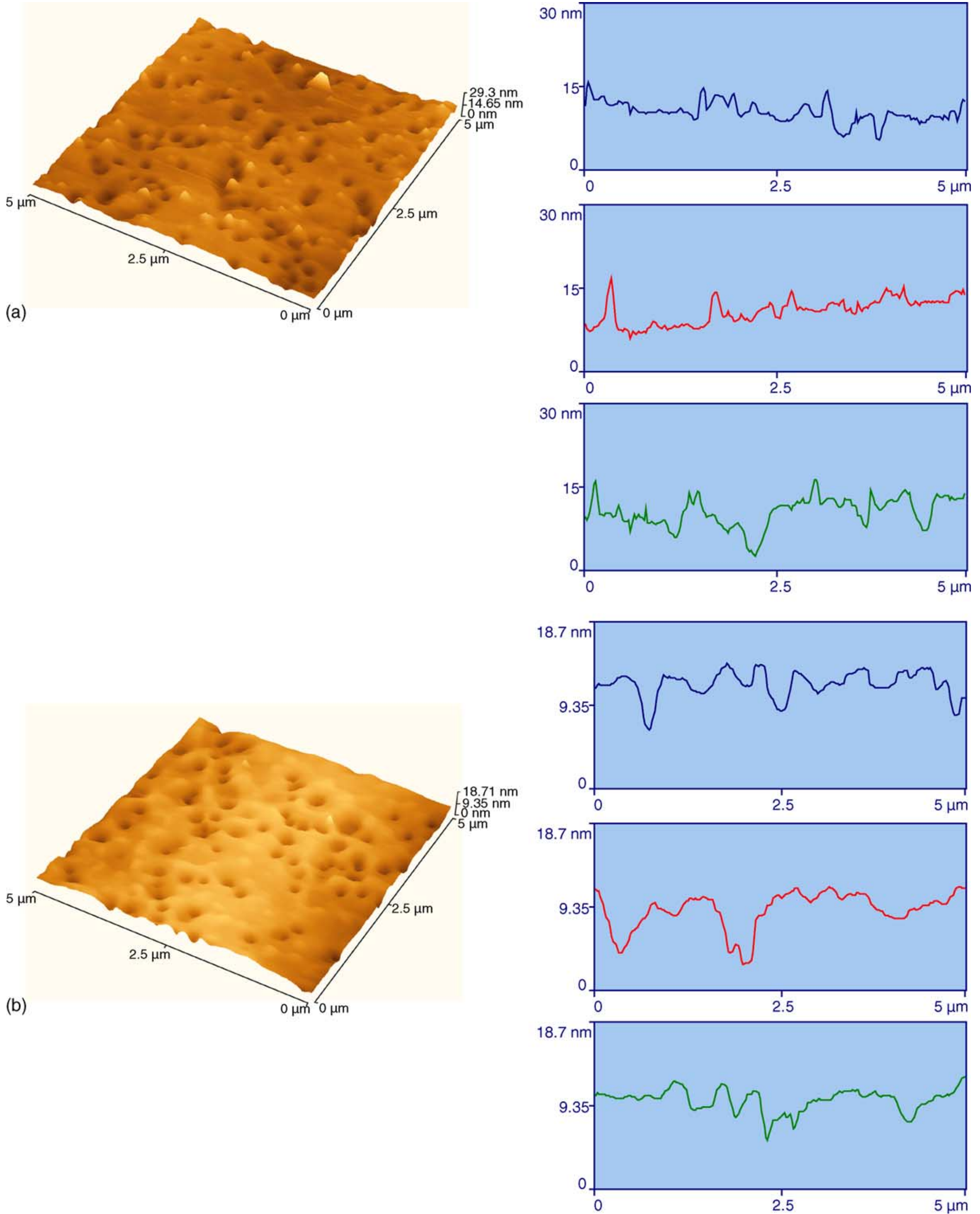

Fig. 2. AFM images taken from selected 5 μm × 5 μm areas of GaN surfaces etched as indicated and the corresponding line profiles.

UNIVERSITEIT VAN PRETORIA
UNIVERSITY OF PRETORIA
YUNIBESITHI YA PRETORIA

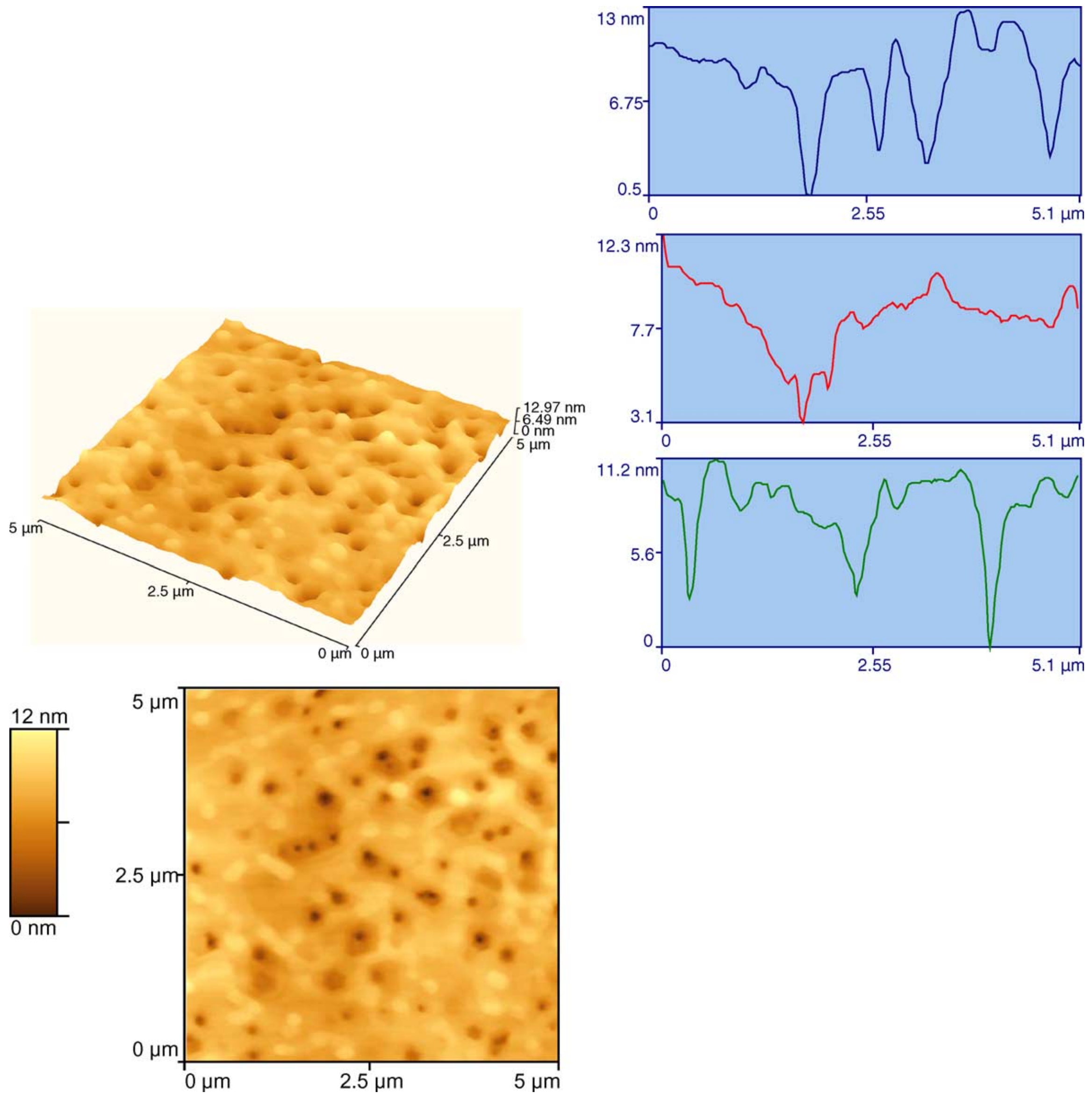

Fig. 3. AFM images taken from selected 5 µm × 5 µm areas of GaN surfaces etched as in $(NH_4)_2S$, the corresponding flat image and line profiles.

KOH has been used to characterize defects in GaN, and the defects density was found to be 2×10^9 cm^{-2}. Different values of defect densities have been recorded as 3×10^7 and 4×10^7 cm^{-2} on N-face, and 1×10^7 and 5×10^5 cm^{-2} on Ga-face. The understanding of the mechanisms for the formation thereof, will lead to the reduction of these defects [10].

Using line profiles, statistical parameters were deduced from the AFM for each of the cleaning procedures and are shown in Table 2 [11]. From the analysis of these data, the morphologies of differently cleaned surfaces differ from one cleaning method to the other. The value of R_t changed from 20.5 nm for degreased sample to 2.5 nm after aqua regia treated, implying a removal of surface protrusions. The last three etch processes also differ in the value of R_t, indicating how one chemical is able to etch the GaN surface. KOH and $(NH_4)_2S$ each were able to produce

UNIVERSITEIT VAN PRETORIA
UNIVERSITY OF PRETORIA
YUNIBESITHI YA PRETORIA

Table 2
Statistical characterization of GaN single crystal surfaces by AFM

Cleaning procedures	Maximum topography variation (R_t, nm)	Parameter		
		Mean topography variation (R_p, nm)	RMS surface roughness (nm)	Roughness factor
Degrease	20.05	11.27	1.74	1.006
Aqua regia	2.5	1.55	0.4	1.060
HCl	13.36	7.0	2.02	1.010
KOH	11.03	4.03	2.1	1.077
$(NH_4)_2S$	8.74	2.74	1.2	1.098

new surfaces as compared to HCl, which was not able to produce a new surface. The other parameters, R_p, RMS roughness and the roughness factor all confirm the R_t values. The highest RMS roughness is from the KOH etched surface and the lowest is from the aqua regia cleaned surface. Furthermore, using RMS roughness parameter, we have compared the stoichiometries on each of the cleaned surfaces, and stoichiometry and RMS roughness are compared as shown in Fig. 5.

3.2. AES

AES was used to analyze the surface contaminants and the results are shown in Fig. 4. The effect of the cleaning procedure is seen in the reduction of O and C peaks. In addition to reducing C and O peaks, HCl in aqua regia and $(NH_4)_2S$, respectively, added Cl and S to the surface. The atomic percentage of surface elements present on every surface after wet chemical cleaning procedures was calculated from the relative sensitivity factors. These contaminants may be of advantage to the metal contact formation on the GaN surface as bonding with Au may be enhanced and adhesion improved. Furthermore the use of sulfurants, alkenoids and halogens has proved to enhance adhesion of metals such as Au, Ag, Pt, Pd and Ni to semiconductor surfaces [12,13].

Comparing the AES surface scans of HCl and $(NH_4)_2S$, it is found that using HCl on the GaN surface reduced the O peak, added Cl, and the use of $(NH_4)_2S$ prevents re-oxidation of the surface, adding insignificant amount of S, and reducing the Cl contaminant. This result further confirms the importance of using

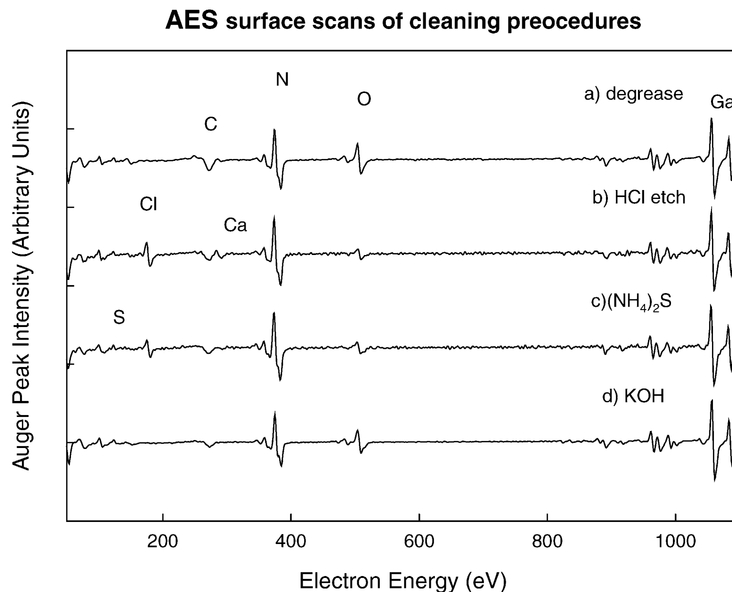

Fig. 4. AES surface scans of GaN surfaces cleaned as indicated.

UNIVERSITEIT VAN PRETORIA
UNIVERSITY OF PRETORIA
YUNIBESITHI YA PRETORIA

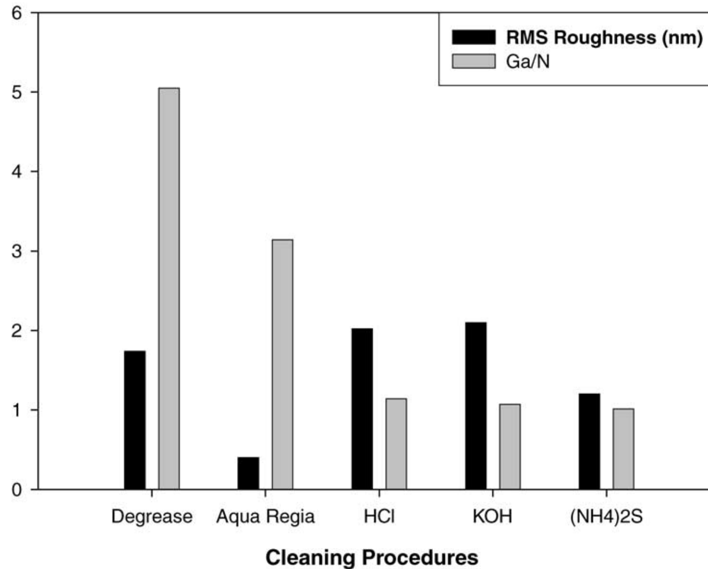

Fig. 5. Graph of root mean square (RMS) surface roughness and Ga/N ratio from AES elemental surface concentrations. Ga/N ratio close to 1 is stoichiometric.

$(NH_4)_2S$ as a chemical that prevents re-oxidation of surfaces. KOH removed all the Cl from the surface, and reduced the C significantly.

There had been reports of improved electrical characteristics of metals/GaN contacts after treatments in HF, HCl, and NaOH. Miller et al. has reported the reduction of reverse bias leakage current in GaN Schottky diodes after treatment in NaOH. The high concentration of OH-ion on the GaN surface is attributed to the reduction of reverse bias leakage in their Schottky contacts [14]. In another report, Lin and Lee has reported the reduction of surface states on InGaN using $(NH_4)_2S$ [15]. Electrically, $(NH_4)_2S$ was reported to reduce the Schottky barrier height. In particular, it was reported that Ga–O, In–O and C–O bonds were removed from the InGaN surface after $(NH_4)_2S$ treatment. Furthermore, repeated exposure of the surface that has a Cl peak to the electron beam in the AES system has resulted in desorption of the surface contaminants, and consequently, complete removal of the Cl peak.

To further analyse the cleaned surfaces, the ratio of Ga/N, and RMS surface roughness are plotted as a function of cleaning method, as shown in Fig. 5. There is a relationship between the RMS surface roughness and the contaminants on the surfaces, which consequently affects the Ga/N ratio. The as-grown surface shows a very high surface roughness and Ga/N ratio and the cleanest surface shows lowest surface roughness and Ga/N ratio. Therefore as the surface is cleaned, the surface roughness reduces as the Ga/N ratio improves, implying that the chemicals used has etch GaN surface to remove contaminants. The RMS surface roughness of KOH etched surface, differ from the as-grown surface by about 0.4 nm. Different wet chemicals used previously in removing contaminants on GaN have shown no effect on the surface roughness of the material [2,3]. The work done previously to etch and remove surface GaN to form etch steps were not achieved by using HCl and KOH [16]. Ultraviolet light illumination and addition of ions were used to etch GaN successfully in KOH [17].

Previous results have recommended the use of thermal desorption after every chemical clean, to completely remove surface contaminants [1–3]. In this work, we have found that thermal cleaning of the degreased GaN surface resulted in almost complete removal of surface contaminants. Fig. 6 is a typical temperature profile of a sample cleaned in UHV under high temperatures. This profile may be divided into two regions: region 1 from 23 to 500 °C and region II from 500 to 1010 °C. In region I, the carbon peak first

UNIVERSITEIT VAN PRETORIA
UNIVERSITY OF PRETORIA
YUNIBESITHI YA PRETORIA

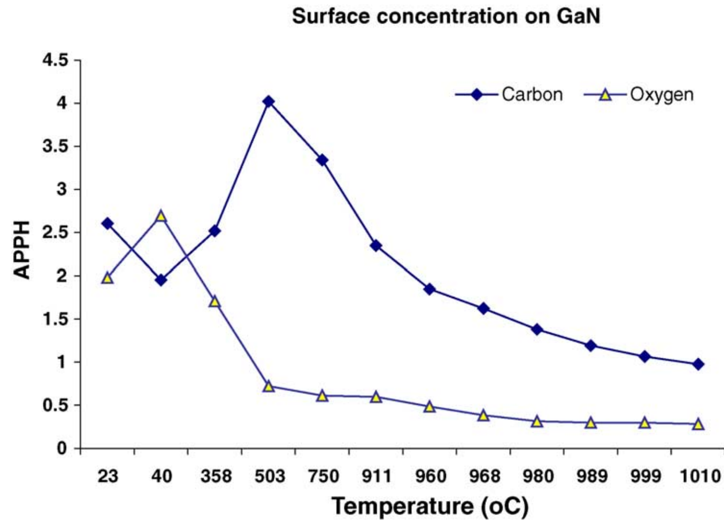

Fig. 6. Surface concentration profiles of O and C on GaN surface during thermal anneal in the AES.

decreases and then increases as temperature increases. In region II, the carbon coverage on the surface of GaN decreases until it drops to below AES detection limit, where average peak-to-peak height is less than 1.5. In the case of oxygen, the surface coverage starts increasing and quickly decreases sharply until the temperature of about 500 °C. At this temperature, all oxides are removed from the surface according to AES sensitivity, in which average peak-to-peak height is less than 0.5. The increase in O from 23 to 50 °C may be attributed to the removal of common surface water that had been covering the surface prior to thermal heating. This water is very sticky and is usually removed at temperatures above 220 °C. On the other hand, the increase in C may be due to segregation from the bulk, which needs further study to confirm.

4. Conclusions

In conclusion, the effectiveness of wet chemical cleaning of GaN with different solutions, have been characterized by AFM and AES. AFM results have shown that GaN surface roughness is affected by the cleaning method used on the surface. Surface defects were characterized by different etch chemicals, with $(NH_4)_2S$ producing a defect-free interface. AES has shown the contaminant as C and O and that using compounds with Cl and S, will leave Cl and S on the surface. This result has given sufficient information on removal of surface contamination; stoichiometry; surface roughness and chemical etch. Using $(NH_4)_2S$ prevented re-oxidation of the surface, and further removes Cl from the surface of the GaN. KOH effectively removes the C on the surface. The effects of S and Cl on the surface may enhance adhesion of metals to GaN surface, thus improving device quality.

Further work is necessary in finding the effects of different cleaning procedures on the optical properties of the material and electrical properties of devices.

Acknowledgements

The National Research Foundation, the University of Pretoria and the University of Free State funded the project.

References

[1] L.L. Smith, S.W. King, R.J. Nemanich, R.F. Davis, J. Electron. Mater. 25 (1996) 805.
[2] S.W. King, J.P. Barnak, M.D. Bremster, K.M. Tracey, C. Ronning, R.F. Davis, R.J. Nemanich, J. Appl. Phys. 84 (1998) 5248.
[3] K.N. Lee, S.M. Donovan, B. Gila, M. Overberg, J.D. Mackenzie, C.R. Abernathy, R.G. Wilson, J. Electro. Chem. Soc. 147 (2000) 3087.

[4] C.M. Pelto, Y.A. Chang, Y. Chen, R.S. Williams, Solid State Electron. 45 (2001) 1597.
[5] F. Machuca, Z. Liu, Y. Sun, P. Pianetta, W.E. Spicer, R.F. Pease, J. Vac. Sci. Technol. A 20 (2002) 1784.
[6] R.J. Shul, G.A. Vawter, C.G. Willison, J.W. Lee, S.J. Pearton, C.R. Abernathy, Solid Stat. Electron. 42 (1998) 2259.
[7] J.M. Nel, C.M. Demanet, K.T. Hillie, F.D. Auret, H.L. Gaiger, Appl. Surf. Sci. 134 (1998) 22.
[8] P.N.K. Deenapanray, F.D. Auret, G. Myburg, K.T. Hillie, C.M. Demanet, Surf. Interf. Anal. 26 (1998) 748.
[9] J. Jasinki, W. Swider, Z. Liliental-Werber, P. Visconti, K.M. Jones, M.A. Reshchikov, F. Yun, H. Morkoc, S.S. Park, K.Y. Lee, Appl. Phys. Lett. 78 (2001) 2297.
[10] H. Morkoc, Mat. Sci. Eng. R33 (2001) 135.
[11] D. Zymierska, J. Auleytner, T. Kobiela, R. Dus, Phys. Solid State (a) 180 (2000) 479.
[12] J. Wang, B. Zeng, C. Fang, X. Zhou, J. Electroanal. Chem. 484 (2000) 88.
[13] I. Shalish, Y. Shapira, L. Burstein, J. Salzan, J. Appl. Phys. 89 (2001) 390.
[14] E.J. Miller, D.M. Schaadt, E.T. Yu, P. Walterit, C. Poblenz, J.S. Speck, Appl. Phys. Lett. 82 (2003) 1293.
[15] Y.-J. Lin, C.-T. Lee, J. Vac. Sci. Technol. B 9 (2001) 1734.
[16] C.B. Vartuli, S.J. Pearton, C.R. Abernathy, J.D. Mackenzie, F. Ren, Solid State Electron. 41 (1997) 1947.
[17] D.A. Stocker, E.F. Schubert, J.M. Redwing, Appl. Phys. Lett. 73 (1998) 2654.

UNIVERSITEIT VAN PRETORIA
UNIVERSITY OF PRETORIA
YUNIBESITHI YA PRETORIA

Contents lists available at ScienceDirect

Physica B

journal homepage: www.elsevier.com/locate/physb

Effects of chemical treatment on barrier height and ideality factors of Au/GaN Schottky diodes

M. Diale *, F.D. Auret

Department of Physics, University of Pretoria, Lynwood Road, Pretoria 0002, South Africa

ARTICLE INFO

PACS:
73.30.+y
79.40.+z

Keywords:
Surface treatment
Schottky contact

ABSTRACT

We have studied Au/*n*-GaN Schottky barrier diodes. GaN surfaces have been prepared by cleaning in HCl and $(NH_4)_2S$ prior to metal deposition. The zero-biased barrier heights and ideality factors obtained from the current–voltage characteristics differ from diode to diode, although all the samples were prepared identically. The statistical analysis for the reverse bias *C–V* data yielded mean value of (1.35 ± 0.04) eV for Schottky barrier height of HCl treated sample and (1.20 ± 0.03) eV for $(NH_4)_2S$ sample, where 9 dots were considered from each cleaning method. It was found that the barrier height values obtained from the C^{-2}–V (1.43 eV) and *I–V* characteristics (0.89 eV) are different from each other by 0.54 eV. The inhomogeneous barrier heights were found to be related to the effect of the high series resistance on diode parameters (Akkiliç et al., 2004) [1].

© 2009 Elsevier B.V. All rights reserved.

1. Introduction

Rectifying contacts with low leakage currents and high barrier height are required for the successful fabrication of GaN-based devices. Schottky barrier diodes (SBD) are the choice structure for many semiconductor devices, including microwave diodes, field-effect transistors and photodiodes [2–4]. Their technological importance requires a full understanding of the nature of the electrical characteristics of SBDs. It is well known that SBD has a thin layer of an oxide between the metal and the semiconductor, which cannot be removed by conventional chemical cleaning. Such an oxide converts the diode to metal–insulator–semiconductor (MIS) and usually influences the electrical characteristics of the diode, causing a change in the interfacial charge with bias, giving rise to an electric field at the interfacial layer between the metal and the semiconductor [5,6]. The oxide layer reduces the barrier height and consequently increases the series resistance.

Generally, the forward biased current–voltage (*I–V*) characteristics are linear in the semi-logarithmic scale at low voltages, but deviate considerably from linearity due to the effects of series resistance, R_s resulting from the presence of the thin oxide layer and other surface contaminants. The series resistance is only effective in the curvature downward region or non-linear region of the forward *I–V* characteristics at sufficiently high voltages. The concavity of the current–voltage characteristics at higher voltages increases with increasing series resistance. Increasing series resistance decreases the barrier height and this result in non-ideal current–voltage characteristics. Other parameters such as the ideality factor, $n(V)$ and zero bias barrier height, $\Phi_{b,0}$ are effective in both the linear and the non-linear regions of the *I–V* curve, accompanying the changes in the Schottky barrier height (SBH) [7]. The effect of the series resistance between the depletion region and the ohmic contact of the neutral region of the semiconductor bulk causes the *I–V* characteristics of the metal–semiconductor contact to deviate from the expected [8].

The interface states at the metal–semiconductor junction play a vital role in evaluating the Schottky barrier height and the ideality factor. These manifest themselves as deviations from the ideal Schottky barrier formation and are localized within a few atomic layers of the intimate metal–semiconductor contact with energies which fall inside the forbidden gap. Bardeen showed that such charge accumulated at the metal–semiconductor contact reduces the effective potential difference between the semiconductor and the metal contact [9]. Interface states arise from semiconductor surface states due to discontinuity in the lattice potential, metal-induced-gap states due to wave-function tunneling from the metal into the semiconductor, surface states due to contamination and defects; and any new compounds formed as a result of the interaction of the metal and the semiconductor.

A study of the importance of series resistance in calculating the characteristic parameters of Si Schottky contacts was done by Aydin et al. [1], obtaining their estimations from determination of interface states density distribution from the analysis of the current–voltage measurements. Kampen and Monch studied the barrier heights of different metals on GaN using metal-induced gap states (MIGS) and the electronegativity model, concluding that the experimental values of the barrier height are excellently reproduced by the theoretical predictions, which follow from

* Corresponding author. Tel.: +27 12 420 4418; fax: +27 12 362 5288.
E-mail address: mmantsae.diale@up.ac.za (M. Diale).

0921-4526/$ - see front matter © 2009 Elsevier B.V. All rights reserved.
doi:10.1016/j.physb.2009.09.039

UNIVERSITEIT VAN PRETORIA
UNIVERSITY OF PRETORIA
YUNIBESITHI YA PRETORIA

physical MIGS and the electronegativity concept [10]. A review of metal-contact technology has revealed the importance of surface preparation prior to metal deposition [11]. In this study, two different surface chemicals were used to treat GaN surface prior to metal deposition. The effects of chemical treatments on Schottky characteristics were investigated using capacitance–voltage (C–V) and current–voltage (I–V) characteristics. The average barrier height for the diodes was 1.43 and 1.20 eV for C–V; and 0.81 and 0.89 for I–V measurements, respectively.

2. Experimental

For this investigation, we have used GaN samples with carrier density of $1\times10^{17}\,\mathrm{cm}^{-3}$, obtained from TDI. Before contact fabrication, samples were cleaned using trichloroethylene (TEC), Isopropanol and HCl:HNO_3 aquaregia. Each of these samples was finally etched in 1:1 HCl:H_2O (sample 1) and $(NH_4)_2S$ (sample 2), respectively. Using patterned surface, Ti/Al/Ni/Au (150/2200/400/500 Å) ohmic contacts were deposited by electron-beam and annealed in ultra pure Ar for 5 min at 500 °C. Thereafter, Au Schottky contacts, 0.25 mm thick, were deposited in the resistive evaporator at room temperature. The values of zero-biased barrier height and ideality factor were determined from I–V and C–V measurements at room temperature and corrected afterwards for the effect of series resistance.

3. Results and discussion

In Schottky diodes, the depletion layer capacitance can be expressed as [2]

$$C^{-2}=\frac{2(V_{bi}-V_A)}{q\varepsilon_s A^2 N_D} \tag{1}$$

where A is the area of the diode, V_{bi} the diffusion potential at zero bias and is determined from the extrapolation of the linear $C^{-2}-V$ plot to the V axis and V_A is the applied voltage. The value of the barrier height can be obtained from the relation:

$$\Phi_{b,0}(C-V)=V_{bi}+V_0 \tag{2}$$

where V_0 is the potential difference between the bottom of the conduction band and the Fermi level; and can be calculated knowing the donor concentration N_D obtained from the following relation:

$$V_0=(kT)\ln\left(\frac{N_C}{N_D}\right) \tag{3}$$

where $N_C=4.6\times10^{16}\,\mathrm{cm}^{-3}$ is the effective density of states in the conduction band [3].

Nine dots with the same diameter (0.25 mm) on each sample were evaluated. Fig. 1 shows the reverse bias $C^{-2}-V$ characteristics for one diode from sample 1 and sample 2, respectively. For these particular diodes on samples 1 and 2, the C–V barrier heights are 1.43 and 1.20 eV, respectively. The carrier concentration of 1.9×10^{16} and $2.4\times10^{16}\,\mathrm{cm}^{-3}$ from the reverse bias $C^{-2}-V$ plots was obtained for samples 1 and 2. The C–V barrier heights ranged from 1.28 to 1.50 eV for sample 1 and from 1.14 to 1.25 eV for sample 2. The statistical analysis for the C–V data yielded SBH mean value of 1.35 ± 0.04 eV for sample 1 dots and SBH mean value of 1.20 ± 0.03 eV for sample 2.

In Schottky barrier diodes, the barrier height depends on the voltage and surface conditions prior to metal deposition. The surface condition includes the thickness of the interfacial oxide, which affects the current–transport mechanisms. These include the thermionic emission, which is characterized by ideality close to unity and thermionic field emission and field emission. These mechanisms are affected by series resistance, tunneling and generation recombination in the depletion region. Table 1 gives the summary of the electrical characteristics of the diodes.

For a Schottky contact with series resistance, the net current of the device is due to thermionic emission and it is written as [2]

$$I=I_0\exp\left(-\frac{q(V_A-IR_s)}{nkT}\right) \tag{4}$$

where the saturation current, I_0 is expressed as

$$I_0=AA^{*}T^2\exp\left(-\frac{q\Phi_{b,0}}{kT}\right) \tag{5}$$

where q is the electron charge, A^* is the effective Richardson constant and is equal to $26\,\mathrm{A/cm^2\,K^2}$ for n-type GaN [12], A is the

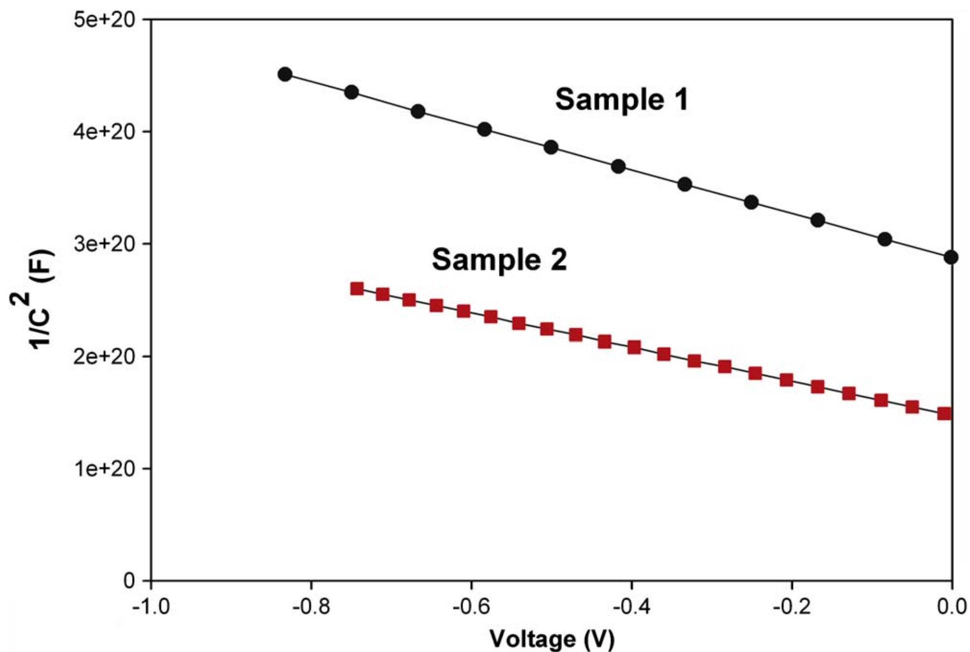

Fig. 1. Reverse bias C^2–V curves of the HCl and $(NH_4)_2S$ samples. For these particular diodes on samples 1 and 2, the C–V barrier heights are 1.43 and 1.20 eV, respectively.

diode area, T is the absolute temperature, k Boltzmann constant, n the ideality factor of the SBD and $\Phi_{b,0}$ the zero bias barrier height. When $V_A \geq 3kT/q$, the extrapolated current, I_0 and the zero bias barrier height can be expressed as

$$\Phi_{b,0} = \frac{kT}{q} \ln\left(\frac{A^*AT^2}{I_0}\right) \quad (6)$$

and the ideality factor from Eq. (4) can be written as

$$n = \frac{q}{kT} \frac{dV}{d(\ln I)} \quad (7)$$

The ideality factor of the SBD, n is a measure of the conformity of the diode to pure thermionic emission. From Fig. 2, current–transport mechanisms displayed are thermionic emission and the series resistance effect at high voltages. The values of the ideality factor, n and the barrier height, Φ_b were calculated from the forward I–V characteristics according to Eqs. (6) and (7). For sample 1 the barrier height, $\Phi_{b.0}$ ranged from 0.79 to 0.89 eV and the ideality factor n ranged from 1.02 to 1.17. Sample 2 $\Phi_{b.0}$ values ranged from 0.71 to 0.85 eV and the n from 1.31 to 1.36. The statistical analysis yielded mean values of 0.84 ± 0.05 eV for the 1.06 ± 0.50 for barrier height and ideality factor of sample 1 (9 dots), respectively, and the mean values of 0.80 ± 0.01 eV and 1.34 ± 0.20 (9 dots) for sample 2 diodes. Ideality factors above unity has been attributed to interface states due to thin oxide layer between the metal and the semiconductor, including other contaminants, tunneling currents in highly doped semiconductors, image-force lowering of the Schottky barrier in electric field at the interface and generation-recombination currents within the depletion region [2]. Our previous results have shown S and Cl residues onto GaN after cleaning in HCl and $(NH_4)_2S$ using Auger electron spectroscopy (AES) and X-ray photoelectron spectroscopy (XPS) [13]. The work done on GaAs and GaP nitridation has shown anion exchange where a thin layer of Ga–N was formed on each of the materials [14]. Surface Ga–N in turn passivates the GaAs and GaP, affecting the I–V and C–V characteristics of these materials. In addition, the work done by Liu et al. has shown that the Ga peak becomes larger when samples are cleaned in $(NH_4)_2S$ than in HF/HCl [15]. Furthermore, $(NH_4)_2S$ has been found to reduce the barrier height on GaN, and preventing re-oxidation of the surface [16]. We suggest that there exist Ga–Cl and Ga–S on sample 1 and sample 2, respectively. Previous XPS results have shown that as-grown GaN surface has oxides in the form of Ga_2O_3 and GaOH. In addition, while rinsing GaN in water, addition of OH to GaN to form the GaOH, may occur, and be part of sticking surface water that may contribute to interface states [17].

Table 1
Values obtained experimentally from the current–voltage characteristics of the Au/GaN Schottky diodes.

Sample 1	
n	1.17
R_s (Ω)	22.3
$\Phi_{b,c}$ (eV), C–V	1.43
$\Phi_{b,0}$ (eV), I–V	0.82
Sample 2	
n	1.89
R_s (Ω)	17.1
$\Phi_{b,c}$ (eV), C–V	1.20
$\Phi_{b,0}$ (eV), I–V	0.71

The difference in series resistance for the samples 1 and 2 is due to the surface state after different chemical treatment.

The values of R_s and $\Phi_{b.0}$ for both samples 1 and 2 were obtained as 0.82 eV and 22.3 Ω; and 0.71 eV and 17.0 Ω, respectively. As mentioned above, the barrier height values of 1.43 and 1.20 eV for samples 1 and 2 were obtained from the C^{-2}–V plots, respectively. These barrier height values obtained from the C^{-2}–V (1.43 eV) and I–V characteristics (0.89 eV) are different from each other by 0.54 eV. We attribute the difference between the I–V and C–V barrier height in the metal–semiconductor to SBH inhomogeneity. This is the fact that the barrier heights of the diodes on the same sample differs from diode to diode and at different positions on the same diode. The measured I–V barrier height is significantly lower than the weighted arithmetic average of the SBHs. On the other hand, the C–V measured barrier height is influenced by the distribution of charge at the depletion region follows the weighted arithmetic average of the barrier height inhomogeneity; hence the BH determined by C–V is close to the weighted arithmetic average of the barrier heights. Therefore, the

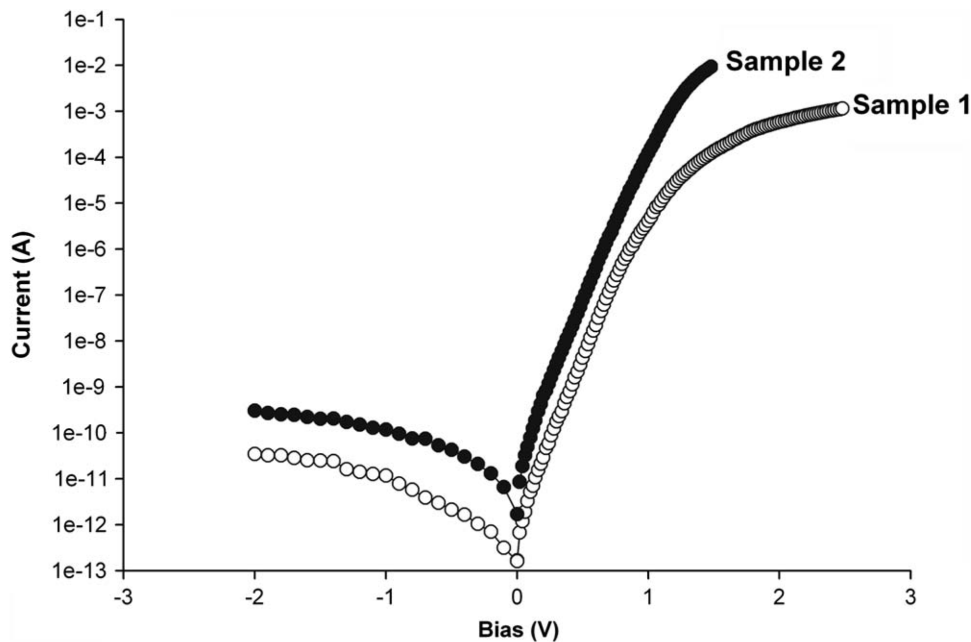

Fig. 2. The I–V curves of the treated samples. The series resistance values of HCl samples are generally higher than those treated in $(NH_4)_2S$, which presented less oxide and reduced barrier height.

barrier height determined from zero bias intercept assuming thermionic emission as current transport mechanism is well below the measured BH and the weighted arithmetic average of the barrier heights [18,19]. Furthermore, the surface damage at the metal–semiconductor interface affects the *I*–*V* measurements because defects may act as recombination centers for trap-assisted tunneling currents. *C*–*V* measurements are generally less prone to interface states, so that the determined barrier height is considered more reliable, though the depletion width can be altered by the interface defects if they are deeper into the space charge region [20].

4. Summary

In conclusion, we have fabricated Au/*n*-GaN SBDs using different cleaning procedures. From the current–voltage characteristics, we obtained the values of ideality factor, SBH and R_s for the samples. The *I*–*V* characteristics are near ideal with thermionic emission as the dominant current transport mechanism. Furthermore, HCl treated samples behave like a MIS diode due to the amount of oxide remaining on the surface after treatment. The series resistance values of HCl samples are generally higher than those treated in $(NH_4)_2S$, which presented less oxide and reduced barrier height, in agreement with published results. Most published results on GaN have only reported their findings without specifics on current transport mechanism. Thus further work is needed for the investigation ideality factor far above unity, which will need the knowledge of the oxide layer thickness on GaN, effects of passivation of GaN surface on electrical characteristics, and analysis of barrier height inhomogeneities on the rectifying diode characteristics on GaN.

Acknowledgment

The authors gratefully acknowledge financial assistance from the South African National Research Foundation.

References

[1] K. Akkiliç, M.E. Aydin, A. Türüt, Physica Scripta 70 (2004) 364.
[2] E.H. Rhoderick, R.H. Williams, Metal–Semiconductor Contacts, Clarendon Press, Oxford, 1988.
[3] S.M. Sze, Physics of Semiconductor Devices, second ed., Wiley, New York, 1981.
[4] L. Wang, M.I. Nathan, T.-H. Lim, M.A. Khan, Q. Chen, Applied Physics Letters 68 (9) (1996) 1267.
[5] P. Hanselaer, W.H. Laflere, R.L. Meirhaeghe, F. Cardon, Applied Physics Letters 56 (1984) 2309.
[6] E. Monroy, F. Calle, J.L. Pau, E. Mu ńoz, F. Omnes, Electronic Letters 36 (25) (2000) 2096.
[7] J.C. Card, E.H. Rhoderick, Journal of Applied Physics D 4 (1971) 1589.
[8] M.E. Aydin, K. Akkiliç, T. Kiliçoglu, Applied Surface Science 225 (2004) 1304.
[9] J. Bardeen, Physical Review 71 (1947) 771.
[10] T.U. Kampen, W. Monch, Applied Surface Science 117/118 (1997) 388.
[11] Q.Z. Liu, S.S. Lau, Solid State Electronics 42 (1998) 677.
[12] A.C. Schmidt, A.T. Ping, M. Asif Khan, Q. Chen, J.W. Yang, I. Adesida, Semiconductor Science and Technology 11 (1996) 1464.
[13] M. Diale, F.D. Auret, N.G. van der Berg, R.Q. Odendaal, W.D. Roos, Applied Surface Science 246 (2005) 279.
[14] G. Bruno, Applied Surface Science 235 (2004) 239.
[15] J. Liu, B. Shen, Y.G. Zhou, H.M. Zhou, M.J. Wang, Z.W. Zheng, B. Zhang, Y. Shi, Y.D. Zheng, Optical Materials 23 (2003) 133.
[16] X.A. Cao, S.J. Pearton, G. Dang, A.P. Zhang, F. Ren, J.M. Van Hove, Applied Physics Letters 75 (1999) 4130.
[17] M. Diale, F.D. Auret, N.G. van der Berg, R.Q. Odendaal, W.D. Roos, Surface and Interface Analysis 37 (2005) 1158.
[18] J.H. Werner, H.H. Guttler, Journal of Applied Physics 69 (3) (1991) 1552.
[19] R.T. Tung, A.F.J. Levi, J.P. Sullivan, F. Schrey, Physical Review Letters 66 (1) (1971) 72.
[20] C. Fontaine, T. Okumura, K.N. Tu, Journal of Applied Physics 54 (1983) 1404.